CELLULAR RNA TARGETING BY PLATINUM (II) ANTICANCER THERAPEUTICS

by

MAIRE F. OSBORN

A DISSERTATION

Presented to the Department of Chemistry and Biochemistry
and the Graduate School of the University of Oregon
in partial fulfillment of the requirements
for the degree of
Doctor of Philosophy

March 2014

DISSERTATION APPROVAL PAGE

Student: Maire F. Osborn

Title: Cellular RNA Targeting by Platinum (II) Anticancer Therapeutics

This dissertation has been accepted and approved in partial fulfillment of the requirements for the Doctor of Philosophy degree in the Department of Chemistry and Biochemistry by:

Diane Hawley	Chair
Victoria DeRose	Advisor
Andy Berglund	Core Member
Jim Remington	Core Member
Alice Barkan	Institutional Representative

and

Kimberly Andrews Espy	Vice President for Research and Innovation; Dean of the Graduate School

Original approval signatures are on file with the University of Oregon Graduate School.

Degree awarded in March 2014.

DISSERTATION ABSTRACT

Maire F. Osborn

Doctor of Philosophy

Department of Chemistry and Biochemistry

March 2014

Title: Cellular RNA Targeting by Platinum (II) Anticancer Therapeutics

Cis-diamminedichloroplatinum (II), or cisplatin, is a widely prescribed anticancer compound, currently one of only three platinum (II) complexes FDA approved for cancer treatment. Despite its widespread use, we lack a comprehensive picture of global drug targets, which would lend valuable insights into the molecular mechanisms of action and resistance in different tissues. Drug binding to genomic DNA is an accepted cause of downstream apoptotic signaling, but less than 10% of Pt (in the case of cisplatin) accumulates within genomic DNA. Non-genomic contributions to cisplatin's therapeutic action are also under active investigation. In particular, cisplatin treatment can disrupt RNA-based processes such as splicing and translation. Pt(II) targeting of non-DNA species such as RNA may contribute to or sensitize a cell to the downstream effects of this drug, including the induction of apoptosis.

Chapter I summarizes the activity profile of Pt(II) therapeutics, describing cellular uptake, cellular localization, incidences of Pt(II) accumulation within RNA, and RNA processes affected following drug treatment. Chapter II reports our thorough investigation of the distribution of Pt species throughout messenger and ribosomal RNA, with the discovery that *Saccharomyces cerevisiae* ribosomes act as a *de facto* cellular Pt sponge. In Chapter III, we report the synthesis of an azide-functionalized platinum (II)

species, picazoplatin, for post-treatment click labeling and isolation of drug targets *in vivo*. Picazoplatin was designed to circumvent mislocalization and misprocessing of Pt typically encountered when trying to track small molecules tethered to large, charged fluorophores. This chapter contains several proof-of-principle studies validating the use of this class of reagents for future purification and sequencing of Pt-bound nucleic acids. Chapter IV describes the first application of the click-capable Pt reagent technology: the demonstration of significant in-gel fluorescent detection of Pt-bound ribosomal RNA and transfer RNA extracted from picazoplatin-treated *S. cerevisiae* and the first evidence that cellular tRNA is a platinum substrate. Chapter V summarizes these data, which suggest a potential ribotoxic mechanism for cisplatin cytotoxicity and broadly describe a convenient click chemistry methodology that can be applied to identify other metal or covalent modification-based drug targets.

This dissertation includes previously published and unpublished co-authored material.

CURRICULUM VITAE

NAME OF AUTHOR: Maire F. Osborn

GRADUATE AND UNDERGRADUATE SCHOOLS ATTENDED:

University of Oregon, Eugene, Oregon
McGill University, Montreal, Quebec, Canada

DEGREES AWARDED:

Doctor of Philosophy, Chemistry, 2014, University of Oregon
Bachelor of Science, Chemistry, 2008, McGill University

AREAS OF SPECIAL INTEREST:

RNA Biochemistry (Structure, Function, Catalysis, Regulation)
Platinum Anticancer Therapeutics
RNA Therapeutics

PROFESSIONAL EXPERIENCE:

Chair of Business Development, The RNA Society, 2013-2014

HHMI Science Literacy Program Fellow, Department of Chemistry, University of Oregon, Eugene, Oregon, 2012-2014

Graduate Teaching Fellow, Department of Chemistry, University of Oregon, Eugene, Oregon, 2008-2014

GRANTS, AWARDS, and HONORS:

NIH Molecular Biophysics Training Grant, Institute of Molecular Biology, University of Oregon, Eugene, Oregon, 2009-2011

RNA Society Travel Fellowship, 2011

Travel Fellowship, Department of Chemistry, University of Oregon, 2012

PUBLICATIONS:

White, J.W.*, Osborn, M.F.*, Moghaddam, A.D., Guzman, L.E., Haley, M.M., DeRose, V.J. (2013). Picazoplatin, an Azide-Containing Platinum(II) Derivative for Target Analysis by Click Chemistry. *J. Am. Chem. Soc. 135* (32): 11680–11683.
*Co-first authors

Hostetter, A.H., Osborn, M.F., DeRose, V.J. (2012). RNA-Pt Adducts Following Cisplatin Treatment of Saccharomyces cerevisiae. *ACS Chem. Biol. 7* (1):218-25.

Chapman, E.G., Hostetter, A., Osborn, M.F., Miller, A., DeRose, V.J. (2011). Binding of kinetically inert metal ions to RNA: the case of platinum(II). *Met. Ions Life Sci.* (9):347-77. Review.

Henderson, J.N., Osborn, M.F., Koon, N., Gepshtein, R., Huppert, D., Remington, S.J. (2009). Excited state proton transfer in the red fluorescent protein mKeima. *J. Am. Chem. Soc. 131* (37):13212-3.

ACKNOWLEDGEMENTS

I came to the University of Oregon on the recommendation of a respected advisor at McGill University, Dr. Eric Salin, who completed his Ph.D. at OHSU. Recognizing my love for both chemistry and the outdoors, I think he knew this environment would cultivate a period of great academic and personal achievement. I owe my sincerest thanks to all those who made that possible. First and foremost, I gratefully acknowledge my advisor Dr. Victoria J. DeRose for always holding me to the highest standard, and for providing me with the training and tools necessary to succeed in my future career. I am very thankful for the support of my dissertation committee: Dr. Diane Hawley, Dr. Jim Remington, Dr. Alice Barkan, and Dr. Andy Berglund. It has been an honor to develop as a scientist under their guidance. I would like to thank all those in IMB and the Department of Chemistry and Biochemistry who have provided training, reagents, or scientific discourse, especially those in the Berglund, Prehoda, Stevens, and Stankunas laboratories. I am very thankful for the mentorship of Chris S. Larson, who helped me develop the self-confidence and self-assurance crucial to my professional development.

I am enormously lucky to have surrounded myself with an inspiring group of peers, both in my academic and athletic circles. Former DeRose lab members Dr. Erich G. Chapman, Dr. W. Luke Ward, and Dr. Alethia A. Hostetter welcomed me into the group, patiently showed me the ropes, and fostered my excitement for RNA biology as a whole. Since then, we have had many new faces join us, each bringing a new aspect of expertise to our research. The synthetic prowess of Jonathan D. White laid the foundation for our click chemistry endeavors. I thank Alan D. Moghaddam for his significant contributions to our picazoplatin manuscript. Although he worked on different aspects of

cisplatin chemistry, I am very grateful to Kory J. I. Plakos for providing insight into challenging problems I faced in my own work, especially regarding data and image processing. I would also like to acknowledge Rachael M. Cunningham and new recruits Emily R. Morris and Emelia H. Padilla. It has been a great pleasure to work in close proximity with these people over the past few years. Although not formally a DeRose lab member, I am especially grateful for the friendship of Ruth B. Siboni, who has been a trusted confidante since her rotation with me in early 2011.

My research success would not have been possible without a strong support network outside of the lab. First, I would like to acknowledge my family, especially my mother, Annie C. Osborn, who recognized my love of science at an early age and made it possible for me to be where I am today. I thank my brother, Patrick J. C. Osborn, for his continuous love and support, and for ensuring I keep everything in perspective. Finally, I am grateful to David R. Wells for helping me through some of the most challenging moments and pushing me to become a better version of myself.

I couldn't have done this without all of you.

This dissertation is dedicated to my mom.

Thank you for always believing in me.

TABLE OF CONTENTS

LIST OF FIGURES

LIST OF TABLES

CHAPTER I

MOLECULAR MECHANISM OF PLATINUM (II) THERAPEUTICS

Introduction and Recognition of the Contribution of Others in This Dissertation

The research described in this dissertation was performed in the laboratory of Dr. Victoria J. DeRose, as part of an effort to understand the diverse molecular mechanisms of platinum anticancer therapeutics. The projects described herein, specifically the concept of ribosomal RNA targeting by cisplatin, were co-developed and guided by Dr. DeRose with helpful input from fellow graduate students Dr. Erich G. Chapman, Dr. Alethia A. Hostetter, and Dr. W. Luke Ward. Chapter I outlines the discovery and history of Pt(II) drugs, and recent work suggesting that non-DNA targets, such as RNA, may play critical roles in cytotoxicity. This chapter contains excerpts from a co-authored review written in 2011 with Dr. Chapman, Dr. Hostetter, Amanda L. Miller, and Dr. DeRose.[1] Chapter II recounts our investigation of the biochemical interactions of cisplatin in *S. cerevisiae.* This work was published in *ACS Chemical Biology* in 2012, comprises research performed by Dr. Hostetter and myself and was co-authored with Dr. Hostetter and Dr. DeRose.[2] Chapter III reports on an exciting new technology conceived by Dr. DeRose and developed through my collaboration with Jonathan D. White and Alan D. Moghaddam (the self-titled "Captains of Click"). In this chapter, published in the *Journal of the American Chemical Society* in 2013, we have described the *in vitro* and *in vivo* applications for novel click-capable platinum complexes synthesized by Jonathan D. White with assistance from Lindsay E. Guzman.[3] Chapter IV contains the major product of my graduate work, a comprehensive study of platinum adduct formation within the catalytic core of the *S. cerevisiae* ribosome. Dr. DeRose and I co-designed the experimental strategy and I performed the bench work. For these studies, I am very grateful to Jonathan D. White for providing reagents and to Rachael M. Cunningham for assisting with the *in vivo* experiments. This chapter comprises a manuscript co-authored with Jonathan D. White and Dr. DeRose that is being prepared for submission to *PNAS*. Finally, I would like to gratefully acknowledge co-workers in the Department of Chemistry and Biochemistry who have assisted with experimentation and provided

training, helpful discussion, and project guidance: Kory J. I. Plakos, Ruth B. Siboni, Devika S. Gates, Oggie Golub, and former mentored students Folashade Olwloro, Suzanne Mirashrafi, and Lindsay Guzman.

Platinum Anticancer Drugs: Discovery and Early History

Cis-diamminedichloroplatinum (II), or cisplatin, is the flagship compound of a small class of FDA-approved platinum (II) anticancer therapeutics. Cisplatin was first synthesized by Michael Peyrone in 1844, but not recognized to have biological activity until the serendipitous discovery of its antiproliferative activity against *E. coli* in 1965 by Barnett Rosenberg and colleagues at Michigan State University.[4,5] Interested in the potential for inorganic metal cancer therapeutics, Rosenberg led an effort to characterize the efficacy of cisplatin and derivatives in sarcoma- and leukemia-bearing mouse models. Shockingly, it was discovered that select *cis* platinum (II) complexes were capable of increasing the lifespan of treated animals by almost four-fold following a single injection at 8 mg/kg.[6] Interestingly, the *trans* isomers were found to be clinically ineffective. In early preclinical trials, cisplatin toxicology was hampered by acute and chronic side effects including nephro-, oto-, and peripheral neurotoxocity.[7] Alleviation of these symptoms through dose limitation, hydration, and combinatorial therapy allowed for FDA approval in 1978. These studies were the foundation of a discovery that would revolutionize cancer treatments; cisplatin therapy increased the cure rate of testicular cancer from 4% to over 90% in early detection cases, and is presently included in over half of cancer drug regimes.[8]

Structure-activity relationships have identified the approximate geometry and ligand set for optimal drug activity (such as *cis* conformation), but only two additional platinum therapeutic agents have been FDA approved since cisplatin in 1978 (**Figure 1.1**). Carboplatin, *cis*-diammine-1,1'-cyclobutane-dicarboxylato-platinum(II), was patented in 1979 and FDA approved in 1989. This complex retains the *cis*-diammine configuration of cisplatin, but replaces the chloride leaving groups with a chelating dicarboxylate ligand designed to reduce its chemical reactivity and mediate oto- and nephrotoxicity. Oxaliplatin, (1*R*,2*R*-(N,N'-1,2-diamminocyclohexane)-(O,O')-ethanedioato)platinum(II), was FDA approved in 2002 and avoids issues with cross-

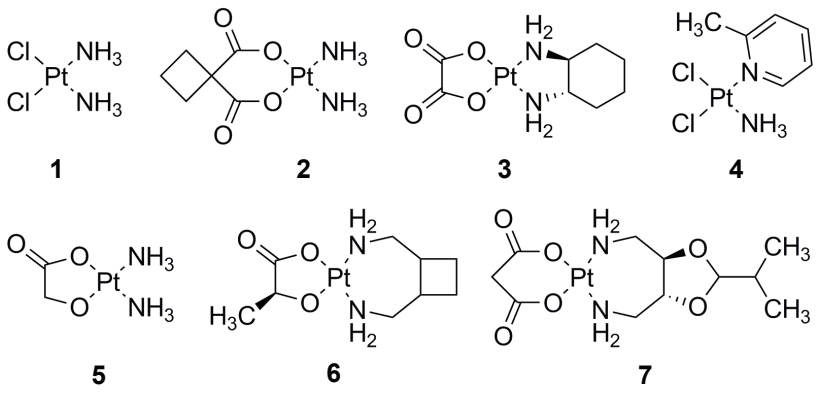

Figure 1.1. Structures of the three currently FDA approved platinum (II) therapeutics (1) cisplatin, (2) carboplatin and (3) oxaliplatin, as well as four newer complexes approved internationally that are currently or have recently gone through U.S. clinical trials: (4) picoplatin, (5) nedaplatin, (6) lobaplatin, and (7) heptaplatin.

resistance typically encountered with cisplatin and carboplatin. **Figure 1.1** portrays several other platinum species already approved internationally but presently in U.S. preclinical trials, including picoplatin (U.S), nedaplatin (Japan), lobaplatin (China), and heptaplatin (South Korea).[5] The underlying challenge faced by all these platinum therapeutics is acquired or intrinsic resistance, due in part to an incomplete comprehension of their intracellular localization and processing. The following chapter describes the current body of knowledge on the activity profile of platinum(II) therapeutics.

Molecular Mechanism of Action

Early studies investigated the broad impact of cisplatin treatment on the synthesis of DNA, RNA, and proteins using isotopically labeled nucleotide or amino acid precursors. The major observation was selective inhibition of DNA synthesis, with a lesser effect on RNA and protein synthesis until higher intracellular concentrations of platinum were achieved.[9] Another indication of DNA damage was the filamentous growth of *E. coli* observed upon cisplatin treatment, typical of DNA damaging agents such as UV and ionizing radiation.[10] This led to an initial hypothesis that cisplatin was acting analogously to a subset of bifunctional alkylating agents containing two active chloride groups, such as chlorambucil, which crosslink genomic DNA and lead to replication stalling.[6] Such bifunctional alkylating agents form interstrand crosslinks

between the N_7 imino atoms of purine bases, across a distance of approximately 8 Å. However, this distance is on the periphery of the coordination sphere of an active *cis* platinum (II) isomer, and cisplatin was thus proposed to form intrastrand crosslinks on adjacent purine-N_7's, which span just ~3-5 Å in B-form DNA.[11] Since the publication of this mechanistic theory in 1970, the majority of research has focused on platinum targeting of genomic DNA. It is commonly accepted that in DNA, intrastrand chelation induces structural distortions within the helix, which cause replication arrest and transcription inhibition, as well as secondary cell cycle arrest and DNA repair. The inability of DNA repair pathways such as nucleotide excision repair to remove Pt(II)-containing nucleotides results in the activation of HMG family proteins, which trigger p53 to initiate an apoptotic signal (**Figure 1.2**).[10] Although this theory describes one aspect of cisplatin cytotoxicity, it does not fully account for the properties of Pt(II) complexes that differentiate them from bifunctional alkylating species. The square-planar Pt(II) compounds represent a different class of metal-based complexes that have defined geometric ligand constraints, slow- to inert-ligand exchange, and binding that is influenced by kinetics rather than thermodynamics in most settings. Platinum complexes are soft Lewis acids, which preferentially react with biological targets containing nitrogen and sulfur donor ligands.[1] Therefore, with a simplistic model, coordination chemistry

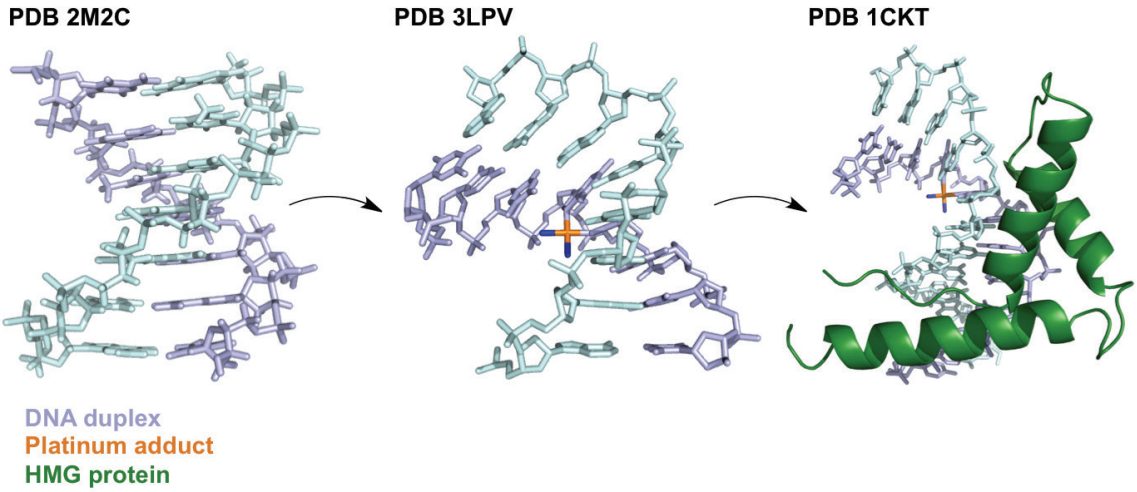

Figure 1.2. Model of platinum drug binding within duplex DNA. B-form DNA duplex (light blue, purple) is conformationally restrained upon platinum adduct formation (orange). Failure of DNA repair pathways to excise the lesion results in high-mobility group (HMG, green) protein recruitment to the structural distortion. All images created in PyMOL using PDB files 2M2C, 3LPV, and 1CKT.

would predict that reactive platinum species would be rapidly sequestered by S-donor ligands in the plasma membrane and cytoplasm. This reactivity greatly expands the breadth of potential cytotoxic targets for this complex and warrants a thorough investigation of reactive partners encountered when first entering the cell, prior to nuclear translocation.

Platinum Drug Cellular Uptake and Activation

In patients, cisplatin is administered intravenously in doses ranging from 50-120 mg/m^2.[10] Following entry into the bloodstream, cisplatin is subject to relatively high chloride concentrations (100 mM), which suppress exchange of its two active chloride ligands. The same principle applies to carboplatin and oxaliplatin, allowing them to remain as inert dicarboxylate species. This mediates reactivity towards circulating proteins, although significant cisplatin accumulation on human albumin is observed 24 h post-treatment.[7] Active transport of the neutral complex across the plasma membrane can occur via copper transporter 1 (Ctr1), copper transporter 2 (Ctr2), the P-type copper-transporting ATPases (ATP7A and 7B), and organic cation transporter 2 (OCT2). Differential expression of these membrane-associated proteins regulates cisplatin translocation into different tissues.[12]

Following cellular uptake, cisplatin becomes intracellularly activated by aquation of one or both of its chloride ligands, forming either a mono- or diaquadiammine platinum(II) cation. The substitution of water with chloride as a leaving group confers a positive charge to the complex, increasing its reactivity. Pt(II) is subsequently able to form coordinate covalent bonds to nucleophilic centers of its bimolecular targets. In nucleic acids, *in vitro* studies reveal that activated cisplatin preferentially binds the accessible and reactive imidazole N_7 atoms on proximal purine bases. This is especially true for studies using duplex nucleic acids where other potential Pt(II) ligands such as the N_1 of adenine and N_3 of cytosine are precluded from platinum binding by their participation in Watson-Crick base pairs.[13] The major DNA adducts formed are 5'-dGpdG-3' 1,2-intrastrand adducts (47-50%), followed by 5'-dApdG-3' 1,3-intrastrand adducts (23-28%), with platinum occasionally forming monofunctional adducts, interstrand crosslinks, or DNA-protein crosslinks (**Figure 1.3**).[14] Other Pt(II) targets may

include mitochondrial DNA (which lack the nucleotide excision repair pathway)[15], purine-N_7's of cytoplasmic RNA, nucleophilic amino acids such as histidine and cysteine, and thiol-containing small molecules such as glutathione. It is well acknowledged that cisplatin binds many species throughout the cytosol; the slow dissociation kinetics of the bis-chelating leaving groups on carboplatin and oxaliplatin were designed to result in latent activation and decreased reactivity towards non-DNA targets.[10]

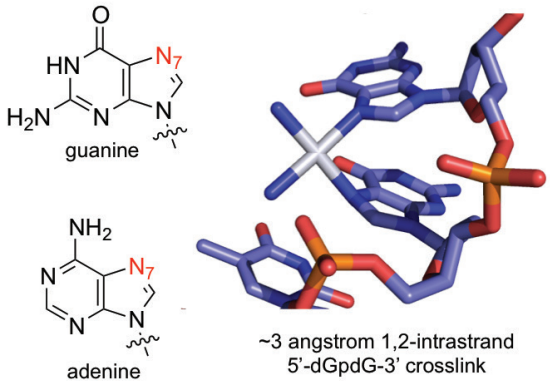

Figure 1.3. (Left) Purine nucleotides guanine and adenine, with N7 positions highlighted in red. (Right) Model of the major 5'-dGpG-3' crosslink (white) observed following *in vitro* treatment of DNA with cisplatin. Figure created in PyMOL using PDB file 3LPV.

Cellular Pt (II) Drug Trafficking and Localization

Characterizing the spatial distribution of Pt(II) binding within a cell provides critical information regarding the types of the cellular machines and architectures that Pt(II) complexes may target. Major cellular targets, with regions important for RNA processes, are highlighted in **Figure 1.4**. Atomic absorption spectroscopy (AAS) and inductively coupled plasma mass spectroscopy (ICP-MS) have been utilized to quantify Pt drug accumulation in subcellular organelles. Nuclear accumulation, presumably from DNA binding, is observed for cisplatin and other Pt(II) therapeutics, in good agreement with predicted mechanistic theory.[16] Although it is generally accepted that cisplatin-DNA adducts are responsible for the majority of a cell's apoptotic response, studies in HeLa cells have proposed that 75-85% of the drug becomes covalently linked to protein, while only 1-5% of the drug actually reaches nuclear DNA.[17] In our lab, we have directly quantified Pt(II) accumulation within yeast RNA and DNA using ICP-MS at therapeutically relevant concentrations of cisplatin, and have demonstrated there is 4-20% more accumulation of Pt in

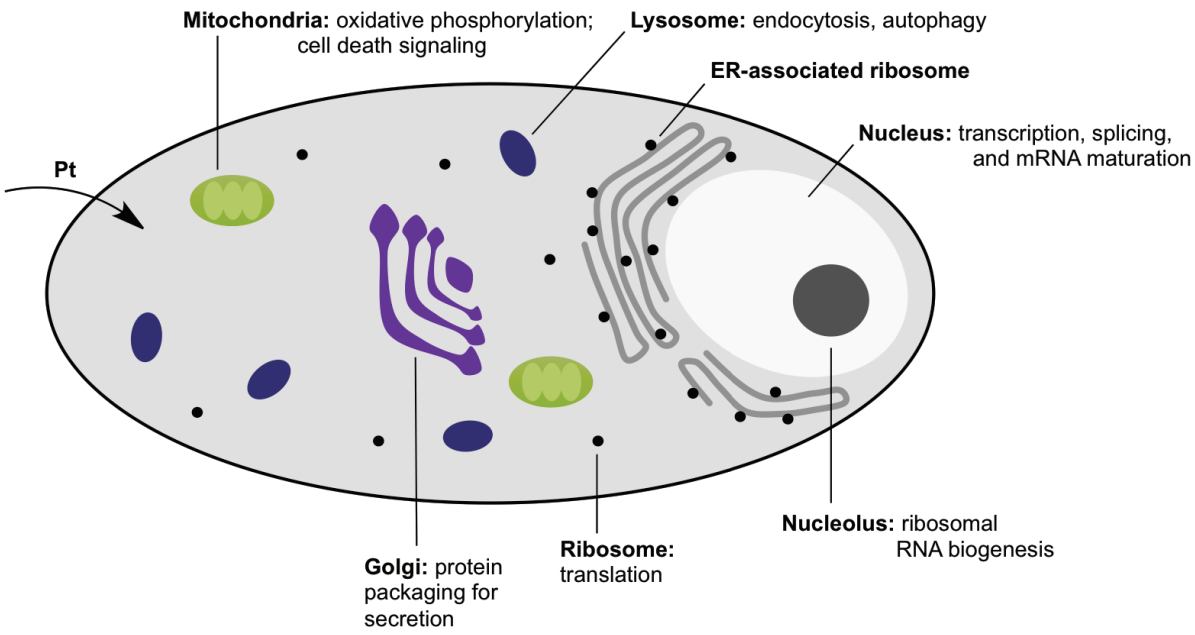

Figure 1.4. Subcellular sites of platinum accumulation, listing the organelles that accumulate Pt drugs in cancerous cells and the locations of important RNA processes within the cell.

total RNA than DNA (further described in Chapter II).[2] Cisplatin accumulation in intact mitochondria[18] as well as drug binding to mitochondrial DNA have been quantified using AAS and by immunodetection techniques.[19–21] More recently, Pt accumulation has been detected in vesicles by ICP-MS following the treatment of cells with cisplatin, carboplatin and oxaliplatin.[22,23] The importance of vesicular Pt(II) accumulation is currently unknown, but may lend insight into biological processing of drug damaged biomolecules.

Direct imaging techniques have also provided a powerful means to study platinum distribution in treated cells. Fluorescently tagged platinum compounds are exceptionally useful for visualizing the cellular localization of platinum drugs in real time. These drug conjugates typically utilize the chelating ligand ethylenediamine (en) as an anchor for attaching labels such as fluorescein.[24] The effects of attaching a large, non-polar fluorophore on the biological distribution and processing of platinum drugs must be taken into account in interpreting these data. However, supporting biological assays show that while the Pt(II)-fluorophore conjugate is ~4-fold less potent that cisplatin, Pt(II)-resistant cell lines are similarly insensitive to the two complexes suggesting that the complexes may be similarly processed *in vivo*.[25]

In one of the first studies of this type, Reedjik and coworkers used a carboxyfluorescein diacetate-tagged [Pt(en)Cl_2] complex to monitor localization of the compound within human osteosarcoma cells. Initially diffuse throughout the cell, the Pt(II) complex accumulates in the nucleus after 1-2 hours and after 6-8 hours, the compound appears to migrate out of the nucleus and into Golgi bodies.[26,27] In a human ovarian carcinoma cell line, a similar Pt(II)-fluorophore species can be tracked to the periphery of the cellular membrane, in the nucleus, and in small vesicular structures scattered throughout the cytoplasm.[25] Fluorescent Pt(II) complexes have been used in concert with specific small molecule inhibitors to show that these compounds are first sequestered by lysosomes, subsequently transferred to Golgi apparatus and finally packaged into secretory vesicles.[28] This approach of fluorescently tagging Pt drugs has produced, over several studies, a more uniform picture of Pt(II)-conjugate localization. Initially, cisplatin and other Pt(II) drugs enter the cell and accumulate to varying degrees in the vesicles and organelles of the cytoplasm, including lysosomes, Golgi, and mitochondria. From there Pt enters and accumulates in the nucleus, often accumulating along the periphery of the nucleus and in nucleoli. Depending on the treatment conditions and cell type this nuclear accumulation may become greater than cytoplasmic accumulation after 1-4 hours. Finally, export from the cell may involve the Golgi and vesicles of the secretory export pathway. However, in general, platinum distribution is highly variant throughout different cell lines and over different treatment conditions, highlighting the need for a uniform method for characterization of kinetically preferred species. In Chapter III, I describe our recent work using the click reaction to fluorescently *post-label* platinum bound species *in vitro*, demonstrating the potential for highly accurate and unbiased real time future Pt(II) tracking studies.[3]

DNA-Pt(II) Binding Not Required for Cisplatin Cytotoxicity

Importantly, alternative cellular pathways that execute apoptosis following cisplatin treatment have been identified. Recent studies in mammalian cells have exhibited rapid and nucleus-independent cytoplasmic initiation of cisplatin toxicity. In these studies, enucleated cytoplasts were treated with cisplatin, and probed for active (cleaved) caspase 3. Levels of cleaved caspase 3 were found to greatly increase relative

to an untreated control.[29,30] The signaling pathways responsible for initiating this apoptotic signal, and whether cytosolic RNA targets could be involved, are yet unexplored. These discoveries, in conjunction with the relatively long timescale of nuclear DNA accumulation (up to 4 hours), describe an undefined cytoplasmic initiator of cytotoxicity, which may very well be mediated by RNA damage. Therefore, this evidence premises our investigation into RNA as a potential target for platination *in vivo*, and its contribution to the antitumor activity of the drug.

RNA: A Putative Therapeutic Target

RNA plays critical roles in the transfer of genetic information, protein synthesis, and signaling events.[31] In addition, novel noncoding RNA species and their corresponding functional roles are continuously being discovered. Such findings include the discovery of siRNA, microRNA, piwi-interacting RNA, long noncoding RNAs, and most recently, competing endogenous RNAs (ceRNAs). This fascinating RNA-dependent RNA regulatory network centers around the concept that a myriad of different RNA species, including lncRNAs, pseudogenes, circular RNAs, and protein-encoding mRNAs, communicate with and co-regulate each other by competing for shared miRNAs.[32] This intricate network of RNA interactions implies roles for RNA well beyond the normal scope of gene expression.

Broadly, this functional range is due to rich structural diversity facilitated by intramolecular tertiary contacts and intermolecular interactions, which are defined by hydrogen bonding and electrostatics. A general description of the many stable structures accessed by RNA is provided in **Figure 1.5a**. Common motifs include hairpins, internal loops, bulged nucleotides, and 3-helix junctions. These secondary and tertiary structural facets enable recognition by other RNAs, proteins, and small molecules. For instance, the sarcin-ricin loop, a solvent exposed region of the large ribosomal RNA subunit, contains several unique RNA-specific structural motifs which enable its recognition and binding by translation factors (**Figure 1.5b**).[33] Disruption of these interactions by ribotoxins such as α-sarcin and ricin results in rapid apoptotic signaling.[34]

RNA is a promising small molecule target, but when compared to nuclear DNA, there are relatively few complexes that target RNA with the specificity and affinity of

those which intercalate DNA. Moreover, RNA-targeting small molecule therapies have been restricted due to insufficient exploration of the structural qualities of small molecules that target RNA, and conversely, the classes of RNA structures that can bind small molecules.[35] However, the interactions of metal ions with RNA have been extensively investigated and are critical for RNA folding, structure, and biochemical activity. A significant number of RNAs adopt structures capable of hosting cationic metal ions, such as Mg^{2+}, K^{+}, and Na^{+}. Only a fraction of the ions that are involved in RNA folding and catalysis can be deduced from crystal structures, and necessitate concurrent biochemical and biophysical studies.[36] Cationic binding pockets predicted from molecular simulations based on NMR structural data within the sarcin-ricin loop[37] are described in **Figure 1.5b**. These regions of high negative charge density are typically coordinated by a network of water molecules and metal ions, and make kinetically favorable platinum (II) binding targets, especially true for abundant cytoplasmic species such as ribosomal RNA. It is interesting to note that the repetitive structure of the DNA double helix may offer a limited number of potential Pt(II) coordination geometries. In contrast, RNA exhibits a diverse array of secondary and tertiary architectures, which include these specific and pre-organized metal-ion binding sites[13,38,39] as well as solvent-excluded folds where nucleobase pK_a's can be significantly altered from those observed in solution.[40,41] Consequently, these structures greatly expand the chemical space in which physiological metal complexes could find appropriate binding pockets. The limited collection of studies describing known Pt(II) lesions on isolated RNA are outlined below.

RNA-Pt(II) Lesions: *In Vitro* Molecular Investigations

Seeking to understand how cisplatin may target RNA structures on a molecular scale, a handful of recent studies have described the formation of Pt(II) adducts within isolated RNAs. These studies examine cases ranging from the platination of relatively short single-stranded RNAs[42] to studies involving coordination of cisplatin to ribosomes.[2,43] In accordance with the observations above, an emerging feature of these studies seems to be ability of Pt(II) complexes to bind in non-Watson-Crick base paired regions of RNA.

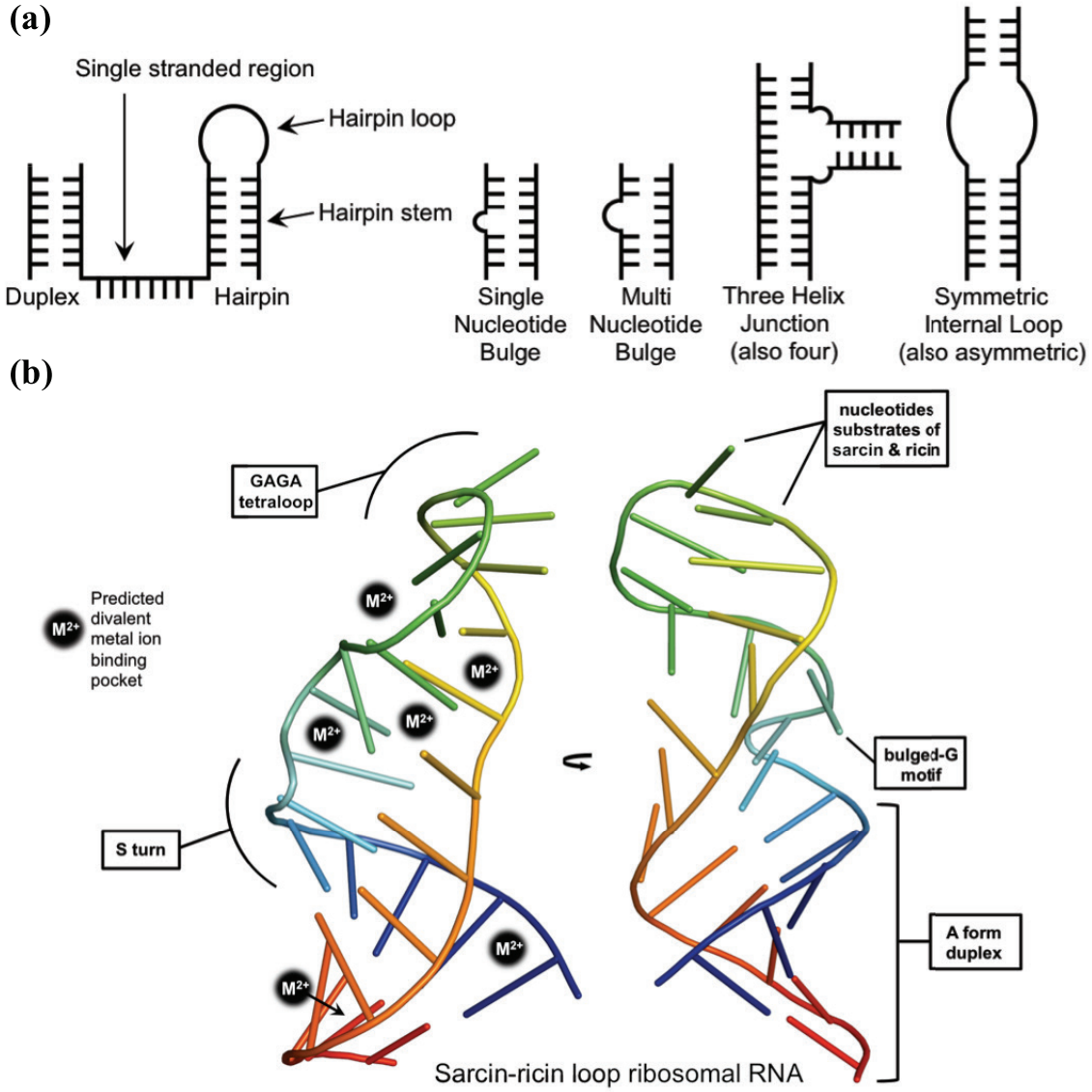

Figure 1.5. (a) Common secondary structures accessed by cellular RNA, including hairpins, single-stranded regions, single and multi-nucleotide bulges, three and four-helix junctions, and symmetric or asymmetric loops. **(b)** *S. cerevisiae* sarcin-ricin loop ribosomal RNA, a distorted hairpin with several RNA-specific structural motifs including a GAGA tetraloop, a bulged-G motif, and an S turn. These features facilitate recognition by a variety of protein co-factors, including the ribotoxins α-sarcin and ricin. Nucleotides predicted by molecular simulations to host cation binding pockets[37] are indicated by "M^{2+}".

Several labs showed a keen interest in characterizing platinum lesions within isolated transfer RNAs. Following incubation with activated cisplatin, Pt(II) adducts formed within the purine-rich acceptor stem and anticodon loop of purified $tRNA^{Phe}$ and $tRNA^{Ala}$.[44,45] However, these adducts were very dependent on sequence; conversion of a GU wobble pair to a canonical GC base pair in the tRNA stem precluded platinum

binding in that region. Cisplatin has also been used as a chemical probe for identifying solvent exposed purine nucleotides in intact bacterial ribosomes.[43] Stable platinum adducts formed within helix 24 of *E. coli* ribosomes were identified by primer extension as stop sites caused by platination. Using this method, it was found that G nucleotides in several non-Watson-Crick base-paired regions of the RNA were targeted by cisplatin. This targeting provides another example of platinum coordination within regions of complex RNA structure, notably even in the presence of competing GG sequences in duplex regions of the same RNA. Chapter IV describes additional instances of Pt(II) binding within the catalytic core of the *S. cerevisiae* ribosome, specifically throughout the sarcin-ricin loop. More recently, the processing, stability, and silencing capacity of cisplatin-modified siRNA and miRNA were investigated *in vitro*. Pt(II) lesions enhanced the stability of the biologically active antisense strand to nuclease degradation. However, metalation severely reduced the silencing capacity of these RNAs in a luciferase assay.[46] Interestingly, platination of the sense strand does not appear to adversely affect early siRNA processing.[47]

In our lab, Erich Chapman and Alethia Hostetter have characterized cisplatin binding within a 41nt RNA subdomain (the 'branch-bulge domain') of the U2-U6 snRNA complex, part of the catalytic core of the spliceosome. This BBD RNA consists of a hairpin structure in which base paired regions flank a purine-rich, asymmetric internal loop. Reaction of this RNA with an aquated form of cisplatin resulted in a novel GpG Pt-induced intramolecular crosslink, which was confirmed by alkali hydrolysis mapping.[48] While the structure of this RNA is currently unknown, the nucleotides involved in this crosslink have been proposed as metal ion binding sites in the full U2-U6 snRNA complex.[49,50] In light of this information, it is intriguing to speculate that cisplatin may compete with native metal ion binding sites in RNA. This type of mimicry would be particularly interesting as metal ions often mediate important tertiary contacts between interacting RNA domains[51] where crosslinking could potentially disrupt the dynamic function of these structures. Although many similar instances of RNA-Pt adduct formation have been reported, the link between specific Pt(II) lesions and downstream functional consequences is still unclear. In the next section, the broad impact of cisplatin on RNA-dependent cellular processes is described.

Influence of Pt on RNA-Based Processes

RNA-based processes in cells are influenced by treatment with Pt(II) compounds (**Figure 1.6**). Each of these processes depends heavily on complex RNA structures as well as on RNA-protein and protein-protein interactions. With the exception of carefully designed RNA polymerase experiments in which a single Pt(II) adduct is specifically placed within a DNA template,[52,53] the studies in **Figure 1.6** have been conducted in a heterogeneous environment where platination may interfere in many possible ways. Pt(II) adducts formed with RNA or DNA templates, RNA products, or ribonucleoprotein complexes all have the potential to disrupt these RNA-dependent processes.

Platinum interference has been implicated in almost every step of the RNA lifecycle, from transcription of pre-mRNA to translation of mature mRNAs into functional proteins. Cisplatin has been observed to preferentially block transcription of ribosomal RNA in HeLa cells and drug treatment results in a redistribution of the RNA

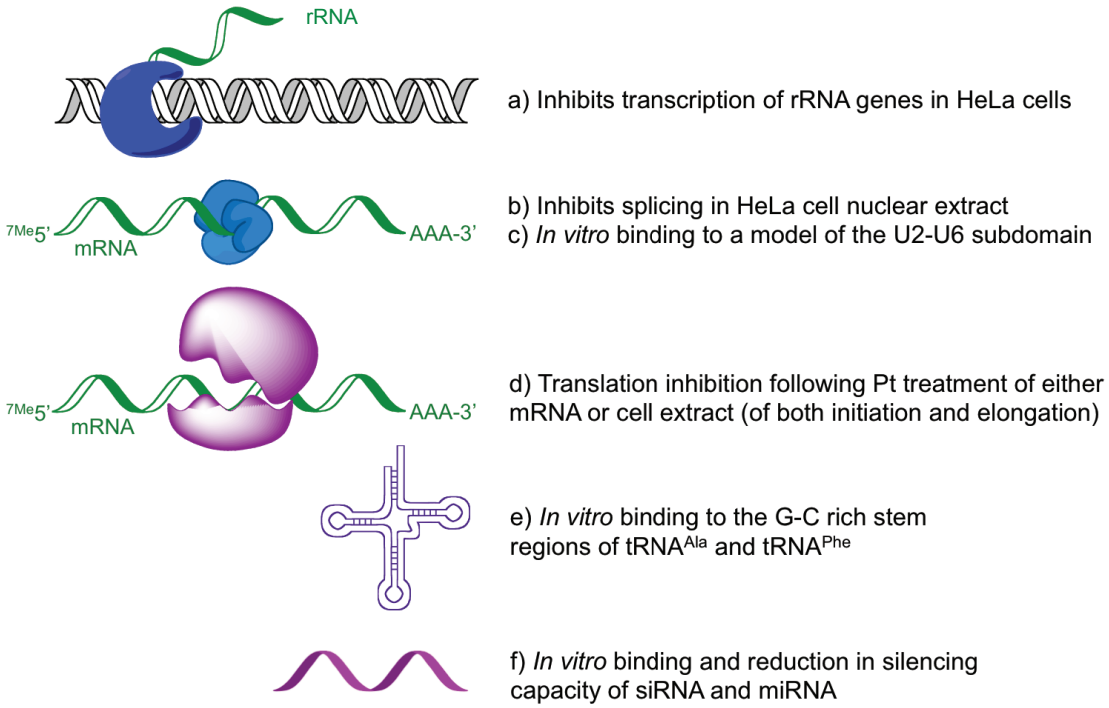

Figure 1.6. Incidences of stable RNA-Pt adducts and disruption of RNA-based cellular processes by cisplatin, including inhibition of the following processes: (a) nucleolar rRNA transcription, (b) pre-mRNA splicing, (c,-e) mRNA translation, following either mRNA or cell extract pre-treatment with Pt(II), (f) siRNA and miRNA silencing capacity in cell culture.

polymerase I transcription machinery.[53] In mammalian cells, arrest of RNA polymerase II at a platinum-DNA lesion has been demonstrated *in vitro*,[54] in cellular extracts,[52] and recently, *in vivo*.[55] The structural basis for this inhibition has also been reported, in which it was found that transcriptional inhibition was a result of the inability of the DNA lesion to enter the active site of the enzyme. Interestingly, this mechanism of polymerase stalling is unique from that of similar DNA lesions that occur upon UV irradiation.[56]

Splicing is a critical step in the RNA lifecycle and is responsible for the successful maturation of pre-mRNA transcripts. In HeLa cell nuclear extract, a dose-dependent inhibition of pre-mRNA splicing was observed after treatment with tetraplatin (tetrachloro[d,l-*trans*]1,2-diaminocyclohexane platinum(IV) and cisplatin. The inhibition of splicing observed in these experiments can be correlated to a disruption in formation of spliceosomal complexes on pre-mRNA.[57] An inhibition of splicing has also been observed following cisplatin treatment of the protein-independent self-splicing *Tetrahymena* rRNA, possibly through the formation of interstrand cisplatin-RNA crosslinks.[58]

Efficient translation is highly dependent on intact and functional RNA molecules such as ribosomes, messenger RNA, and tRNA. Platinum disruption of translation has been described to a great extent *in cellulo* in rabbit reticulocyte lysate. Early studies by Rosenberg and Sato demonstrated that Pt(II)-bound mRNA added to platinum-free cellular lysate inhibits protein synthesis by 85%, while Pt(II)-incubated lysate treated with platinum-free mRNA showed a 19% decrease in translation.[59] In a later study, it was found that the rate of translational inhibition by cisplatin matched that of NaF, an inhibitor of translational initiation. In addition, the polysome profiles of both cisplatin and NaF showed an apparent decrease in polysome intensity.[60] This was interpreted to mean that cisplatin disrupted translation by preventing initiation. Heminger and coworkers later revisited this study and noted a slightly different result, in which the steady accumulation of higher order polysomes was observed on mRNA templates following Pt(II) treatment.[61] They concluded that their data showed Pt(II) inhibition of elongation, not initiation. However, despite the appearance of higher-order polysomes, the apparent intensity of the polysome fractions decreases upon Pt(II) treatment in both studies in conjunction with an increase in the population of free ribosomes. Therefore, it

is likely that platinum interferes in both the initiation *and* the elongation of ribosomes *in cellulo* to cause an overall decrease in protein synthesis.

Recent work has documented specific platinum binding events within the translation machinery. As mentioned previously, stable cisplatin adducts have been mapped to various locations within *E. coli* and *S. cerevisiae* ribosomal RNA through primer extension of RNA extracted from treated cells.[2,43] The effects of platinum binding in these locations on overall protein synthesis have not been investigated.

Cellular Response to Damaged RNAs and Initiation of Stress Responses

There is a growing literature on the sophisticated mechanisms of RNA surveillance, repair and damage control.[62] Nonfunctional mRNA surveillance is reasonably well-studied, and can proceed via nonsense mediated decay, nonstop mediated decay, and no-go decay.[63] The TRAMP complex mediates errors in ribosome biogenesis by tagging nonfunctional and defective rRNAs for exonucleolytic degradation.[64] Other defined RNA degradation pathways include noncoding RNA decay[62], nonfunctional ribosome decay[65], and rapid tRNA decay[66].

In some cases, damaged RNA molecules can be repaired. Instances of RNA repair appear to be best understood within the context of a viral or bacteriophage response to host immune cleavage of transfer RNA, an innate mechanism to prevent the spread of infection. Cellular stresses such as amino acid deprivation can also trigger transfer RNA cleavage within the anticodon loop. Following 3' and 5' end-remodeling by RNA editing enzymes, tRNA ligases recognize and re-anneal the cleaved ends (typically 3'-OH and 5'-PO_4).[67,68] RNA repair is also described for the 3' ends of positive-strand viral RNAs subjected to exonucleolytic cleavage by host RNases.[69] There is only one known class of enzymes, the AlkB family, capable of repairing base alkylation by small molecules. Methyl methanesulfonate-induced lesions on mRNA and tRNA, specifically 1-methyladenine and 3-methylcytosine, inhibit translation *in vitro* but can be rescued by treatment with human AlkB.[70] During methyl methanesulfonate treatment in AlkB-deficient *E. coli,* 10-fold more lesions were repaired in RNA than DNA. This activity was predominant in RNAs less than 200 nt (mainly tRNAs).[71]

Recently, researchers have illuminated a link between specific incidences of cellular RNA damage and the induction of apoptosis *in vivo*. Aberrant RNA cleavage events that cause disruption of RNA-protein interactions have been linked to early disease progression and programmed cell death, suggesting the potential for a global cellular response to small RNA structural modifications.[72–74] Onconase, a cytotoxic ribonuclease, initiates apoptosis through tRNA cleavage and is currently being harnessed for chemotherapeutic purposes.[75] The specific mechanistic pathway for this activity is not known, but it is speculated that onconase-mediated tRNA cleavage directly activates cytochrome c, an effector of apoptotic signaling. Ribotoxic damage to the sarcin-ricin ribosomal RNA loop (**Figure 1.5b**) by ricin and α-sarcin results in the rapid onset of an apoptotic signal. Ricin depurinates the adenine at position 2660 and α-sarcin irreversibly hydrolyzes the bond between the two adjacent purines at the terminal helix loop. These modifications cause structural distortions that prevent recognition by the elongation factor eEF2. Inhibition of eEF2 binding inhibits protein synthesis and initiates an apoptotic signal.[34] The mechanism by which rRNA damage is sensed is not fully understood, but it is clear that the structural integrity of this loop is essential for translation and cell viability. In Chapters II and IV, I describe Pt(II) lesions within ribosomal RNA, specifically within the sarcin-ricin loop itself, which may be sufficient to initiate apoptotic signaling.

Summary of Chapter I and Bridge to Chapter II

In this chapter, I have described the history of platinum anticancer therapeutics and the current body of knowledge regarding the cellular uptake, activation, distribution, and processing of cisplatin. I have summarized the predominant view of the importance of nuclear DNA targeting by this complex and provided strong evidence for RNA as a potent alternative Pt(II) target. In Chapter II, entitled "RNA-Pt (II) Adducts Following Cisplatin Treatment of *Saccharomyces Cerevisiae*", we perform a thorough assessment of RNA-Pt species *in vivo*. The impact of cisplatin in *S. cerevisiae* is measured using growth curves, clonogenic assays, and tests for apoptotic markers. Pt(II) lesions are quantified and characterized in DNA and RNA using ICP-MS, and cisplatin adduct formation within ribosomal RNA is mapped to nucleotide resolution.

CHAPTER II

RNA-PT(II) ADDUCTS FOLLOWING CISPLATIN TREATMENT OF *SACCHAROMYCES CEREVISIAE*

This chapter contains important contributions from Alethia A. Hostetter and Dr. Victoria J. DeRose. A.A.H. performed the ICP-MS experiments, the growth and clonogenic assays, the DAPI and TUNEL staining. I performed the rRNA mapping experiments. A.A.H. and I co-wrote the manuscript. V.J.D. guided the project and provided significant editorial feedback. This chapter includes work published in *ACS Chemical Biology* (**2012,** *7*, 218-25, © 2013 American Chemical Society).

RNA as a Drug Target

As a modulator of gene expression at multiple levels, RNA is an important potential drug target (*1–5*). In addition to the well-defined functions of mRNA, tRNA, and rRNA, novel regulatory roles are continuously being defined in both transcription and translation (*1, 6*). Such findings include the discovery of siRNA, microRNA, piwi-interacting RNA, and long noncoding RNAs. Moreover, RNA damage and RNA-protein interactions have been linked to early events in disease and to programmed cell death (*7-10*). RNA targeting by small molecule interactions has the potential to influence these cellular pathways through both specific and nonspecific mechanisms.

While drug-RNA interactions have the potential to impact cell fate by disrupting RNA regulatory pathways, a challenging aspect for this field is assessing RNA-drug interactions and RNA accessibility *in vivo*. For this purpose, a covalent RNA-drug adduct is of value in quantifying target binding and following the fate of the targeted RNA. The inertness of metal-RNA adducts formed following treatment with Pt(II) anticancer drugs provides one method of monitoring small-molecule distribution on cellular RNA. Cisplatin (*cis*-diamminedichloridoplatinum(II)) is a potent antitumor agent that has had a particularly major clinical impact on the treatment of testicular and ovarian cancers. Currently, cisplatin and the structurally related carboplatin and oxaliplatin are used in the treatment regimes of 50-70% of cancer patients (*11*). *In vivo*, cisplatin-derived Pt(II)

species form kinetically inert 'covalent' adducts with biomolecule targets (*12, 13*). Drug binding to adjacent purines on genomic DNA has been linked to cell cycle arrest at the G2 phase and the induction of programmed cell death, one foundation of antitumor activity (*14*). Non-genomic contributions to cisplatin's therapeutic action are also under active investigation. In particular, cisplatin treatment can disrupt RNA-based processes such as splicing and translation (*15-17*). Targeting of non-DNA species, including RNA, by cisplatin may contribute to or sensitize a cell to the downstream effects of this drug, including the induction of apoptosis.

The distribution of Pt in different RNA species has not been previously determined *in cellulo* in eukaryotes. Here, we use *Saccharomyces cerevisiae* for *in cellulo* analysis of Pt adduct formation on mRNA, rRNA, and total RNA and DNA. *S. cerevisiae* was selected as a model and has been used previously for drug studies due to the high level of conservation between mammalian and yeast cellular processes, including components of cell-cycle regulation and mRNA turnover (*18,19*). We report the action of cisplatin on *S. cerevisiae* in minimal media based on growth curves, clonogenic assays, and tests for apoptotic markers. Despite high cytotoxicity, under the conditions studied cisplatin does not induce apoptosis. Estimated in-cell Pt concentrations and platinum accumulation on mRNA, rRNA, total RNA, and DNA were determined using inductively coupled plasma mass spectrometry (ICP-MS). Interestingly, while similar Pt accumulation was observed on rRNA and total RNA, significantly less accumulated on mRNA. Mapping by reverse transcription demonstrated specific Pt adduct formation on rRNA sequences conserved between yeast and humans. Taken together, these data highlight important differences in the relative accumulation of Pt on different RNA species and provide insight into the accessibility of cellular RNA to small, cationic molecules.

Cisplatin Treatment Causes Acute Cell Death

S. cerevisiae has been used previously to investigate cisplatin toxicity, including drug transport, DNA repair, and the genes involved in drug resistance and sensitivity (*20-22*). Within these reports, however, the sensitivity of *S. cerevisiae* to cisplatin treatment varies widely. In addition, although cisplatin causes apoptosis in mammalian systems (*23*), this

topic had not been addressed for *S. cerevisiae* despite a growing body of work on yeast apoptotic-like cell death pathways (*24,25*). Therefore, we established cisplatin cytotoxicity in *S. cerevisiae* (strain BY4741) by growth and survival curves as well as with apoptotic markers .

Cisplatin is activated by hydrolysis of the labile chlorido ligands, which in patients occurs upon exposure to relatively low intracellular [Cl^-] (*26*). For cultured cells, however, significant cisplatin aquation may take place in the media. In rich media such as YEPD (yeast extract peptone dextrose), the highly reactive aquation products may interact with soft sulfur- and nitrogen-containing nucleophiles to effectively sequester the drug, which could be one reason for higher IC_{50} measurements than those observed in mammalian and cancer cell lines (e.g. 500 µM in *S. cerevisiae* in YEPD media (*27*)

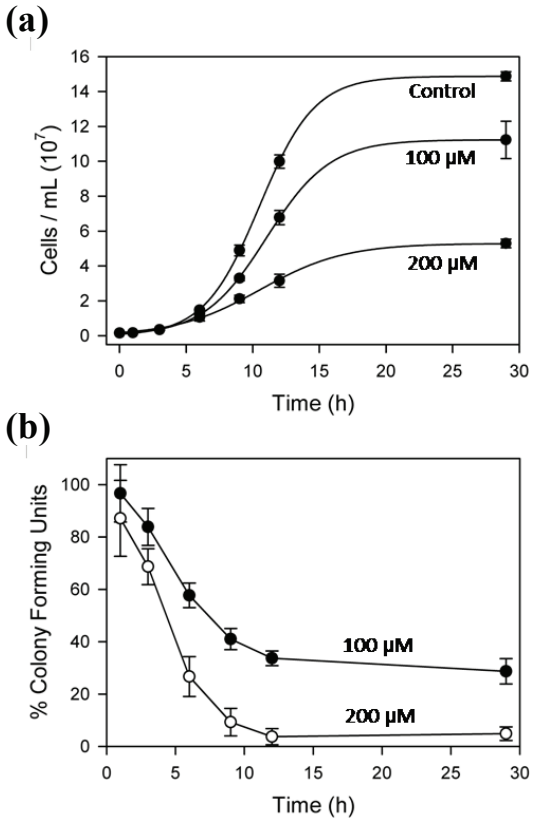

Figure 2.1. Cisplatin inhibits yeast growth and viability. (a) Exponential growth curves of BY4741 *S. cerevisiae* continuously treated with 0, 100, and 200 µM cisplatin in SD media. (b) Viability of cisplatin-treated yeast plated onto drug-free media,. Results presented as the means ± standard deviation from four (a) and three (b) independent experiments.

versus 2–40 μM for human cancer cell lines (*28-30*)). In **Figure 2.1**, we assayed drug toxicity in minimal SD (synthetic dextrose) liquid media (**Figure 2.1a**), and found a moderate (76 ± 8%) and severe (36 ± 1%) reduction in culture density at saturation for 100 and 200 μM drug, respectively. The effect of cisplatin on the viability of BY4741 cells, monitored by clonogenic assay (**Figure 2.1b**), shows a marked decrease in the number of dividing cells that begins after just 1–2 h incubation in the drug. The majority of irreversible cisplatin toxicity coincides with the onset of exponential growth that is observed in **Figure 2.1a**. We therefore chose 6 h (**Table 2.1**) as a relevant timepoint to investigate the distribution of cisplatin-derived Pt species on different RNAs within the cell.

Table 2.1. Cisplatin influence on *S. cerevisiae*

	[Cisplatin]	
	100 μM	**200 μM**
Culture Density[a]	87 ± 6%	71 ± 12%
Cell Viability[a]	58 ± 5%	27 ± 8%

[a]Measured at 6 h relative to control.

Cell Death Is Not Apoptotic

Cell death via apoptotic pathways has been reported for *S. cerevisiae* treated with several agents including anticancer drugs such as bleomycin and valproate, but has not been reported for metallodrugs such as cisplatin (*24,25*). We assayed cell cultures for hallmarks of apoptosis after continuous treatment with cisplatin for 6–12 h. Similar to mammalian systems, yeast apoptosis results in chromatin condensation and DNA fragmentation (*31*). DAPI DNA staining of BY4741 cells in 200 μM cisplatin at 6 h treatment showed significant differences from the control in chromatin morphology (**Figure 2.2a**). In almost all samples, nuclei were either fragmented and diffuse, or abnormally enlarged. These findings are consistent with an activation of apoptosis or an alternative programmed death pathway. Cell cycle arrest, previously reported in cisplatin-treated yeast and mammalian cultures (*32, 33*) was observed with an increase in both parent cell and bud size. Such examples of oncosis are generally associated with necrotic

cell death (*34*), with some exceptions (*35*), and contrast with the reductions in cell sizes generally observed from slow cell division due to metabolic factors (*36*).

Apoptosis was further assayed through terminal dUTP nick-end labeling (TUNEL) (*31*), to detect cleaved DNA. Despite disruptions in cell and chromatin morphology, cells were TUNEL-negative following treatment with 200 μM cisplatin for both 6 h (**Figure 2.2b**) and 12 h (data not shown). This suggests that under these conditions, cisplatin treatment disrupts normal chromatin segregation but is insufficient to initiate an apoptotic signal culminating in double-stranded DNA breaks.

The majority of yeast apoptosis pathways are mediated by YCA1, a type 1 metacaspase, or by AIF1, a homolog of mammalian apoptosis-inducing factor (*24, 31*). To determine if cisplatin-induced toxicity involves either of these pathways, we assessed cell viability in *YCA1* and *AIF1* deletion mutants treated with 200 μM cisplatin for 6 h. For both Δ*YCA1* and Δ*AIF1*, no differences in cell viability were observed, indicating that neither protein is mediating cytotoxicity in yeast (**Figure 2.2c**). In summary, cisplatin-treated *S. cerevisiae* are undergoing a non-apoptotic form of cell death, but whether it is uncontrolled necrosis, a programmed necrosis, or alternate form of cell death cannot be determined by the present data (*35*).

Other antitumor agents including the DNA fragmenting bleomycin and the microtubule directed paclitaxel, as well as the ribosome targeting toxin ricin, appear to induce apoptotic markers in yeast (*25, 37*). From several reports, a stimulus can induce yeast apoptosis at low doses and necrosis at high doses (*36,38*). It is therefore plausible that cisplatin induces yeast apoptosis in a different treatment window than used here. It is also possible that, unlike the case for other toxins, yeast lacks a key component of a pathway through which cisplatin treatment triggers apoptosis. One candidate is the tumor suppressor p53, which has no yeast homologue (*21*). Significantly, mismatch repair pathways have been linked to p53-driven apoptosis in mammalian cell lines, while deletion of parallel MMR components in yeast does not influence cisplatin sensitivity (*39*). In mice, it has been demonstrated that cell cycle arrest occurs in a p53-independent manner, despite its requirement for the initiation of apoptosis (*40*). Thus, p53-independent cisplatin-induced cell toxicity pathways appear to be present that in yeast result in acute cell cycle arrest and disrupt chromatin morphologies, but not the hallmark

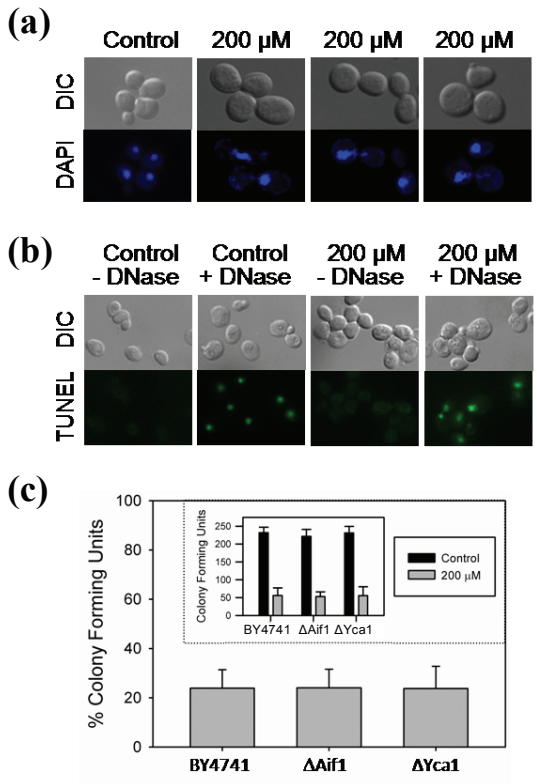

Figure 2.2. Tests for apoptotic markers. (a) DAPI staining of yeast treated with 0 and 200 µM cisplatin for 6 h. (b) TUNEL assay of yeast treated with 0 and 200 µM cisplatin for 6 h, +/- 5 U DNase I. (c) Viability of BY4741, ΔAif1 and ΔYca1 treated with 200 µM cisplatin for 6 h, Inset: average cfu for control and cisplatin-treated cultures. Results presented as means ± standard deviation from three independent experiments.

DNA cleavage events associated with apoptosis. Similar phenotypes have been observed in *S. cerevisiae* following treatment with tunicamycin, an X-type agent that also causes cell-cycle arrest and the unfolded protein response, but death by non-apoptotic methods (*41*).

Intracellular Pt Concentrations

The concentration of Pt species inside a cell following cisplatin treatment is affected by a complex set of dynamics including passive diffusion, active transport, and active efflux from the cell (*21,26*). To assess intracellular Pt levels, the accumulation of Pt in whole yeast cells was measured by ICP-MS (**Figure A.1, Appendix A**). Values of $5.0 \pm 0.6 \times 10^6$ and $2.1 \pm 0.1 \times 10^7$ Pt/cell for 100 µM and 200 µM cisplatin treatment after 12 h reflect previous results of $7\text{-}30 \times 10^6$ Pt/cell for yeast incubated with 130 µM

cisplatin for 18 h (*42,43*) and are in line with values for cisplatin-treated HeLa cells when differences in cell volume are taken into account (*30,44*).

The increased volumes of cisplatin-treated yeast cells were estimated for calculating intracellular Pt concentrations (Methods). An average volume of (~40 fL) is calculated for untreated yeast, consistent with previous measurements (*34,45*). The average size of 200 μM cisplatin-treated yeast continuously increases, while that of 100 μM cisplatin-treated yeast is consistent after 6 h, potentially reflecting differences in cell viability between these two treatment conditions at extended time points (**Figure 2.3a**). The resulting calculated in-cell Pt concentrations (**Figure 2.3b**) are 47 ± 10 and 84 ± 5 μM measured at 6 h for 100 and 200 μM cisplatin, respectively. At 12 h the in-cell Pt concentration exceeds the concentration of cisplatin in the media. This effect, observed

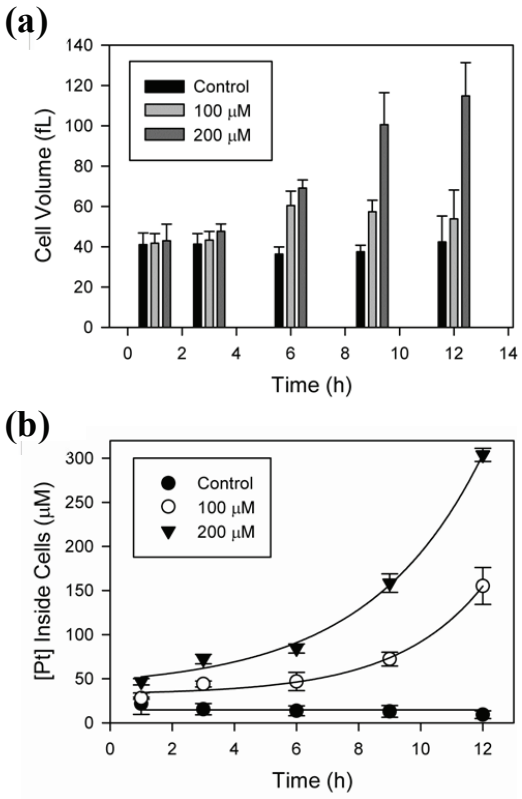

Figure 2.3. Estimated cell volumes and in-cell Pt concentrations. (a) Average estimated cell volumes following treatment with 100 μM and 200 μM cisplatin (see Methods). (b) Calculated in-cell Pt concentrations based on Pt/cell ICP-MS measurements and the average estimated cell volumes. Results averaged from at least three independent experiments presented as means ± standard deviation.

previously for other anticancer metallodrugs (*46*), is consistent with both an active transport process (*47*) and the fact that these drugs produce kinetically inert adducts with cellular targets, placing drug binding under kinetic rather than thermodynamic control (*48*).

Pt Accumulation in Different Nucleic Acids

To lend insight into the exposure of cellular RNAs to intracellular Pt species, Pt adduct formation on total RNA extracted from cisplatin-treated yeast was quantified with ICP-MS. An exponential increase in Pt-RNA content was observed in parallel with the exponential increase in cellular Pt concentrations (**Figure 2.4a**), indicating that accumulation of Pt in RNA is proportional to whole-cell Pt accumulation. At 6 h, Pt accumulation corresponds to one Pt every 14,600 ± 1,500 and 5760 ± 580 nt for 100 and 200 μM cisplatin, respectively. For perspective, the yeast ribosome is roughly 5600 nt (*49*).

A comparison of Pt accumulation on whole-cell RNA and DNA, performed following 12 h treatment with cisplatin (**Materials and Methods, Appendix A**), yields ~ 3-fold more Pt bound to DNA than RNA on a per nucleotide basis (**Figure 2.4b**). Cellular distribution studies performed in human cell lines have observed an accumulation of cisplatin-derived Pt in the nucleus and nucleolus (*50*), consistent with the higher density of Pt on DNA. However, there is 10–50 fold more RNA in a yeast cell than DNA (*51,52*), resulting in ~4–20 fold more Pt accumulation in the total cellular RNA than in the total cellular DNA (**Table 2.2**).

Pt accumulation on poly(A)-mRNA and rRNA was compared in total cellular RNA harvested from yeast after 6 h of continuous cisplatin treatment. Poly(A)-messenger RNA was extracted with an mRNA Miniprep Kit while intact 25S and 18S rRNA were isolated by gel purification (**Materials and Methods, Appendix A**). Pt accumulation on rRNA is similar to that of total RNA on a per nucleotide basis, while significantly less accumulation per nucleotide is observed on poly(A)-mRNA (**Figure 2.4c and Table A.1, Appendix A**). Given that yeast RNA is 80% ribosomes, 15% tRNA, and 5% mRNA (*51*), it appears that Pt measured in total RNA is largely due to accumulation on ribosomal RNA. Assuming a statistical distribution of Pt adducts, these data indicate an average of 1

and 2 Pt adduct for every 3 ribosomes following 6 h treatments with 100 and 200 μM cisplatin, respectively.

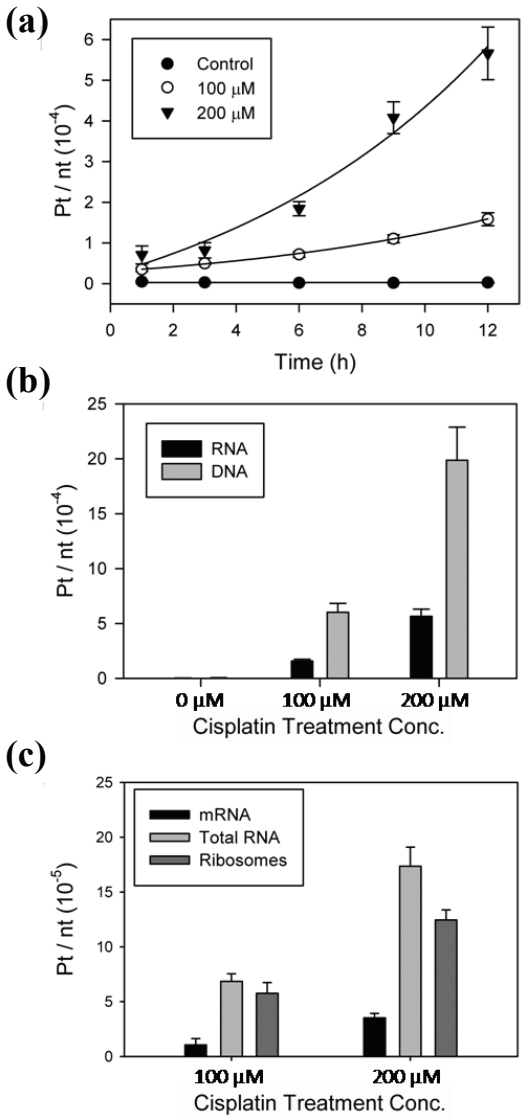

Figure 2.4. Pt accumulation per nucleotide in total RNA, DNA, rRNA, and mRNA. (a) Total RNA from yeast treated with cisplatin. (b) Total RNA and genomic DNA at 12 h treatment. (c) mRNA, total RNA, and rRNA at 6 h. Data values provided in Supplementary Table S1, and presented as means ± standard deviation for at least three independent experiments.

In yeast, global protein synthesis is dramatically reduced as early as 2-4 hr post-cisplatin treatment, indicating a compromised translation machine, which may be a result of mRNA, tRNA, or rRNA modifications (*27*). In general, cationic aquated Pt species are expected to associate more readily with accessible sites in higher-order RNA structures,

which present a larger electrostatic driving force (*50*). The enrichment of Pt on rRNA relative to poly(A)-mRNA (**Figure 2.4c**) may be due to the high negative charge density of the ribosome and may present a contributing factor to cisplatin's cytotoxicity, although the probability of Pt adducts associating with higher-order regulatory structures amidst otherwise single-stranded regions of cellular mRNAs is yet unknown. Additional factors that remain to be determined include the influence of Pt-RNA adducts on mRNA surveillance pathways and message turnover (*53*).

Table 2.2. Estimated Pt atoms accumulated in the total RNA or DNA of one yeast cell[a]

	[Cisplatin]	
	100 μM	**200 μM**
DNA (10^4)	2	6
RNA (10^4)	7–34	24–120

[a]Calculation based on the mass of DNA and RNA in one haploid *S. cerevisiae* cell (*60*)

Platinum Adduct Identification on rRNA

Specific locations of platinum adducts within *S. cerevisiae* ribosomal RNA were probed by RT primer extension, which stalls 3' to adduct sites (*54-56*). Pt adducts may reflect the solvent accessibility and electrostatic potential of specific rRNA motifs. Using similar methods to probe for potential antibiotic sites, Rijal and Chow reported major platination sites within helix 24 of the *E. coli* small ribosomal subunit (*56*), revealing a significant RT stall at U801 that reflects Pt binding to adjacent guanines at positions 799 and 800 (**Figure 2.5**). Secondary binding was observed at A792, suggesting the formation of a 3'-GA-5' adduct between G791 and A790. As an ideal antibiotic drug differentially targets bacterial and eukaryotic ribosomes, we compared platinum adducts in this region (helix 18 in *S. cerevisiae*), which is located in close proximity to the peptidyltransferase center (**Figure A.2, Appendix A**) and fully conserved between yeast and humans but not *E.* coli (**Figure 2.5**).

Primer extension was performed on total RNA extracted from yeast cultures treated with 0–150 μM cisplatin for 6 h. **Figure 2.5** shows a dosage-dependant increase

in termination intensity at several positions, predicting sites of platinum binding. Significant platinum adduct formation occurs at the purine-rich capping loop of helix 18, as evidenced by two major stops in the sequencing gel at positions A792 (***) and A790 (***) (**Figure 2.5**). Minor stalling is observed at A802 and G786. An additional minor stop site occurs directly on purine residue G797. This particular guanine lies 3' to a 2'O-methylated cytosine residue, which is known to pause primer extension under certain conditions (*62*). Alternatively, stalling at this site may be the result of an interstrand crosslink between G797 and G786, whose N7 atoms are stacked favorably for such an interaction (**Figure 2.5**).

Certain RNA sites are expected to be more accessible and/or reactive. To detect early Pt accumulation on rRNA, helix 18 was probed after exposure to 100 µM cisplatin for 0, 1 and 3 h (**Figure A.3, Appendix A**). As expected, platinum targets the same

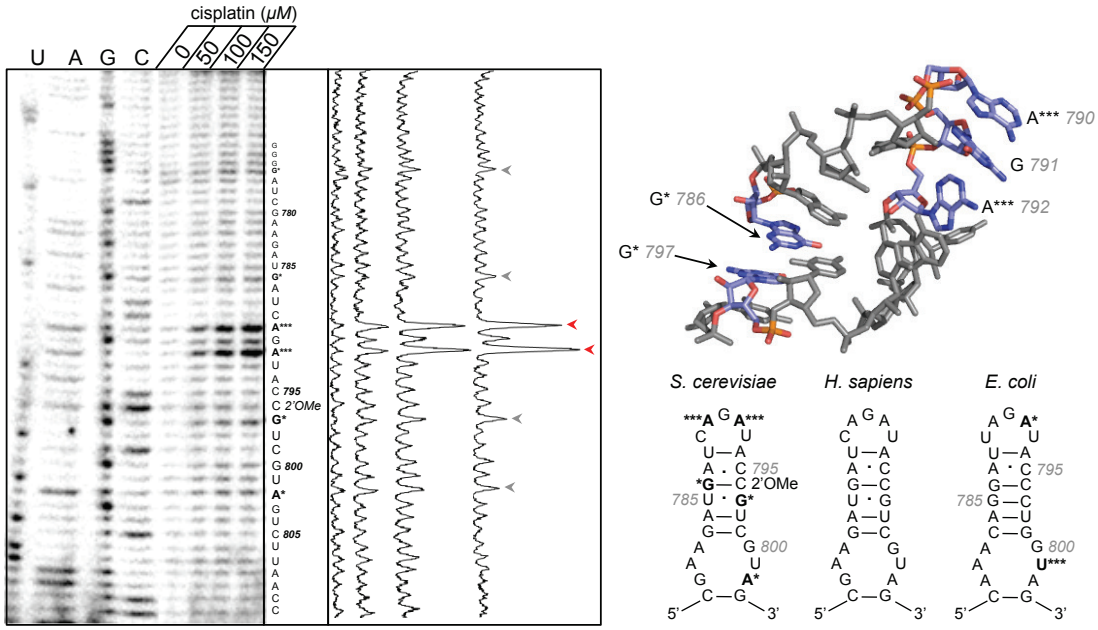

Figure 2.5. Primer extension analysis of *S. cerevisiae* small ribosomal subunit helix 18. Primer extension analysis of RNA isolated from 6 h cisplatin-treated BY4741 (left) shows a dosage-dependant increase in termination intensity at the starred sites, indicating major (***) and minor (*) Pt binding sites. Dideoxy sequencing ladders denoted by U, A, G, and C. Experimental results are summarized on secondary structure of the *S. cerevisiae* helix 18 (right, lower panel). Results from Rijal and Chow (*56*) are summarized on the *E. coli* secondary structure (right, lower panel). *E. coli* numbering used for comparison. Major platinum binding sites and a potential crosslink between G797 and G786 are depicted on a helix 18 crystal structure (right, upper panel, PDB 3O30).

purine residues as observed following 6 h treatment (**Figure 2.5**), showing transcription stops at positions A790 and A792 within the capping loop as early as 1 h post exposure to drug (**Figure A.3, Appendix A**). Stalling at A802 appears stronger at early timepoints, although its signal is minor in comparison to banding patterns observed within the terminal loop (A792 and A790) after 6 h cisplatin treatment. Importantly, at all timepoints, the reversal of the G783-C799 basepair in yeast and humans, which removes the preferred G799-G800 Pt binding site observed in *E.* coli, is sufficient to preclude Pt binding to G800 in yeast. Instead, binding within the stem is diverted to residue A802. These findings demonstrate that although aquated cisplatin products are highly reactive, they are remarkably sequence-specific in the context of complex RNA structures.

Conclusions

In this study, the ability of the anticancer drug cisplatin to form stable adducts with RNA was used to assess accumulation of Pt species on cellular RNA following drug treatment. Under the conditions of this study cisplatin toxicity was characterized by irreversible inhibition of cell division, but not apoptotic cell death. This suggests that in comparison with mammalian systems, a mediator of cisplatin-induced apoptotic pathways, such as p53, is lacking in *S. cerevisiae*. Comparison of Pt accumulation in RNA and DNA at 12 h shows ~4–20 fold more Pt accumulation in the total cellular RNA than in genomic DNA. Intact 25S and 18S ribosomal RNA accumulates the majority of cellular Pt, while significantly less accumulates on poly(A)-mRNA when compared on a per-nucleotide basis. Mapping by reverse transcription demonstrates that specific Pt adducts in eukaryotic ribosomes form in a dose- and time-dependent fashion, accumulating after just 1 h of treatment. Taken together, these data show significant accumulation of Pt adducts in eukaryotic RNA following treatment *in cellulo* with cisplatin, with significantly larger amounts of irreversible Pt-RNA adducts accumulating in ribosomal RNA as compared to mRNA, and a demonstrated specificity for particular binding sites in the eukaryotic ribosome. The results from these data emphasize potential for rapid and specific accumulation of small molecules on cellular RNA. The potential of such interactions to impact complex RNA regulatory pathways is of great interest.

Bridge to Chapter III

In Chapter II, we assessed the impact of cisplatin treatment on *S. cerevisiae* and quantified accumulation of Pt(II) on nucleic acids following drug treatment, discovering that 4-20 fold more Pt(II) accumulates on cellular RNA than DNA and identifying the ribosome as a cellular Pt sponge. In Chapter III, we describe a new click-chemistry based methodology for high-throughput analysis of Pt-bound species *in cellulo*.

CHAPTER III

PICAZOPLATIN, AN AZIDE-CONTAINING PLATINUM (II) DERIVATIVE FOR TARGET ANALYSIS BY CLICK CHEMISTRY

This chapter contains contributions from Jonathan D. White, Alan D. Moghaddam, Lindsay E. Guzman, Dr. Victoria J. DeRose, and Dr. Michael M. Haley. V.J.D. and M.M.H. initiated the development of click-enabled Pt(II) compounds for this research. J.D.W., with direction from V.J.D. and M.M.H and assistance from L.E.G., was responsible for the synthesis and characterization of novel azide-modified Pt(II) reagents and corresponding alkyne-containing fluorophores. A.D.M. contributed to the *in vitro* DNA-Pt(II) studies. I also performed *in vitro* DNA-Pt(II) studies, including the gel analysis of Cu-mediated degradation and MALDI-MS, and was wholly responsible for the RNA-Pt(II) work, both *in vitro* and *in vivo*. The manuscript was co-authored by J.D.W., A.D.M., V.J.D., M.M.H., and myself. This chapter includes work published in the *Journal of the American Chemical Society* (**2013,** *135*, 11680-3, © 2013 American Chemical Society).

Picazoplatin, a Novel Azide-Modified Pt(II) Reagent

Platinum (II) compounds comprise up to 50-70% of anticancer treatment regimes in use today.[1] Unlike other classes of common therapeutics such as antibiotics, however, a molecular-level understanding of the specific targets of Pt(II) drugs is lacking.[2] Pt(II) drugs preferentially target purine nucleobases, and drug binding to genomic DNA is an accepted cause of downstream apoptotic signaling.[3] Less than 10% of Pt (in the case of cisplatin) accumulates within genomic DNA,[4] and questions remain regarding additional targets that could impact cytotoxicity and resistance. A facile and sensitive method for drug target analysis would greatly aid such investigations.

One synthetic-based strategy for target identification involves modifying Pt(II) complexes to contain sterically small bioorthogonally reactive handles. Chemical trans-formations at this handle (such as reaction with a fluorophore) following drug treatment would allow for accurate Pt localization in vivo or subsequent purification of cellular

targets.[2c] Post-treatment labeling circumvents problems associated with using compounds modified with bulky or charged fluorophores, which may not accurately represent cellular processing of the native drug.[2d] An ideal candidate for post-treatment labeling is the azide-alkyne dipolar cycloaddition, the prototypical click reaction.[5] Click chemistry has been broadly used for localization and functional studies of modified biomolecules, including proteins and nucleic acids.[6,7] Despite the importance of Pt(II) compounds in therapeutics and catalysis, applications of click reactions on Pt(II) complexes have been limited.[8] Click reactions have been used as a synthetic route to generate libraries of Pt-based therapeutics[8d-f] and for fluorescent post-labeling of a monofunctional Pt(II)-acridine derivative.[9] Our goal is to modify small bifunctional Pt(II) reagents such as cisplatin and related compounds (**Figure 3.1**) for post-treatment analysis.

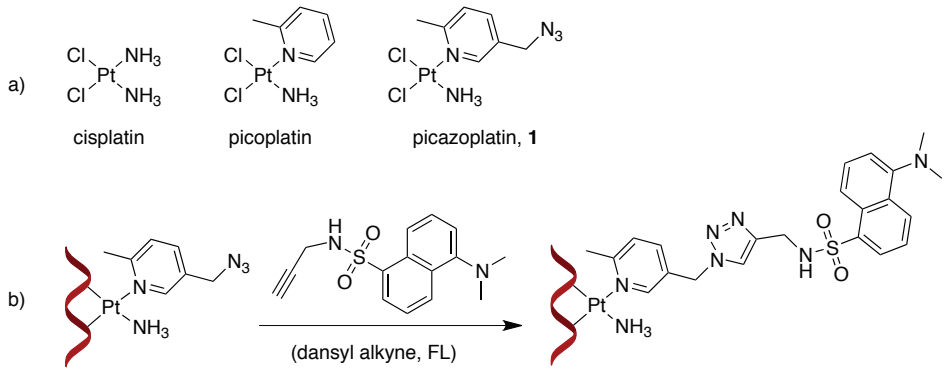

Figure 3.1. (a) The anticancer drugs cisplatin and picoplatin, with the novel picoplatin analogue 1, picazoplatin. (b) Reaction scheme of biomolecule-bound picazoplatin clicking to a dansyl fluorophore.

Here, we report the synthesis of the novel azide-functionalized Pt(II) complex 1 and present DNA oligonucleotide binding and subsequent click reactivity with alkyne-modified fluorophores (**Figures 3.2 and 3.3**). We extend these studies to show in vitro labeling of a structured RNA oligonucleotide (**Figure 3.4**) and in vivo treatment and post-labeling of yeast ribosomal RNA (**Figure 3.5**). This tandem Pt binding and post-modification technique enables visualization and quantification of the cellular targets of Pt(II) compounds, and may be broadly applicable towards identification of other metal-ion based drug targets.

We designed complex 1 with the azide-functionalized 2-picoline ligand, similar to the well-known complex picoplatin (**Figure 3.1a**).[10] Since Pt(II) is capable of catalyzing hydroamination and other undesirable side reactions with alkynes,[11] the azide-functionalized complex remained the initial focus of this work. In addition, organoazide complexes of Pt, where the azide moieties are connected through organic linkers and not directly bound to the Pt center, are known compounds.[12] Furthermore, an azide-Pt(II) click reagent allows for the future use of nonlinear, ring-strained alkynes and thus copper-free click chemistry.[13] The steric hindrance provided by the 2-methyl group of picoplatin and its derivatives slows the kinetics of substitution reactions on Pt and is an important effector of therapeutic activity.[10,14] The presence of the 2-methyl substituent also prevents the formation of dipicoline adducts and generally yields cleaner syntheses compared to other asymmetrically substituted cisplatin derivatives.[15] Complex 1 was synthesized and fully characterized by ^{1}H and ^{195}Pt NMR, IR, and HRMS (**Materials and Methods, Figures B.1-B.6, Appendix B**).

Picazoplatin-DNA Interactions *In Vitro*

Cisplatin, picoplatin, and similar Pt compounds bind readily to 5'-GG-3'-containing short DNA oligonucleotides and hairpin structures.[3a,c,16] Binding of 1 to double-stranded DNA and click labeling were analyzed by dPAGE (**Figure 3.2**). Resolution between the denatured strands is clearly observed, and reaction with two-fold excess 1 (4 h, 37 °C) results in a new band corresponding to Pt-bound T_6GGT_5 (**Figure 3.1b, left and center lanes**) in yields similar to those observed with the parent compound picoplatin (not shown). Reaction of the Pt-bound oligonucleotide with an alkyne fluorophore (dansyl propargylamine)[17] in the presence of CuI (4 h, 50 °C) results in fluorescent labeling of the Pt-bound species (**Figure 3.2b, right lane**). Observation of the expected click product with a single-stranded T_6GGT_5 construct was confirmed by MALDI mass spectrometry (**Figure 3.2c**).[18] The observed Pt-bound species (**Figure 3.2c, black**) shifts to a higher m/z as predicted from cycloaddition of the dansyl fluorophore (**Figure 3.2c, blue**). The click reaction efficiency appears to be high, as the Pt-bound peak disappears completely in the clicked (blue) spectrum.

Additional work examining nonspecific interactions between the dansyl alkyne fluorophore and the terminal azide of the Pt-bound DNA scaffold was performed with a pyrimidine rich DNA hairpin (**Figure 3.3a**).[16] This sequence was selected to minimize potential Pt interstrand crosslink formation between hairpins (as was occasionally observed for single-stranded T_6GGT_5, data not shown). A Pt-bound species is not

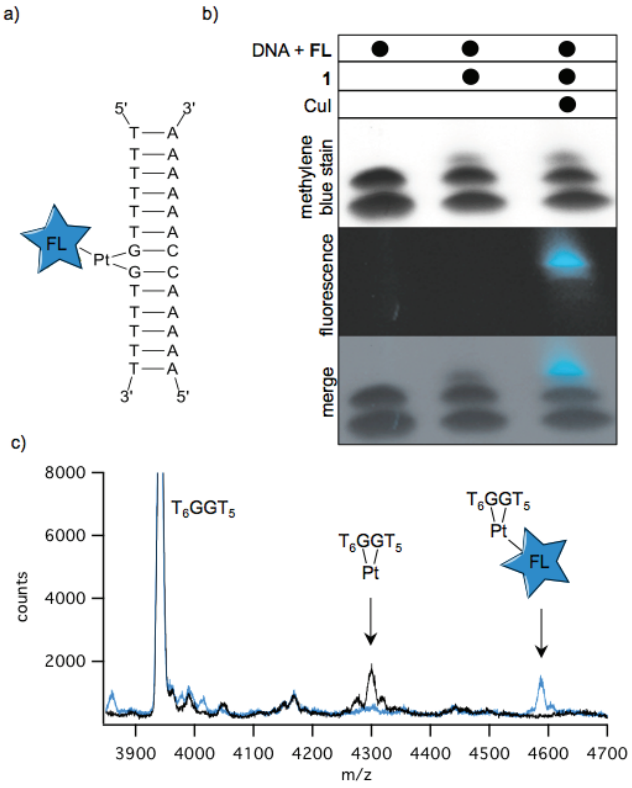

Figure 3.2. (a) DNA duplex with picazoplatin (**1**) bound and labeled with dansyl alkyne fluorophore. (b) dPAGE analysis showing the denatured complementary strands (left) and higher molecular weight Pt-bound species (center). Click reaction with the fluorophore results in fluorescence of the Pt-DNA band under UV light (right). (c) MALDI mass spectra of Pt-DNA (black) and Pt-DNA-click product (blue) showing the change in mass upon binding **1** and reacting with the fluorophore. Expected m/z of 4301.7 and 4590.8 compared to the observed 4300.03 and 4587.3, respectively. Conditions are outlined in **Appendix B**.

resolved under these gel conditions, but fluorescence detection of the subsequent click reaction clearly identifies a platinated species. No nonspecific fluorescent labeling is observed under Cu-free conditions (**Figure 3.3, lane 1**) following the reaction of the hairpin with two-fold excess 1 (18 h, 37 °C). Proficient fluorescent labeling of the 1-bound GG DNA hairpin is observed with either CuI-catalyzed (**Figure 3.3, lanes 2-3**) or

$CuSO_4$-catalyzed click protocols (**Figure 3.3, lanes 4-5**) following incubation at 50 °C for 1 h.

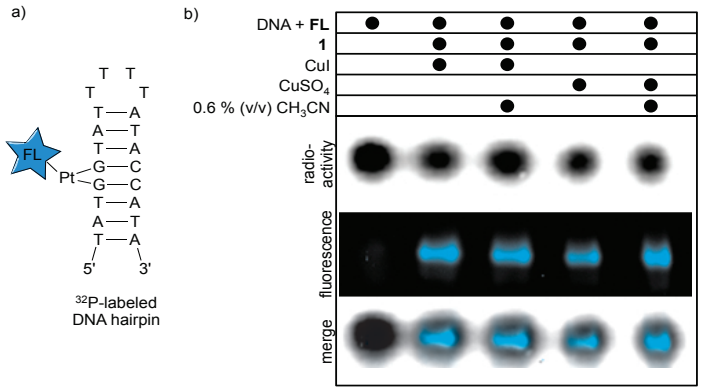

Figure 3.3. (a) DNA hairpin with **1** bound and labeled with the alkyne fluorophore. (b) dPAGE analysis showing fluorescent labeling of DNA hairpin by Cu-catalyzed click chemistry. Lane 1 contains *non*platinated DNA hairpin and shows no nonspecific DNA-fluorophore interaction. Lanes 2-5 contain platinated DNA under varying click condition sets (**Appendix B**), all of which show successful DNA-fluorophore labeling.

Picazoplatin-RNA Interactions *In Vitro* and *In Vivo*

The presence of Pt(II) lesions in cellular RNAs and their potential downstream consequences have become an increasingly important consideration given the many regulatory roles of RNA in essential cell processes.[19] Recent studies in our laboratory have demonstrated that in *S. cerevisiae*, cisplatin-derived Pt species accumulate to a significantly greater extent in RNA versus DNA, with ribosomal RNA acting as a *de facto* cellular Pt sponge.[19a] In context of *E. coli*[20] and *S. cerevisiae*[19a] ribosomal RNA, specific Pt binding sites have been identified within the small ribosomal subunit. Pt adducts are also observed in the sarcin-ricin loop (SRL), a universally conserved exogenous loop essential for elongation factor binding and GTP-dependent translocation (unpublished data).[21] To establish potential for using Pt-click reagents on cellular RNA, we investigated the interaction and click reactivity of **1** on a model SRL RNA construct (**Figure 3.4**).

The sensitivity of unmodified (i.e., 2'-OH) RNA species towards degradation by Cu-mediated chemistry has previously limited studies of click reactions with RNA sequences like the SRL in the absence of protective ligands such as TBTA or under O_2-free conditions.[22] We have independently observed significant degradation of our SRL

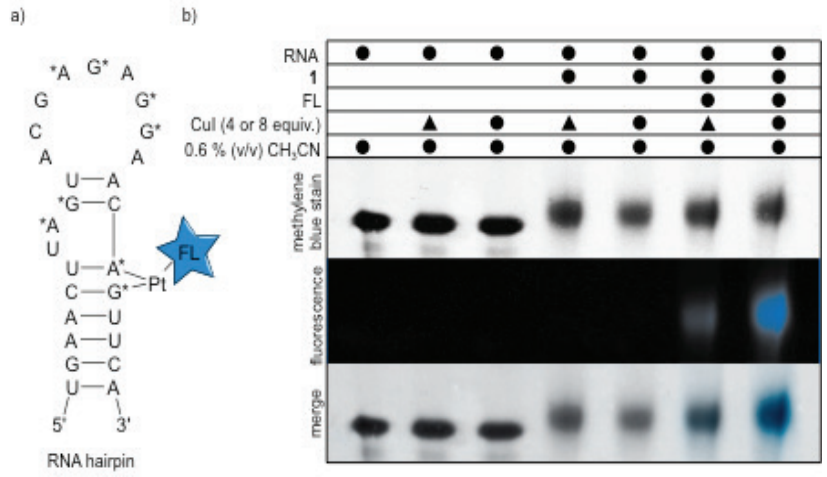

Figure 3.4. Fluorescent labeling of Pt-bound RNA SRL hairpin by click chemistry. (a) RNA SRL hairpin. Potential Pt binding sites are indicated by starred nucleotides. (b) Lanes 1-3: non-platinated RNA is stable in click reaction conditions with 0.4 (triangle) or 0.8 equivalents (circle) CuI. Lanes 4-7: SRL RNA treated with 4 equivalents **1** shows increasing yields of fluorophore labeling following click reactions with 0.4 (lane 6) and 0.8 (lane 7) equivalents CuI and the dansyl alkyne. Conditions are given in **Appendix B**.

RNA construct under various Cu-catalyzed click conditions (not shown). Recent work has demonstrated that trace amounts of acetonitrile stabilize free Cu(I) in aqueous solution while still facilitating efficient cycloaddition catalysis.[22] Here, we demonstrate substantial click product formation from picazoplatin-bound RNA in the presence of 0.6% v/v acetonitrile (**Figure 3.4 and Figure B.7, Appendix B**). Lanes 1-3 of **Figure 3.4** show that the SRL RNA is stable in up to 0.8 molar equivalents of Cu(I). In lanes 4-7, a supershift demonstrates Pt-adduct formation following RNA treatment with four-fold excess 1 (18 h, 37 °C). Notably, lanes 6 and 7 demonstrate efficient Cu(I)-catalyzed click labeling to dansyl alkyne fluorophore (1 h, 50 °C). Thus, post-treatment labeling by click chemistry is also successful for the analysis of RNA-Pt adducts.

To assess the feasibility of identifying cellular picazoplatin-bound species, we extracted and labeled ribosomal RNA from 1-treated S. cerevisiae with Alexa Fluor 488 DIBO alkyne (**Figure 3.5**). Lane 1 contains a 200 nucleotide RNA ladder. Lanes 2-4 contain 5.8S ribosomal RNA treated with an excess of alkyne fluorophore (18 h, 37°C). Lane 2 indicates the absence of nonspecific labeling. Lanes 3 and 4 clearly demonstrate picazoplatin accumulation on 5.8S rRNA *in vivo* and successful alkyne fluorophore labeling to an intact azide. These studies show the potential for in-gel quantification of all

cytoplasmic Pt(II) drug targets and/or fluorescent imaging of Pt trafficking in vivo in fixed and permeabilized cells.

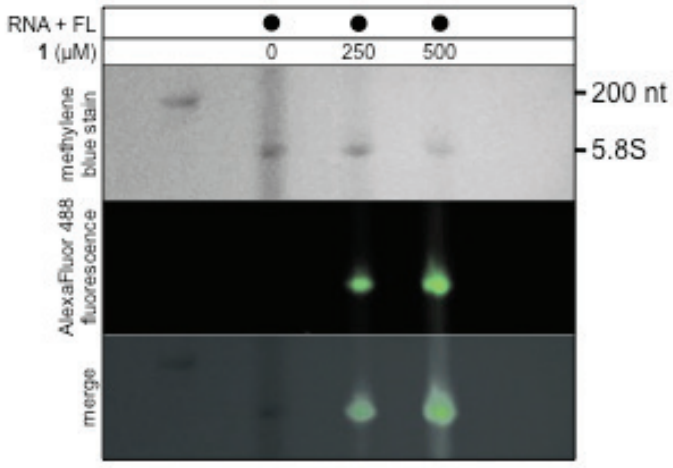

Figure 3.5. Fluorescent labeling of **1**-treated *S. cerevisiae* ribosomal RNA by click chemistry. Lane 1 contains a 200 nucleotide RNA ladder. Lanes 2-4 contain 5.8S ribosomal RNA (approx. 160 nucleotides) extracted from *S. cerevisiae* treated with 0, 250, or 500 μM picazoplatin and clicked to an excess of Alexa Fluor 488 DIBO alkyne (18 h, 37 °C). Proficient fluorescent labeling of the 5.8S rRNA is observed *in vivo.* Conditions are given in **Appendix B**.

Conclusions

In summary, we report the successful synthesis of picazoplatin, an azide-containing picoplatin derivative for Pt-bound drug target analysis by click chemistry. Picazoplatin ready binds DNA oligonucleotides and undergoes high-yielding click reactions with alkyne fluorophores. Moreover, successful fluorophore labeling via acetonitrile-assisted click reactions were demonstrated on an RNA mimic of the ribosomal sarcin-ricin loop construct, demonstrating viability of this approach in the presence of unmodified (i.e. 2'-OH-intact) RNA. Preliminary *in vivo* applications of this technique identified the 5.8S ribosomal RNA as a cellular Pt(II) drug target.
Future applications of Pt-click reactions could include the isolation, purification, and identification of in vivo targets of Pt(II) therapeutics using various alkyne-functionalized scaffolds. Reversal of Pt covalent linkages could be achieved by saturation with thiourea,[18a] releasing Pt-bound constituents for analysis via high-throughput sequencing, proteomics, or other analytical methods.[2c] The ability of Pt(II) compounds to crosslink

RNA and RNA-protein complexes[23] suggests additional applications in RNA and ribonucleoproteins structure-function analyses. Such efforts towards using Pt-mediated click chemistry to isolate and quantify Pt-bound species are currently underway in our laboratory.

Bridge to Chapter IV

Chapter III decribes a novel technology for identification, characterization, or purification of post-labeled platinum-bound species using click chemistry. This work has described picazoplatin (an azide-modified derivative of picoplatin) binding throughout RNA and DNA oligomers *in vitro*, confirmed by in-gel fluorescent detection and MALDI-MS analysis. Importantly, this is the first example of fluorescent post-labeling of platinum bound 5.8S rRNA as observed in RNA from picazoplatin-treated cells. Chapter V uses this technique to characterize platinum accumulation within rRNA and tRNA in picazo- and cisplatin treated *S. cerevisiae*.

CHAPTER IV

CLICK FLUORESCENT LABELING AND ENZYMATIC MAPPING OF PLATINUM (II) COVALENT DRUG MODIFICATIONS IN *SACCHAROMYCES CEREVISIAE* RIBOSOMAL RNA

This chapter contains ideas co-developed by Dr. Victoria J. DeRose and myself. I wrote the entirety of the manuscript, and received significant editorial feedback from V.J.D. Picazoplatin was synthesized by Jonathan D. White.

Introduction

Cis-diamminedichloroplatinum (II), or cisplatin, is a widely prescribed anticancer compound and currently one of only three Pt(II) complexes that are FDA approved for cancer treatment. In tumors, nuclear DNA damage from Pt(II) initiates apoptotic signaling, but this activity is not necessary for cytotoxicity. The accumulation and consequence of Pt(II) lesions on non-DNA targets, such as RNA, are largely unexplored. We previously reported the synthesis of an azide-functionalized Pt(II) species, picazoplatin, for post-treatment click labeling and isolation of Pt targets *in vivo* (White et al., *JACS* 2013). Here, we report in-gel fluorescent detection of Pt-bound ribosomal RNA and transfer RNA extracted from picazoplatin-treated *S. cerevisiae* and labeled using copper-free click chemistry. These data provide the first evidence that cellular tRNA is a platinum substrate and demonstrate a convenient click chemistry methodology that can be applied to identify other metal or covalent modification-based drug targets. We assessed Pt(II) binding within regions of ribosomal RNA where damage is linked to significant downstream consequences. Pt(II) lesions were mapped to nucleotide resolution on the sarcin-ricin loop (SRL) Helix 95 from ribosomal RNA extracted from cisplatin-treated *S. cerevisiae* as well as on a model SRL oligomer. Binding occurred on the nucleotide substrates of ribosome-inactivating proteins, as well as on the bulged-G motif critical for elongation factor recognition of the loop. At therapeutically relevant concentrations, Pt(II) also binds robustly within conserved cation-binding pockets in

Domains V and VI rRNA at the peptidyl transferase center. Taken together, these results suggest a ribotoxic mechanism for cisplatin cytotoxicity.

Pt(II) Lesions within Cellular RNAs

Cisplatin is the preeminent compound in a limited class of universally prescribed platinum (II) anticancer therapeutics. These small molecules form exchange-inert crosslinks with a variety of biomolecular targets, particularly across stacked guanine bases of nucleic acids. Formation of irreparable crosslinks on DNA induces programmed cell death in tumors (1). However, as less than 10% of intracellular cisplatin accumulates on DNA, cytotoxicity and alternative cell death pathways caused by additional platinum modifications is a major interest (2). We are specifically interested in assessing platinum modifications in cellular RNA, which may be a significant molecular decoy and secondary Pt(II) target. In *Saccharomyces cerevisiae*, we have shown that cisplatin-RNA adducts are more prevalent than in DNA (3). Cisplatin binding has been observed *in vitro* within rRNA (3, 4), tRNA (5), siRNA (6–8), and miRNA (9). Platinum lesions on RNA are not well-tolerated; disruptions to RNA-based processes are observed where structure and function are tightly coupled, such as ribosomal RNA synthesis, splicing, and translation (10–13). Moreover, there is developing recognition that RNA damage may contribute to cellular apoptotic signaling (14, 15). There is a clear need to characterize the molecular RNA targets of platinum, especially those which may initiate cytoplasmic cytotoxicity.

Here, we show in-gel visualization of post-treatment labeled cytoplasmic cisplatin targets and characterize, to nucleotide resolution, Pt(II) binding within the sarcin ricin loop and peptidyl transferase center of the ribosomal large subunit. These studies show the potential for ribotoxic response to chemotherapies, as well as structural insight into the ability of a small divalent metal to form crosslinks in unique RNA structures.

Click Fluorescent Tagging and Identification of Pt-bound RNA

We recently developed a method to detect platinum-modified targets through bioorthogonal ligation of Pt-bound species to alkyne-containing fluorescent probes (**Figure 4.1**) (16). Post-treatment modification allows the Pt compound to bind without

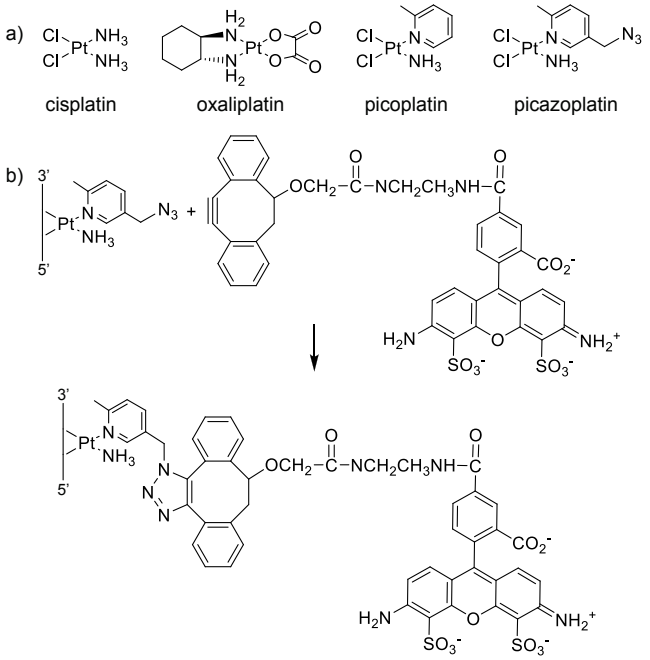

Figure 4.1. (a) The platinum (II) therapeutics cisplatin, oxaliplatin, picoplatin, and click-capable picazoplatin. (b) Copper- free fluorescent labeling of a picazoplatin-bound nucleic acid with Alexa Fluor 488 DIBO alkyne.

potential interference from attached labels, such as fluorescent dyes, and has also been used recently in studies of acridine-modified Pt compounds (17). Here, we use picazoplatin, an azide-functionalized click-capable derivative of picoplatin, to obtain dose-dependent fluorescent post-labeling of *S. cerevisiae* ribosomal RNA and transfer RNA (**Figure 4.2**). In-gel fluorescence scanning reveals significant fluorescent labeling of the 25S, 18S, 5.8S, and 5S ribosomal RNA bands. The broad distribution of fluorescent labeling between all ribosomal subunits demonstrates the environmental accessibility of rRNA towards covalent Pt modifications *in vivo.* This approach allows a rough quantification of Pt lesions per RNA based on signal intensity, with an estimated detection limit of ~1 Pt per 10,000 nt (**see Appendix C**). Using this calculation, we estimate ~0.4 platinum molecules per ribosome following treatment with 250 μM picazoplatin (**Table C.1**). This agrees well with previous work quantifying cisplatin accumulation as 1-2 per ribosome following 6 h of 100 or 200 μM cisplatin treatment (3), especially since picoplatin, the picazoplatin parent compound, has slower substitution kinetics (18, 19). Based on the signal intensity in the smaller 70—100 nt RNAs, it

appears that Pt is accumulating to a much greater degree, on the order of ~0.8 Pt per tRNA (**Table C.1**).

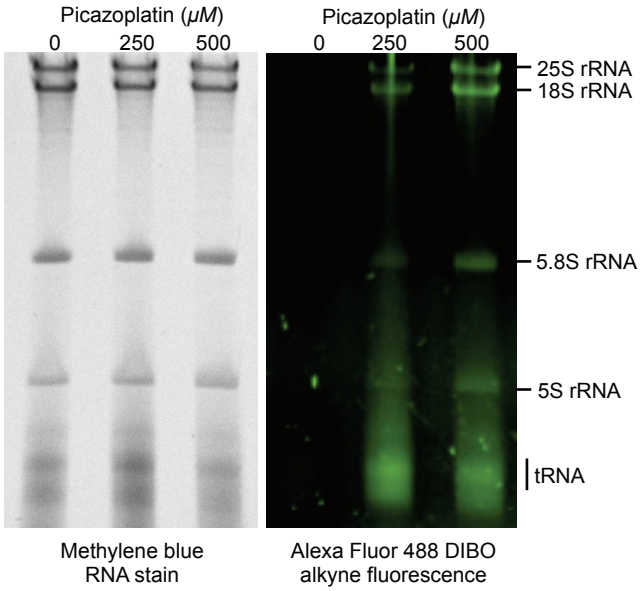

Figure 4.2. In-gel fluorescent analysis of post-labeled Pt-bound rRNA and tRNA purified from picazoplatin-treated *S. cerevisiae*. Cells were treated with 0, 250, or 500 μM for 6 h. Harvested RNAs (~5 μg) were reacted with an excess of Alexa Fluor 488 DIBO alkyne (18 h, 37° C), RNeasy column purified, and analyzed via 15% dPAGE. Dose-dependent labeling of tRNA and 25S, 18S, 5.8S, and 5S rRNA is observed. Fluorescence (panel, R) colored for clarity using Adobe Photoshop. Conditions provided in **Appendix C**.

To our knowledge, this is the first indication of Pt(II) accumulation in cytoplasmic tRNA. The functional consequences of Pt-tRNA adducts are unknown but are predicted to perturb their regulatory function. For instance, damage to tRNAs directly impacts RNA metabolism, may be a cellular signal of oxidative stress, and is indirectly linked to enhanced apoptotic signaling due to an increase in free cytochrome c (15, 20, 21). The observation of the accumulation of Pt(II) species on tRNA is especially intriguing given that damaged tRNAs, once sensed, are expected to have reduced half-lives, sometimes as short as minutes (22). However, given that tRNAs are already highly modified RNA species that fold into complex and diverse tertiary structures, their function may be more tolerant to Pt lesions. For example, certain nucleotide modifications are suggested to exert stabilizing effects by restricting conformational flexibility on the angstrom scale (23), thus reducing the propensity for enzymatic or base-

catalyzed degradation. As an additional factor, cisplatin lesions prevent exo- and endonuclease digestion of a number of RNA species (24). An accumulation of Pt-bound tRNA could result in nuclear mislocalization, as is seen in unspliced or modified tRNAs (25). Furthermore, elevated levels of tRNAs are implicated in some disease states (26, 27).

Enzymatic Mapping of Pt(II) Adducts in *S. cerevisiae* Ribosomal RNA

It is of interest to characterize Pt(II) modifications within RNAs that are functionally susceptible to substitutions, metal ion-mediated cleavage, or structural modifications. In rRNA, these regions are clustered in domains V and VI, within in the functional core of the ribosome (28–31). Certain modifications in these domains are capable of initiating a ribotoxic stress response in actively translating ribosomes, which we hypothesize may contribute to cisplatin cytotoxicity (32, 33). One particularly sensitive rRNA motif is the sarcin ricin loop (SRL), a universally conserved and purine-rich 12 nt sequence located adjacent to the peptidyl transferase center (PTC). The SRL (*S. cerevisiae* helix 95) folds in a robust and energetically stable distorted hairpin containing several flexible non-Watson Crick base pairs and unique motifs, including a GAGA tetraloop, a bulged G-motif, an S-turn, and a terminal A-form duplex (34). It scaffolds several critical protein-RNA interactions within the ribosome and is the target of ribosome inactivating proteins (RIPs) such as α-sarcin and ricin, proteins that catalytically modify the capping loop of the SRL, inhibiting the elongation step of translation and inducing apoptosis (35). Point mutations and structural perturbations within the SRL, such as those which may be induced by platinum crosslinking, are lethal (35, 36). Additionally, the SRL is proposed to host several cation-binding pockets, which could facilitate platinum coordination (37). Therefore, given the structural properties of this motif and potential for its modification to cause significant downstream consequences, we have carefully examined cisplatin accumulation in the SRL of RNA isolated from *S. cerevisiae* following cisplatin treatment.

Primer extension analysis, in which a reverse transcriptase stalls 3’ to a platinum adduct, was used to identify platinum binding pockets in the region of the SRL (helices 95 and 96, **Figure 4.3 and Figure C.1**) and adjacent solvent accessible and mobile

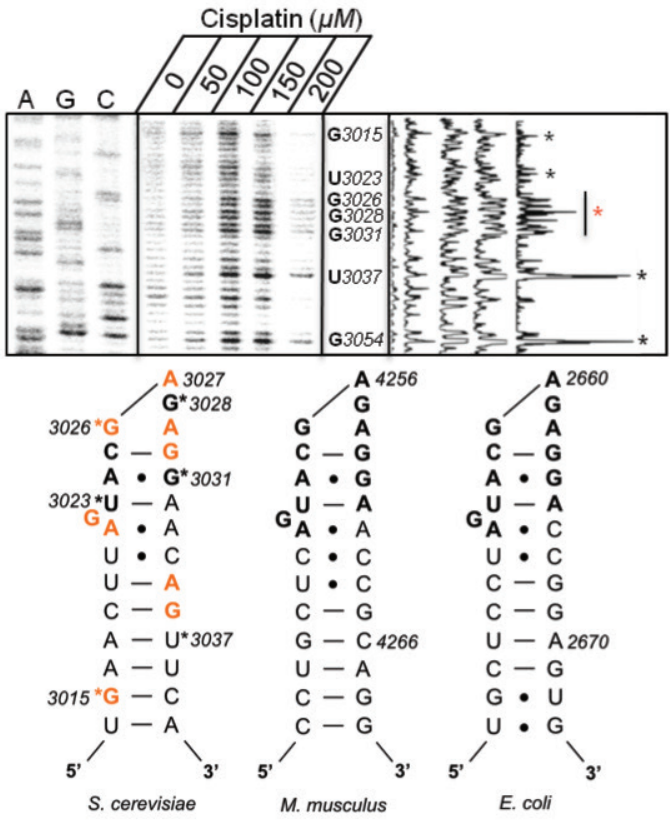

Figure 4.3. Primer extension analysis of the sarcin-ricin loop (SRL) region in ribosomal RNA extracted from *S. cerevisiae* treated with 0—200 μM cisplatin. Dideoxy sequencing ladder labeled by A, U, C, and G. Cisplatin-induced stop sites are denoted by asterisks (*) and represent nucleotides 3' to a stable platinum adduct. Colored asterisk denotes primary stop site in terminal SRL region (at G3028) according to line plot analysis. Predicted platinum crosslinks between adjacent purines based on experimental results are colored on the *S. cerevisiae* secondary structure map. The 12 nt universally conserved RNA sequence is in bold. *M. musculus* and *E. coli* sequences provided for comparison.

helices in the PTC (helices 90 and 93, **Figure C.3**). Such crosslinks are expected to primarily occur between the N7 positions of purines that are in close proximity. Accompanying a quantitative ICP-MS analysis of Pt on *S. cerevisiae* rRNA, we previously performed a limited identification of Pt sites within helix 18 in the small ribosomal subunit (3) and compared them with a prior report from *E. coli* (4). Differences in rRNA sequence led to a shift in preferred Pt binding sites in the two organisms, demonstrating *in vivo* sequence selectivity. Within the *S. cerevisiae* SRL, extension data using two different primers provides clear evidence for concentration-dependent platinum adducts (**Figures 4.3 and C.2**). A strong stop at U3037 indicates a 5'-ApG-3' adduct between G3036:A3035. In DNA helices, this sequence is known to be kinetically

preferred over the opposite 5'-GpA-3' (38). A second clear stop site occurs at U3023, indicating Pt(II) binding at the bulged-G motif (G3022) critical for loop recognition by elongation factor 2 (EF-G, *E. coli*) (39). Depending on the flexibility of this non-Watson-Crick basepaired nucleotide, this could represent a monofunctional Pt(II) adduct on G3022 or a 5'-ApG-3' adduct between A3021:G3022. Disruption of RNA-protein interactions at G3022 is directly linked to translation inhibition and ribotoxic response signaling (39, 40). The third clear stop within the sarcin ricin loop is at the 5' distal end of the helix. Experiments with the 'upstream' SRL primer experiments show significant stops at A3017 (**Figure C.2**). As this is a relatively purine-rich stretch of the stem, we conclude that platinum could form a 5'-GpA-3' diadduct between G3015:A3016.

In primer extension of the highly conserved and purine-rich terminal SRL loop, multiple stop sites arise in RNA isolated from cells treated with increasing cisplatin concentrations. The multiple but nonspecific stop sites in the region between G3033 and G3026 indicate that platinum binding in or near to this loop causes rigid secondary structures that are nonpermissive to RT extension. From the *in vivo* data it is difficult to ascertain specific platinum adducts; for comparison, we extended these studies to investigate *in vitro* platinum binding within a SRL oligomer (vide infra). However, line plot analyses for both primers suggest a primary stop site within this region at A3029 (**Figure C.2**) or G3028 (**Figure 4.3**), suggesting formation of a Pt(II) adduct between G3028:A3027 or a monofunctional adduct at A3027. A3027 is moderately reactive in *in vivo* SHAPE analyses, indicating some degree of conformational flexibility (41). Ricin specifically depurinates A3027, while α-sarcin cleaves the phosphodiester backbone between A3027 and G3028, and both types of damage culminate in apoptosis (33). We hypothesize that the observed Pt(II) lesions may elicit a similar ribotoxic response.

Throughout helix 96, the helix directly adjacent to the SRL, platinum accumulation is observed on adjacent, stacked purines at therapeutically relevant treatment conditions as low as 100 μM cisplatin, which we have previously correlated with a cytoplasmic concentration of 47 μM (3). In regions of stable duplex RNA and longer hairpins, we generally observe stable 3'-GG-5' Pt (II) intrastrand adducts. In regions which may exhibit flexibility, such as the H95:H96:H97 three-helix junction (42),

primer extension is terminated on the first guanine of a 3'-GG-5' pair (G3044:G3045), suggesting a monofunctional adduct or long-range RNA crosslink (**Figures 4.3 and C.1**).

One facet of cisplatin's effect on RNA-dependent cellular processes is the inhibition of translation elongation (43). We therefore assessed platinum binding within helix 93, one of the mobile stalks of the peptidyl transferase center (**Figure C.3**). This structure is adjacent to the aa-tRNA accommodation corridor and hosts A2971 in its stem. This particular adenine is the most conformationally flexible residue in the PTC and was found to be strongly reactive to SHAPE 2'-OH modification in *E. coli* and *S. cerevisiae* in the absence of tRNA in purified ribosomes (41). Moreover, mutations at A2971 strongly interfere with peptide release (29). From our primer mapping data, a strong stop site at G2973 suggests that A2971 is also highly reactive to platinum crosslinking, forming a crosslink with G2972 (**Figure C.3**). This data suggests the Pt(II) adduct occurred in an A-site tRNA unbound (i.e. Pt (II) accessible) state, providing a mechanism to inhibit further translation. Intriguingly, although the broad reactivity of platinum towards adjacent purines is well established, cisplatin binding in this region is remarkably specific; several purines in helix 93 (G2956, A2957, G2965, A2966, G2967, and A2968) are unreactive towards Pt (II). **Figure 4.4** depicts H93 in the context of a $tRNA^{Met}$-bound ribosome. In this structure, the purine nucleotides G2966 and A2967 in the terminal loop of H93 (orange) are organized around a ~2.8Å hydrogen bond to the 2'OH of the G2964 ribose sugar (aqua). This interaction may preclude stable Pt(II) diadduct formation between G2966:A2967, and explain a general mechanism for protection at this loop. However, A2971 (yellow) is clearly flipped out from the helix and in a position ready to bind Pt(II). This may account for our observation of strong targeting to A2971, while the H93 terminal loop appears shielded (**Figure C.3**).

In this investigation of Pt(II) adduct formation within the PTC, we also uncovered several Pt(II) binding sites in helix 90, corresponding to 1,2-intrastrand GpG adducts. These results are somewhat obscured by the prevalence of RNA modifications within these sequences (Figure S3). However, they clearly depict the ability of Pt(II) to target accessible purine bases within a complex RNA structure. The summary of these analyses is presented in the rRNA secondary structure map in **Figure 4.5**.

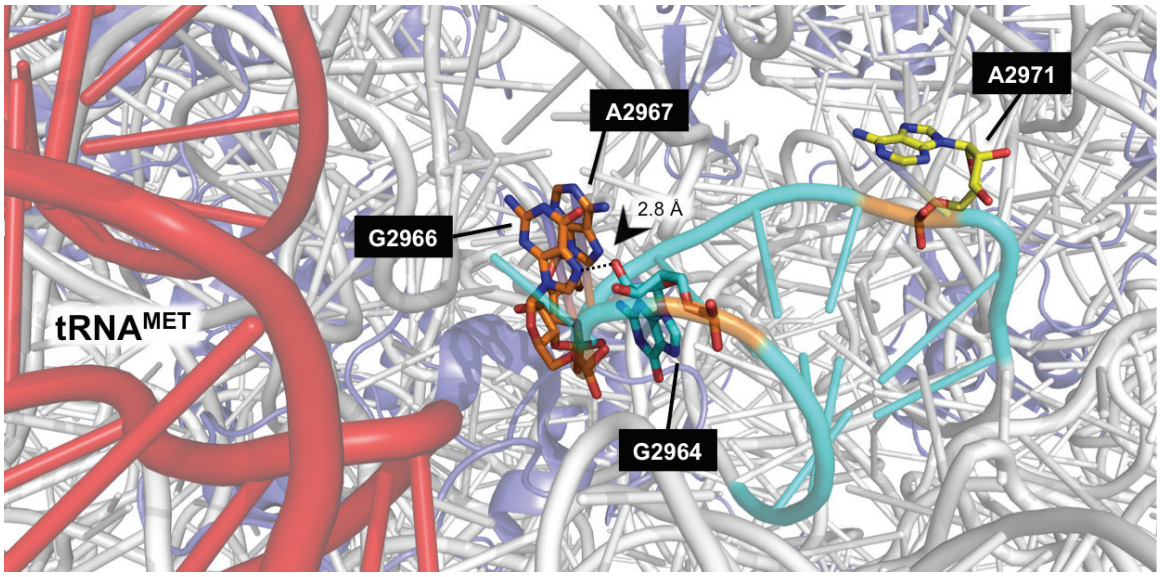

Figure 4.4. Model depicting H93 (aqua) in the context of a tRNA^{Met}-bound ribosome (tRNA: red; rRNA: gray; protein: light purple). G2966 and A2967 in the terminal loop of H93 (orange) are organized around a ~2.8Å hydrogen bond to the 2'OH of the G2964 ribose sugar (aqua). A2971 (yellow) is clearly flipped out from the helix and in a position accessible for Pt(II). Figure generated in PyMOL using PDB files 4BYT, 4BYS, 4BYP, 4BYR, 4BYQ, 4BYO, 4BYN, AND 4BYL.

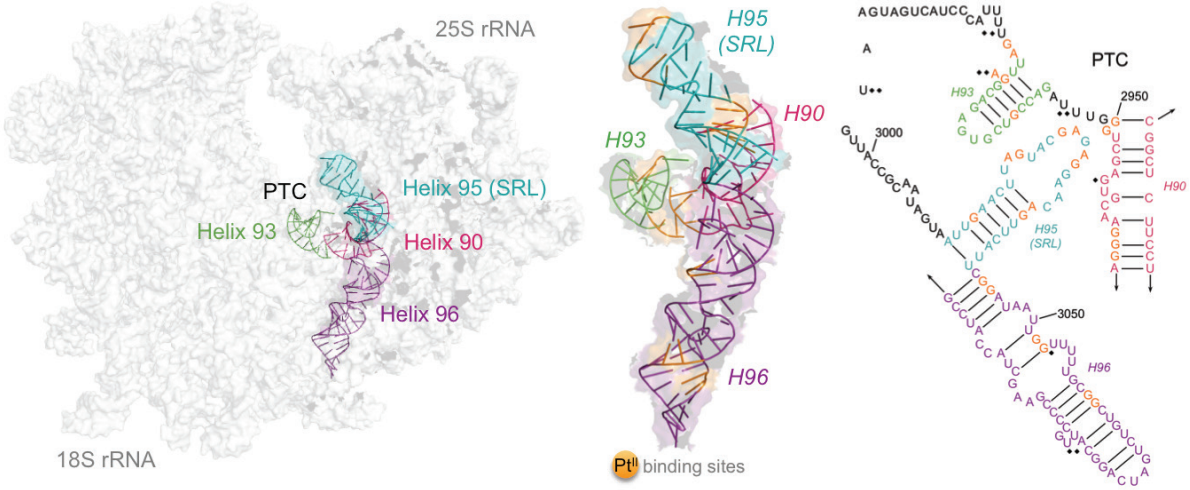

Figure 4.5. Model of platinum binding within helices 90, 93, 95, and 96 of the *S. cerevisiae* large ribosomal subunit RNA. Crystal structure of rRNA (gray left) is shown with probed regions highlighted in color and expanded to show platinum dinucleotide crosslinks in orange (middle). Crosslinks agree well with proposed solvent accessibility and nucleotide position according to the crystal structure. Pt (II) sequence specificity is summarized on the left, with sites of moderate (⬥) and high (⬥⬥) SHAPE reactivity overlaid (41). The 2 D structure map of yeast rRNAs was obtained from the Comparative RNA Website (47).

Enzymatic Mapping of Pt(II) Adducts in a Model SRL RNA

To compare accessibility to Pt *in vivo* with an *in vitro* model, platinum adducts within a 27 nt model SRL oligomer were probed using primer extension analysis. From NMR structural data and molecular simulations, this sequence is well-understood to fold into a stable structure *in vitro*, allowing our 27 nt oligomer to accurately model the SRL in the context of the 25S rRNA (34, 44). We have assessed aquated ("activated") cisplatin binding within the SRL from 0—2 equivalents (**Figure 4.6**). We observe dose-dependent platinum stop sites occurring at U3036, A3031, G3030, and A3026 (*S. cerevisiae* numbering). The platinum adducts predicted by these stop sites are highlighted in color in the *S. cerevisiae* secondary structure map. They include a canonical 3'-GG-5' adduct (G3031:G3030), two putative 3'-GA-5' intrastrand crosslinks (G3036:A3035; G3030:A3029), and a signal at an isolated guanine which could represent a monofunctional adduct or a crosslink bridging the terminal GAGA tetraloop (G3026). As described earlier, there is a strong causal link between damage at this position and downstream apoptotic signaling. It is important to note that under these conditions, it is likely that each RNA is bound by multiple Pt(II) atoms. Due to the 3' bias of this technique, it is difficult to define where 1,2-intrastrand Pt(II) lesions form on the 5' distal

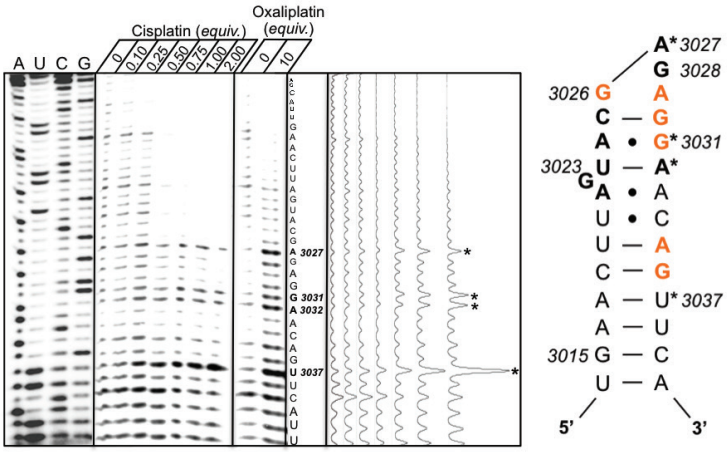

Figure 4.6. Primer extension analysis of a folded model *S. cerevisiae* sarcin ricin loop RNA following treatment with 0—2 equivalents of aquated cisplatin or 0—10 equivalents of non-aquated oxaliplatin (20 h, 37° C). Cisplatin-induced dose-dependent stop sites are denoted by asterisks. Oxaliplatin-induced stop sites mimic those of cisplatin, and are shown for comparison. Mapping results are summarized in the secondary structure diagram using the same notation as in **Figure 4.3**.

region of the duplex.

Cisplatin accumulation within the model SRL was compared to the RT stalling pattern following SRL treatment with non-activated oxaliplatin (**Figure 4.6**). The equilibria, mechanism, and rates of aquation and binding differ between cisplatin and oxaliplatin and depend strongly on pH and ionic environment (45). For oxaliplatin, dissociation of the oxalato ligand is reported to occur with a half-life of 92 min at 37 °C (46). In our studies, 10 equivalents of non-activated oxaliplatin are required to observe RNA-Pt(II) adducts, compared with just 0.5 to 1 equivalents of activated cisplatin. Remarkably, despite these differences, their kinetically preferred binding sites are identical within the SRL. Conservation of Pt (II) binding within the SRL may demonstrate a ubiquitous mechanism for translation inhibition. This differs from

Finally, we report that the pattern of platinum accumulation differs slightly between the sarcin ricin loop *in vitro* model versus the *in vivo* and presumably intact ribosome (**Figure 4.7**). Platinum crosslinking throughout the helix stem (at A3035:G3036) is completely conserved, but the preference of platinum slightly shifts within the GAGA tetraloop *in vivo*. We observe Pt(II) accumulation within A3027 and G3028 by two different primer extension assays. However, neither nucleotide is Pt(II)-bound in our *in vitro* model (**Figure 4.7**). This may be explained in part by anti/syn base

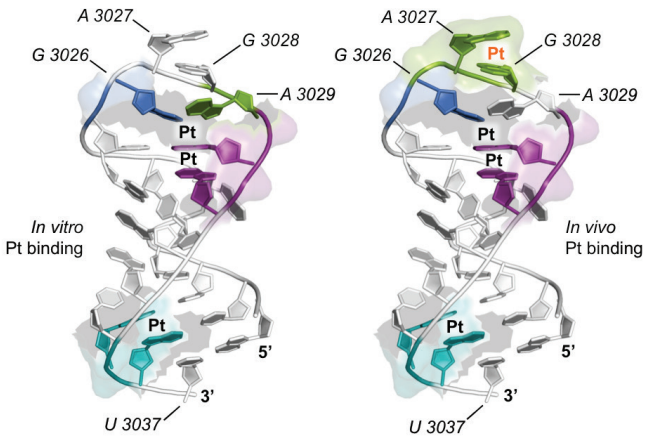

Figure 4.7. Model comparing differences in Pt(II) binding preferences within the SRL *in vitro* and *in vivo*. Predicted platinum adducts are denoted by "Pt". Pt(II) binding is conserved throughout the SRL with the exception of the GAGA tetraloop. *In vivo*, strong Pt(II) targeting is observed to A3027 and G3028 (Pt, orange). This targeting is not conserved *in vitro*. Figure generated in PyMOL using PDB files 3O5H and 3O50.

flipping of the terminal adenine as predicted by molecular simulations (34). According to Sponer *et al.*, although the SRL is highly rigid when compared to other RNA motifs, the tetraloop is dynamic. Given that several protein interactions occur at the tetraloop that may induce unfolding or stabilization, we predict a concurrent change in platinum accessibility and binding. The change in the binding pattern could also reflect RNA-protein crosslinks, which are absent in our *in vitro* model.

Conclusion

To date, we lack a comprehensive understanding of the biological cytoplasmic substrates of Pt(II) therapeutics such as cisplatin. We recently developed a method to detect platinum-modified drug targets using picazoplatin, an azide-containing picoplatin mimetic designed for post-treatment labeling via click chemistry. Here, we demonstrate that ribosomal RNA and transfer RNA purified from picazoplatin-treated yeast accumulate platinum and are efficiently labeled with Alexa Fluor 488 DIBO alkyne to levels detectable by in-gel fluorescence (following 250 μM treatment, ~0.4 Pt per ribosome and ~0.8 Pt per tRNA). This is the first evidence that tRNA is an authentic platinum substrate. Pt-tRNA damage could severely impact cellular processes such as translation and apoptotic signaling. Within ribosomal RNA, we have identified the sarcin ricin loop and peptidyl transferase center as high impact cisplatin targets. Using primer extension analysis, we have mapped platinum accumulation on the sarcin ricin loop *in vivo* on rRNA extracted from yeast treated with cisplatin as well as in a model 27 nt oligomer. This investigation of Pt(II) adducts within Domains V and VI rRNA demonstrate a variety of potential ribotoxic roles for platinum, all of which likely contribute to the general cytotoxicity of the drug. Using picazoplatin, future avenues of research could focus on isolation, enrichment, and sequencing of platinum-bound nucleic acids to gain a global perspective on Pt accumulation and RNA access *in vivo*. We are very interested in dissecting the accumulation of cisplatin on its cellular targets with temporal resolution, as the types of Pt-RNA interactions we have described could be of cytoplasmic or nucleolar origin. Of critical importance is the demonstration that this azide modification technique can be broadly utilized to assess the binding preferences of other small molecules on cellular RNAs.

Bridge to Chapter V

In Chapter IV, we report significant in-gel fluorescent detection of Pt-bound ribosomal RNA and transfer RNA extracted from picazoplatin-treated S. cerevisiae using copper-free click chemistry, and demonstrate the first evidence that cellular tRNA is a platinum substrate. Building on this insight, we have identified the sarcin-ricin ribosomal RNA loop as an impactful drug target. We have mapped cisplatin accumulation to nucleotide resolution on the sarcin-ricin loop (SRL) from ribosomal RNA extracted from cisplatin-treated S. cerevisiae as well as on a model SRL oligomer. At therapeutically relevant concentrations, Pt(II) binds robustly within conserved cation-binding pockets in Domains V and VI rRNA. Taken together, these data suggest a ribotoxic mechanism for cisplatin cytotoxicity, and broadly describe a convenient click chemistry methodology that can be applied to identify other metal or covalent modification-based drug targets. Chapter V summarizes the research described in Chapters I through IV, and provides a perspective on the future outlook of platinum therapeutics.

CHAPTER V

CONCLUDING REMARKS AND FUTURE DIRECTIONS

I am very privileged to have spent my graduate career in a highly collaborative environment. Many of my co-workers research complementary aspects of cisplatin biochemistry, and as such, I have received invaluable input, assistance, and guidance from former and present DeRose lab members, including Dr. Erich G. Chapman, Dr. W. Luke Ward, Dr. Alethia A. Hostetter, Jonathan D. White, Kory J. I. Plakos, Rachael M. Cunningham, and Alan D. Moghaddam. This chapter is a synopsis of the creative ideas seeded by Dr. DeRose and developed throughout generations of graduate work, and my personal view on the future outlook of platinum (II) therapeutics.

Concluding Remarks

This dissertation describes cellular RNA targeting by platinum (II) chemotherapeutic drugs. Chapter I summarizes the history, molecular mechanism, and current literature on Pt(II) therapeutic targets and anticancer activity. Here, I have introduced the concept of Pt(II) sequestration by cellular RNA, and discussed the potential for RNA as a drug target. Chapter II recounts our work characterizing the distribution of Pt(II) within *S. cerevisiae* cytoplasmic RNA, with the discovery that ribosomal RNA acts as a *de facto* cellular platinum sponge, forming stable covalent adducts following just 1 h of drug exposure. We learned about the sequence specificity and reactivity of cisplatin towards complex RNA hairpins *in vivo*, validating many *in vitro* RNA-Pt(II) studies performed by my predecessors. Interested in extending this work to a more high-throughput system, current work is focused on developing a suite of click-capable platinum(II) reagents for the purpose of post-labeling, isolating, or purifying platinum-bound species. Specific routes toward those goals are outlined in **Figure 5.1**. One intriguing possibility would be the use of alkyne-functionalized biotin to enrich for platinum-containing species on streptavidin functionalized beads or surfaces (**Figure 5.1, top right**). Following target capture, the selected biomolecules could be released using thiourea reversal of Pt(II) binding, a method developed by Dr. Erich G. Chapman.[1] Then,

sequences could be subjected to mass spectrometry (proteins, lipids) or high-throughput sequencing (nucleic acids) for characterization. Alan D. Moghaddam and Rachael M. Cunningham are actively pursuing these types of assays.

Chapter III describes our first proof-of-principle studies with picazoplatin, an azide-functionalized picoplatin derivative. Here, we have shown a novel method for in-gel fluorescent detection of Pt-bound DNA and RNA oligomers, as well as labeling of the 5.8S ribosomal RNA subunit from picazoplatin-treated *S. cerevisiae*. Currently, Jonathan D. White and Alan D. Moghaddam are engaging in the synthesis and application of more reactive azide-functionalized complexes, such as 2-ADAP Pt (**Figure 5.1**). These complexes have opened up a number of new avenues for innovative research in the DeRose lab. Currently, Rachael M. Cunningham is developing an assay using 2-ADAP Pt to monitor platinum accumulation on cellular proteins. Kory J. I. Plakos is using 2-ADAP Pt as a platinum crosslinking reagent to study the tertiary structure of folded ribozymes.

In Chapter IV, I recount the first in-gel fluorescent detection of picazoplatin-bound RNA species within total RNA isolated from drug-treated *S. cerevisiae*. From these data, we report Pt accumulation on the order of ~0.5 Pt per ribosome, and ~0.8 Pt per tRNA. This is the first evidence of tRNA as a *bona fide* cisplatin substrate *in vivo*, which could severely affect translation or apoptotic signaling. Chapter IV also describes my methodical investigation of Pt(II) binding within the functional core of the ribosome, in an effort to understand how Pt(II) lesions could contribute to the inhibition of translation observed in cisplatin-treated cellular extracts. We detect stable Pt-RNA modifications throughout several critical RNA motifs, including the sarcin-ricin loop and peptidyl transferase center. These studies demonstrate a variety of potential ribotoxic roles for platinum, all of which likely contribute to the general cytotoxicity of the drug. Translation is not the only RNA dependent process altered following cisplatin treatment; currently, Emily R. Morris is investigating the effects of cisplatin on alternative mRNA splicing. Taken together, the work described in this dissertation highlights the significance of RNA targeting by cisplatin and disseminates a novel technology (Pt(II) click chemistry) which could be broadly applied in the identification of targets of metal-based drugs.

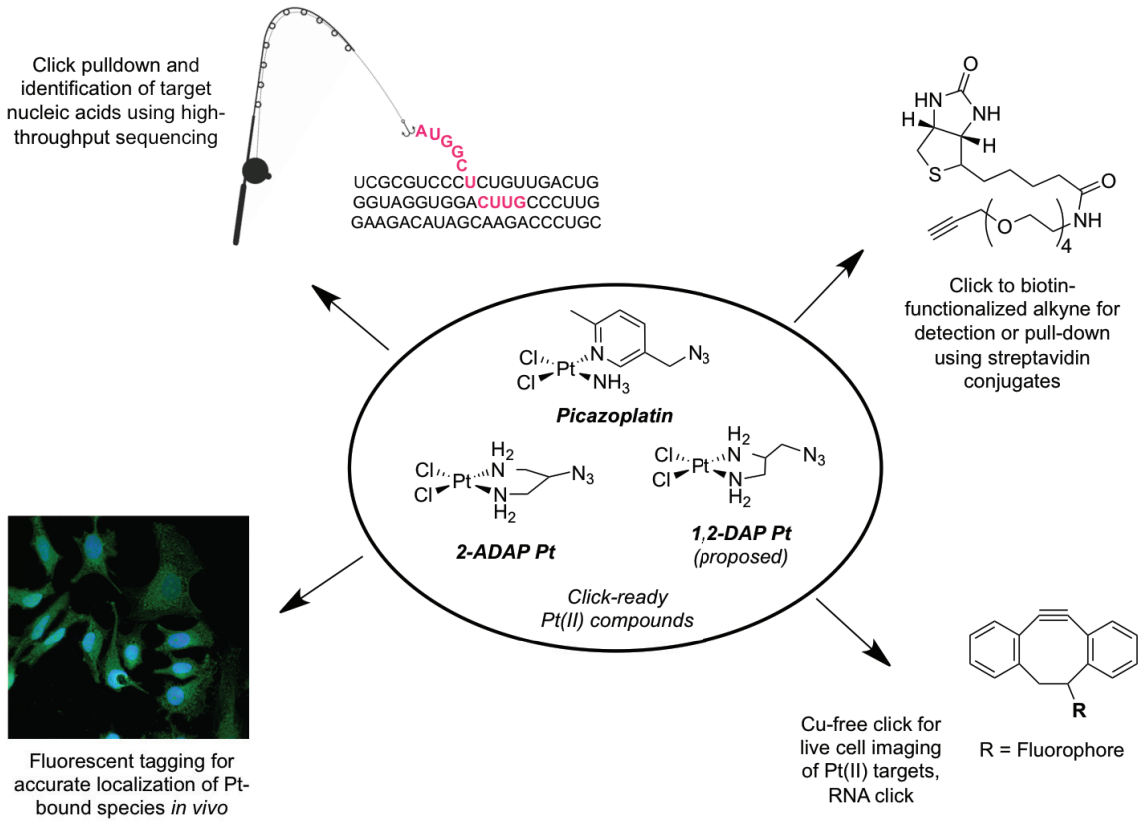

Figure 5.1. Potential applications for click-capable Pt(II) reagents. (Top left) Click pulldown of Pt-bound RNA for high-throughput sequencing. (Top right) Click to biotin-alkyne for facile detection or pulldown of labeled species. (Bottom left) Fluorescent tracking of cellular Pt(II) species in tissue culture. (Bottom right) Use of a strained alkyne fluorophore for Cu-free labeling of RNA *in vitro*.

Current Limitations on Use of Pt(II) Drugs and Future Outlook

Chapter I summarized the historical progression of platinum antitumor agents through the FDA approval process. Cisplatin was approved for use in the U.S. in 1978. Since then, 23 complexes have entered clinical trials, with only two gaining approval (carboplatin and oxaliplatin).[2] No new Pt(II) drug has been promoted to clinical trials since 1999.[3] This is partially explained by an increase in stringency of FDA regulations; however, to date, the major issues of toxicity and resistance are still problematic. High doses of Pt(II) agents results in ototoxicity, neurotoxicity, myelosuppression, and acute nephrotoxicity, as the body attempts to clear the drug through the kidneys. The side effects suffered may require sub-lethal doses, which cause tumor cells to develop resistance. Resistance is mediated through reduced uptake and inactivation of the drug

via sequestration to intracellular thiols.[3] This has led research to shift towards development of DNA-targeting Pt(II) ligands,[4] photoactivatable Pt(IV) prodrugs,[5] and tumor-specific lipophilic delivery systems.[6] These advances may alleviate issues associated with side effects in non-tumorigenic cells, allowing treatment with higher dosages. However, they do not fully address issues of intracellular resistance. If a comprehensive study of Pt(II) cellular targets was performed using reagents such as picazoplatin and 2-ADAP Pt, it would allow precise quantification of the distribution and localization of platinum drugs. Using this technique, we are the first to demonstrate that cellular tRNA is a major target of platinum binding *in vivo* in treated *S. cerevisiae*. Discoveries like this would directly enhance development of novel or non-classical platinum-based anticancer therapeutics. Moreover, there is a clear need to understand the effects of targets such as rRNA and tRNA, especially given the recent expansion of knowledge regarding RNA damage sensing, repair, and regulation. New chemical strategies like our click-capable Pt(II) species will be invaluable for the advancement of platinum therapeutics.

APPENDIX A

SUPPORTING INFORMATION FOR CHAPTER II: RNA-PT(II) ADDUCTS FOLLOWING CISPLATIN TREATMENT OF *SACCHAROMYCES CEREVISIAE*

Materials and Methods

Cell cultures and treatments: *S. cerevisiae* strains BY4741 (MATa; *his3*D1; *leu2*D0; *met15*D0; *ura3*D0), *yca1*D (BY4741 *yca1*::kanMX4) and *aif1*D (BY4741 *aif1*::kanMX4) were gifts from the Stevens laboratory at the University of Oregon. Liquid cultures were grown on Synthetic Complete medium (SC) consisting of 0.67% yeast nitrogen base and 2% glucose supplemented with amino acids and nucleotide bases maintained in the dark at 30 °C with shaking at 200 rpm. Plated cells were grown on YEPD agar plates (1% yeast extract, 2% peptone, 2% glucose, and 2% agar). A 5 mM cisplatin (Sigma Aldrich) stock in 100 mM NaCl (stored in the dark for no more than a week) was used for all cisplatin treatments. Yeast cultures were pregrown to an OD_{600} of 5 then inoculated into 30 °C cisplatin-containing media to an OD_{600} of 0.075.

Culture growth, cell survival, and cell size: Culture growth was measured by absorbance at 600 nm (1 $AU_{600} = 2.0 \times 10^7$ cells/mL). Cell viability was measured by plating serial dilutions of treated and untreated yeast, at given growth times, onto drug-free YEPD agar plates (~250 cells/plate) and counting colonies after 3 d at 30 °C. The number of colony-forming units (cfu) was determined by dividing the cfu counts of treated cultures by those of untreated cultures (assumed to be 100%). Yeast cell radii were measured from differential interference contrast images obtained on a Carl Zeiss Axioplan 2 fluorescence microscope using a 100× objective and AxioVision software (Carl Zeiss, Thornwood, NY) and volumes were calculated by treating the yeast as spheres.

Nucleic acid extraction and purification: For measurements of Pt in total RNA ~1.2×10^8 cisplatin treated yeast cells were pelleted and RNA was extracted using the MasterPure RNA Purification Kit (Epicentre) according to manufacturer's specifications.

For both mRNA and rRNA samples total RNA was extracted from cisplatin treated cells according to the method of Motorin *et al.* (*1*). Poly(A)-mRNA was isolated using GenElute mRNA Miniprep Kit (Sigma), doing the binding and wash steps twice to ensure maximum mRNA purity. Ribosomal RNA was isolated from total RNA using 8% dPAGE. The 25S and 18S bands were visualized by brief staining with methylene blue, cut out and eluted with an Elutrap Electroelution System (Whatman), then desalted (3k Microsep Centrifugal Devices, Pall). DNA samples were purified as in Rose *et al.* including the optional RNase A treatment (*2*). Because Pt adducts on RNA are known to inhibit RNase activity (*2*) DNA was extracted at 12 h, a time at which there is 4–5 fold lower RNA content in yeast cell (*3*), in order to ensure sample purity. All pellets were collected at 4 °C and washed 3 times with deionized H_2O before further processing.

Measurement of Pt content: Isolated RNA and DNA samples were desalted on in-house prepared G-25 sephadex spin columns (BioRad) and quantified by absorbance at 260 nm. Whole-cell and most nucleic acid samples were digested in 70% nitric acid (trace select, Fluka) for 2 hours at 65^{o}C then diluted to 2% (v/v) nitric acid with milli-Q H_2O. Pt content was determined by Inductively Coupled Plasma Mass Spectrometry (ICP-MS) using a Thermo VG PQExcell quadrupole ICP-MS equipped with a Gilson 222 autosampler at the W. M. Keck Collaboratory for Plasma Spectrometry (Oregon State University, Corvallis, Oregon). The instrument was calibrated for ^{194}Pt, ^{195}Pt and ^{196}Pt by developing standard curves from a Pt standard (High Purity Standards). All measurements were done in triplicate using ^{115}In as an internal standard.

Tests for apoptotic markers: Terminal deoxynucleotidyl transferase-mediated dUTP nick end labeling (TUNEL) was performed according to the method of Madeo et. al. (*59*) with the following modifications: cell walls were digested with 2.5 U zymolyase 100T (US biological) for 30 min at 30 °C in 1 mL sorbitol buffer (1.2 M sorbitiol, 0.5 mM $MgCl_2$, 35 mM phosphate buffer pH 6.8), the permiabilization was carried out for 1 min, and the in situ cell death detection kit, fluorescein (Roche), was used with a 30 min incubation (full protocol Supplementary pS4). Positive control samples were incubated with 0.2, 1, and 5 U DNase I (Fermentas) for 1 h at 37 °C in the manufacturer's rxn

buffer. Images were acquired on a Carl Zeiss Axioplan 2 fluorescence microscope as described above. DAPI staining was performed by pelleting 1.0×10^7 yeast cells, washing 3x with PBS, fixing in 70% (v/v) EtOH for 30 min, washing with PBS, and then incubating with 0.5 mg/mL DAPI for 20 min (in the dark). The samples were then washed 3x with PBS and visualized immediately.

Full TUNEL protocol: Yeast cells (3.0×10^7) were pelleted, washed 3x with PBS, fixed with 3.7% (v/v) formaldehyde for 2 h at 24 °C, and then digested with 2.5 U zymolyase 100T (US biological) for 30 min at 30 °C in 1 mL sorbitol buffer (1.2 M sorbitiol, 0.5 mM $MgCl_2$, 35 mM phosphate buffer pH 6.8). A portion of the sample was applied to a polylysine-coated slide and let dry for 1 h at 37 °C. The slides were incubated with freshly prepared permiabilization solution (0.1% Triton X-100, 0.1 sodium citrate) for 1 min at 4 °C, then rinsed 3x with PBS. Positive control samples were incubated with 0.2, 1, and 5 U DNase I (Fermentas) for 1 h at 37 °C in the rxn buffer provided by the manufacturer. Samples were incubated with 10 mM TUNEL reaction mixture (in situ cell death detection kit, fluorescein, Roche) for 30 min at 37 °C in the dark, rinsed 3x with PBS.

5' End-labeling: The DNA primer designed for reverse transcription of helix 18 of the small yeast ribosomal subunit was purchased from Integrated DNA Technologies. γ-^{32}P 5' end-labeling was performed as previously described (4).

Reverse Transcription: Total RNA extracted from cisplatin-treated yeast cells was used as a template for RT. Yeast cells were inoculated at 5×10^6 cells/mL into cisplatin-containing SD-URA and grown for 6 h. Total RNA was isolated using a MasterPure Yeast RNA Extraction kit (Epicentre) and resuspended in 10 mM Tris-HCl (pH 7.5) and 1 mM EDTA to a final concentration of 10 mg/mL. For primer extension, 1 mg of RNA template was annealed to 100 pmol of the specified 5' end-labeled primer in the manufacturer's reaction buffer and incubated in the presence of AMV Reverse Transcriptase (Fermantas) for 1.75 h at 42°C. The resulting cDNA products were diluted in loading buffer containing 0.005% (w/v) xylene cyanol and bromophenol blue and

analyzed by 8% dPAGE. Bands were visualized using a GE phosphor screen in conjunction with a Storm phosphor screen imaging system and then quantified with ImageQuant 5.1 and normalized in Excel.

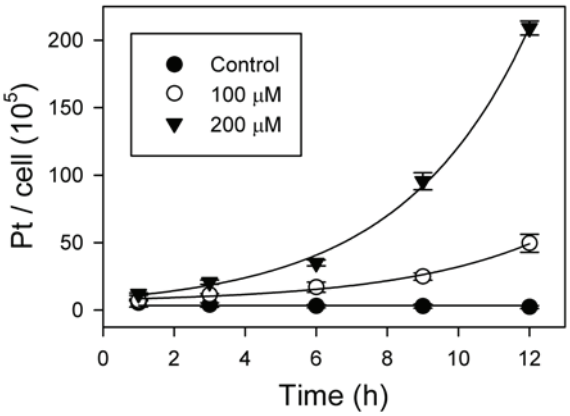

Figure A.1. Accumulation of Pt atoms per yeast cell in yeast treated with cisplatin for 1, 3, 6, 9, and 12 h. Results averaged from four independent experiments, presented as the means ± SD.

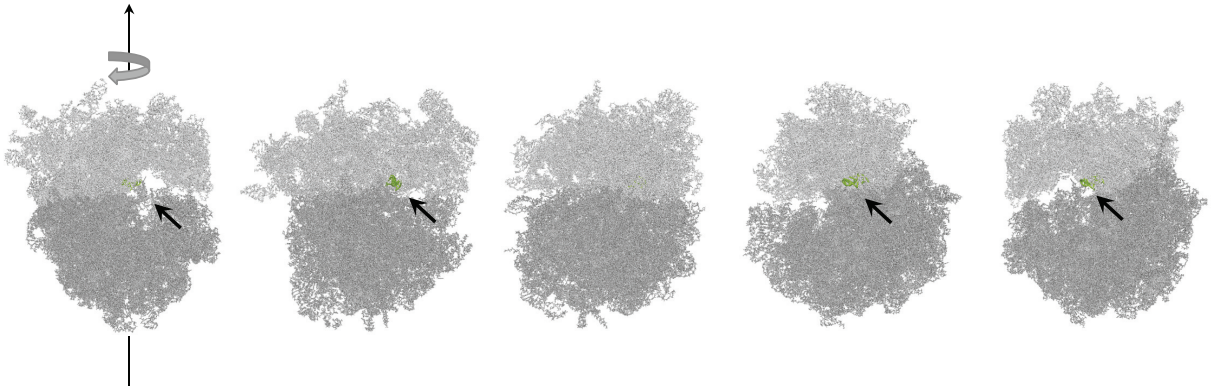

Figure A.2. Helix 18 of the yeast ribosome (green) is located in close proximity to the peptidyl transferase center within the small ribosomal subunit (light gray). Image created with PyMol from PDB files 3O30 and 3O5H (5).

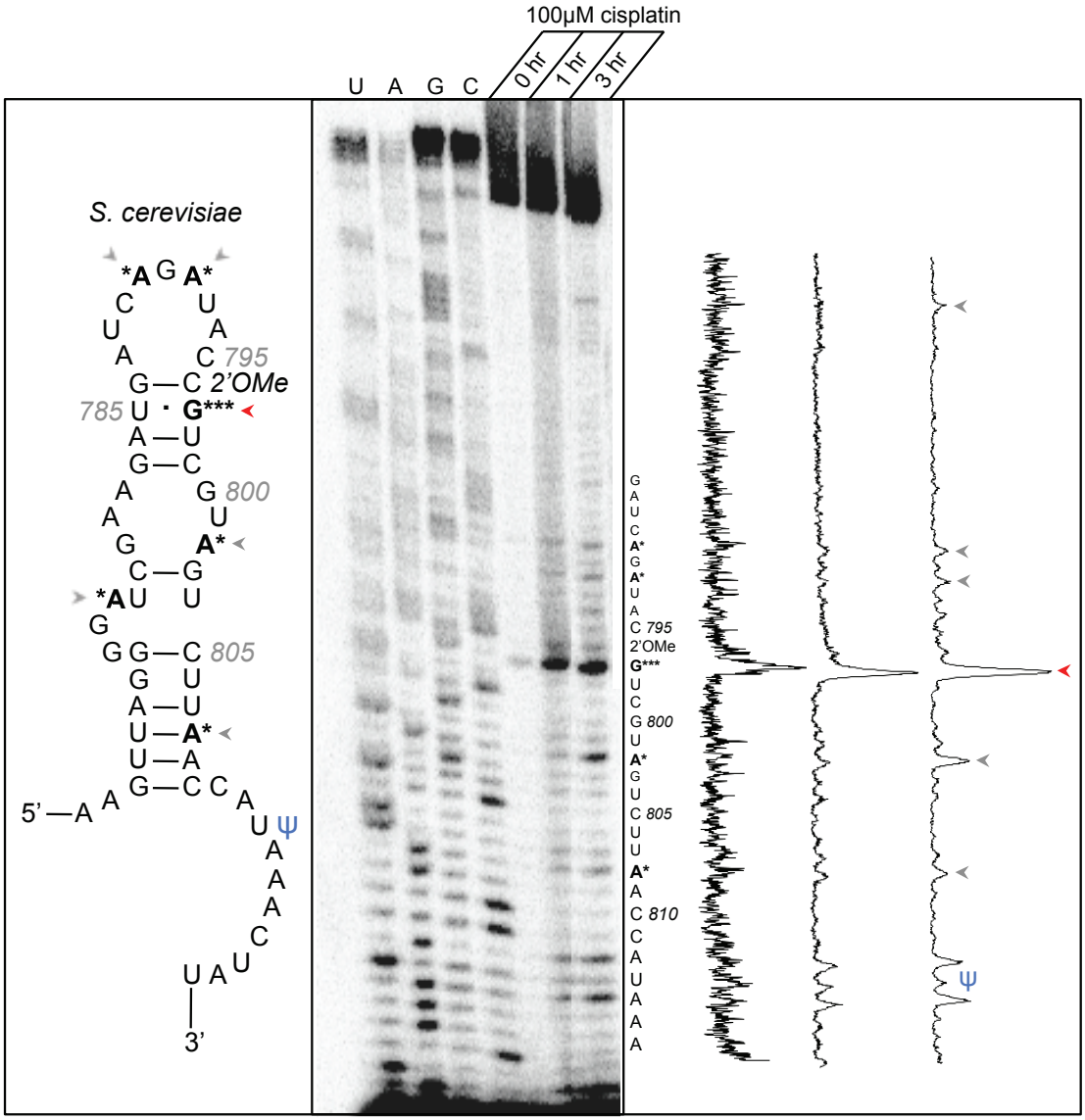

Figure A.3. Primer extension analysis of RNA isolated from 100 mM cisplatin-treated BY4741 at 0, 1, and 3 h shows a time-dependent accumulation of Pt^{2+} at the indicated purine residues (red arrowheads) beginning as early as 1 h following treatment. Specific platination sites are conserved after 6 h continuous exposure to drug (**Figure 2.5**).

Table A.1. Pt atoms accumulated in yeast RNA or DNA

	[Cisplatin]	
	100 mM	**200 mM**
mRNA (Pt/nt, 6 h)	$(1.05 \pm 0.58) \times 10^{-5}$	$(3.53 \pm 0.40) \times 10^{-5}$
rRNA (Pt/nt, 6 h)[a]	$(5.77 \pm 0.96) \times 10^{-5}$	$(12.5 \pm 0.91) \times 10^{-5}$
Total RNA (Pt/nt, 6 h)[a]	$(6.97 \pm 0.69) \times 10^{-5}$	$(18.2 \pm 1.74) \times 10^{-5}$
Total RNA (Pt/nt, 12 h)	$(15.7 \pm 1.59) \times 10^{-5}$	$(56.6 \pm 6.46) \times 10^{-5}$
DNA (Pt/nt, 12 h)	$(60.2 \pm 8.22) \times 10^{-5}$	$(199 \pm 30.2) \times 10^{-5}$
Pt atoms on DNA from one yeast cell (10^4)[b]	2	6
Pt atoms on RNA from one yeast cell (10^4)[b]	7–34	24–120

[a] There is a small but statistically significant increase in Pt/nt values in total RNA vs. rRNA at 200 mM cisplatin treatment, but not at 100 mM cisplatin treatment. A major difference between these two cell populations is the number of viable, dividing cells (60% at 100 uM and only 30% at 200 uM cisplatin treatment, manuscript Table 1). It is possible that the cells in 200 uM cisplatin have begun processing the most heavily platinated rRNA, depleting it from the 'full-length' population.

[b] At 12 h, calculation based on the mass of DNA and RNA in one haploid *S. cerevisiae* cell (*6*).

APPENDIX B

SUPPORTING INFORMATION FOR CHAPTER III: PICAZOPLATIN, AN AZIDE-CONTAINING PLATINUM (II) DERIVATIVE FOR TARGET ANALYSIS BY CLICK CHEMISTRY

Materials and Methods

General Comments: Materials were purchased from commercial vendors and used without further purification unless noted otherwise. Anhydrous THF was purchased from EMD Millipore. 2-Methylpyridine-4-carboxylic acid, $LiAlH_4$, diphenyl phosphorylazide, and 1,8-diazabicycloundec-7-ene (DBU) were purchased from TCI America. K_2PtCl_4 was purchased from Strem Chemicals, Inc. and deuterated solvents were purchased from Cambridge Isotope Laboratories, Inc. Alexa Fluor 488 DIBO alkyne fluorescent dye was purchased from Life Technologies. Column chromatography was performed on Silica Gel Premium R_f (Sorbent Technologies, 75–200 μm).

^1H, ^{13}C, and ^{195}Pt NMR spectra were recorded in d_6-acetone or $CDCl_3$ using a Varian Mercury 300 MHz (^1H: 300.09 MHz), Varian Inova 500 MHz (^1H: 500.11 MHz, ^{13}C: 125.76 MHz), or Bruker Advance III HD 600 MHz (^1H: 600.02 MHz, ^{195}Pt: 128.99 MHz) NMR spectrometer with Prodigy multinuclear broadband cryoprobe. Chemical shifts (δ) are expressed in ppm relative to the residual acetone (^1H: 2.05 ppm) or $CHCl_3$ (^1H: 7.27 ppm, ^{13}C: 77.23) or the external reference K_2PtCl_4 (^{195}Pt: –1604 ppm). IR spectra were obtained from neat solids on a Nicolet 6700 FT-IR instrument with diamond crystal ATR attachment. Gels were visualized with methylene blue stain or radiolabelled phosphate imaging (GE Storm 825), and UV exposure (AlphaImager HP System). High resolution mass spectra were recorded on a JEOL MS-Route mass spectrometer. MALDI spectra were acquired on an Applied Biosystems 4700 Proteomics Analyzer instrument at the Oregon State University mass spectrometry facility. The project described was supported, in part, by Award Number P30ES000210 from the National Institute of Environmental Health Sciences (NIEHS), National Institutes of Health (NIH). The content herein is solely the responsibility of the authors and does not necessarily represent the official views of NIEHS or NIH. The authors acknowledge and sincerely

thank the Biomolecular Mass Spectrometry Core of the Environmental Health Sciences Core Center at Oregon State University.

All DNA substrates were purchased directly from Integrated DNA Technologies, Inc., dissolved in nanopure ddH_2O to a final stock concentration of 1 or 10 mM, and used directly without further purification. The yeast sarcin-ricin loop (SRL) RNA construct was purchased from Dharmacon, Inc., 2'-ACE deprotected according to the manufacturer's protocol, and stored as a 1 mM solution in nanopure ddH_2O. All DNA and RNA substrates were stored in aliquots at –30 °C.

5-(Azidomethyl)-2-methylpyridine (ligand): 2-Methylpyridine-4-carboxylic acid (1.00 g, 7.3 mmol) suspended in dry THF (20 mL) was cooled on ice and purged with N_2. A solution of $LiAlH_4$ (0.41 g, 10.8 mmol) in dry THF (20 mL) under N_2 was slowly added to the carboxylic acid. Upon completion, the flask was removed from the ice and stirred another hour at rt. The reaction was quenched carefully with H_2O (0.5 mL) and then ~10% aq. KOH soln (0.5 mL). The slurry was dried ($MgSO_4$), filtered, and evaporated *in vacuo* to afford the crude alcohol as a thick yellow oil (0.28 g, 2.27 mmol). To a solution of the crude oil (0.28 g, 2.27 mmol) in toluene (10 mL) was slowly added diphenyl phosphorylazide (0.60 mL, 2.81 mmol), then DBU (0.45 mL, 2.95 mmol), and the mixture stirred in the dark at rt for 18 h. The reaction mixture was then washed with 1M HCl soln (3 x 20 mL) and the combined aqueous layers were neutralized with an excess of solid $NaHCO_3$. The aqueous layer was extracted with Et_2O (5 x 30 mL), dried (Na_2SO_4), and evaporated *in vacuo* to obtain a light-yellow oil. The oil was purified by flash silica gel column chromatography (EtOAc) to afford the ligand (0.19 g, 1.3 mmol, 18% from the acid) as a pale-yellow oil. R_f = 0.50 (EtOAc). ^{1}H NMR (500 MHz, $CDCl_3$): δ 8.45 (Ar *H*, d, 1H, *J* = 2.3 Hz), 7.56 (Ar *H*, dd, 1H, *J* = 2.3, 8.0 Hz), 7.19 (Ar *H*, d, 1H, *J* = 8.0 Hz), 4.33 (C*H*$_2$N$_3$, s, 2H), 2.57 (C*H*$_3$, s, 3H); ^{13}C NMR (126 MHz, $CDCl_3$): δ 158.8, 148.8, 136.4, 128.2, 123.5 (Ar *C*), 52.1 (*C*H_2N_3), 24.3 (*C*H_3) ; IR ν (N_3), very strong, 2097 cm.$^{-1}$

***cis*-Ammine(5-azidomethyl-2-methylpyridine)diiodoplatinum(II), iodinated picazoplatin:** To a clear-red solution of K_2PtCl_4 (0.50 g, 1.20 mmol) in H_2O (15 mL)

was added KI (1.0 g, 6.0 mmol) and the reaction was stirred in the dark until all of the KI had dissolved. 5-(Azidomethyl)-2-methylpyridine (0.13 g, 0.96 mmol) in H_2O (10 mL) was added dropwise over ca. 1 h. The resulting brown precipitate was then filtered and washed with cold H_2O and re-suspended in H_2O (10 mL). To this suspension was slowly added 30% aq. NH_3 soln (0.25 mL, 4 mmol) and the reaction watched closely for the brown solid to turn yellow in color. After ca. 2 h stirring at rt, the yellow solid was filtered and washed with excess H_2O and dried *in vacuo*. The crude complex was purified by flash silica gel column chromatography (1:1 acetone/benzene) to furnish the product (0.13 g, 0.22 mmol, 19%) as a yellow solid. R_f = 0.64 (1:1 acetone/benzene). ^{1}H NMR (500 MHz, d_6-acetone): δ 9.04 (Ar *H*, d, 1H, *J* = 2.1 Hz, $^3J_{Pt\text{-}H}$ = 37 Hz), 7.85 (Ar *H*, dd, 1H, *J* = 2.1, 8.1 Hz), 7.53 (Ar *H*, d, 1H, *J* = 8.1 Hz), 4.63 (C*H*$_2$N$_3$, s, 2H), 3.13 (C*H*$_3$, s, 3H). ^{13}C NMR (126 MHz, d_6-acetone): δ 161.7, 153.3, 138.8, 132.4, 127.7 (Ar *C*), 51.3 (*C*H$_2$N$_3$), 26.8 (*C*H$_3$) ^{195}Pt NMR (107.5 MHz, d_6-acetone): δ –3259 (Pt). HRMS (ESI) m/z calculated for $C_7H_{12}N_5I_2Pt$, 614.8830 (M^++H); found, 614.8852. IR ν(N_3), very strong, 2095 cm^{-1}.

Picazoplatin, *cis*-ammine(5-azidomethyl-2-methylpyridine)dichloroplatinum(II), 1: *Cis*-ammine(5-azidomethyl-2-methylpyridine)diiodoplatinum(II) (0.133 g, 0.22 mmol) was dissolved in a minimal amount of acetone. This yellow-orange solution was slowly dripped into a solution of $AgNO_3$ (0.072 g, 0.43 mmol) in H_2O (10 mL) and the solution stirred in the dark for 2 h. The resulting yellow-opaque solution was placed under high vacuum with gentle heating for 15 min, then filtered through a 0.2 μm syringe filter. 1 M HCl soln (ca. 4 drops) and KCl (1.0 g) were added to the clear-yellow filtrate, and the solution left to sit in the refrigerator overnight. The next day the yellow precipitate was filtered, rinsed with water, and dried in a dessicator to afford a light-yellow solid (0.052 g, 0.12 mmol, 11 % from K_2PtCl_4). ^{1}H NMR (300 MHz, d_6-acetone): δ 9.34 (Ar *H*, d, 1H, , *J* = 2.0 Hz, $^3J_{Pt\text{-}H}$ = 37 Hz), 7.85 (Ar *H*, dd, 1H, *J* = 2.0, 8.1 Hz), 7.54 (Ar *H*, d, 1H, *J* = 8.1 Hz); 4.64 (C*H*$_2$N$_3$, s, 2H); 3.23 (C*H*$_3$, s, 3H); ^{195}Pt NMR (129 MHz, d_6-acetone): δ –2041 (Pt); HRMS (ESI) m/z calculated for $NaC_7H_{11}N_5Cl_2Pt$, 453.9939 (M^++Na); found, 453.9962; IR ν (N_3), very strong, 2098 cm^{-1}.

5-(Dimethylamino)-N-(2-propynyl)-1-napthalenesulfonamide (dansyl alkyne fluorophore): The dansyl alkyne was synthesized according to previously published methods (Bolletta, F.; Fabbri, D.; Lombardo, M.; Prodi, L.; Trombini, C.; Zaccheroni, N. *Organometallics* **1996**, *15*, 2415-2417).

Platinum activation (aquation): *Cis*-ammine(5-azidomethyl-2-methyl pyridine)diiodoplatinum(II), iodinated picazoplatin, (3.0 mg, 4.89 μmol) was added to a solution of $AgNO_3$ in ddH_2O (10 mM, 1 mL). The solution was incubated at 50 °C for 4 to 18 h with stirring, at which time AgI precipitated as a white solid and was separated by centrifugation (10,000 RPM for 10 min). The resulting light orange supernatant was removed and used for DNA and RNA binding studies. Solutions were stored in the dark at 4 °C and used for up to 1 week.

Platinum—DNA Duplex Binding (Figure 3.2a): The DNA duplex (280 μM each of 5'-T_5GGT_6-3' and 5'-A_6CCA_5-3', typically 28 nmol) was folded by rapid heating to 90 °C and slow cooling to 4 °C in 10 mM Na_2PO_4 (pH 7.0), 100 mM $NaNO_3$, and 1 mM $Mg(NO_3)_2$. An activated solution of *cis*-ammine(5-azidomethyl-2-methylpyridine)diiodoplatinum(II) was added in 2-fold excess and the solution was incubated at 37 °C for 4 h. Platinum bound DNA was purified with Sephadex G-25 Medium size exclusion resin (GE Healthcare) on laboratory prepared spin columns (BioRad) to remove unbound platinum. The eluent was dried to completion by SpeedVac and the remaining pellet was either resuspended in ddH_2O for click reactions or redissolved in a 50% v/v solution of ddH_2O and formamide without loading dye for cleaner PAGE analysis and UV imaging.

Platinum—DNA Duplex Click reaction (Figure 3.2a): Sodium ascorbate (18 μL, 10 mM), CuI (18 μL, 10 mM), dansyl alkyne (10 μL, 2mM), and Et_3N (10 μL, 7.2 M) were added to an aqueous solution of Pt-bound DNA (18 μL, 180 μM). The samples were incubated at 50 °C for 30 min to 4 h. The samples were then purified with Sephadex G-25 Medium spin-columns. The samples were dried *in vacuo* and then re-suspended in an equal volume mixture of ddH_2O and formamide. The solutions were then analyzed using

20% (29:1) mono/bis polyacrylamide gels.

Platinum—DNA Single Strand Binding (Figure 3.2c): Single-stranded GG DNA (80 μM of 5'- T_5GGT_6-3', typically 8 nmol) for MALDI- MS analysis was reacted with activated *cis*-ammine(5-azidomethyl-2-methylpyridine)diiodoplatinum(II) in 4-fold excess at 37 °C for 18 h. Platinum-bound DNA was purified with Sephadex G-25 Medium size exclusion resin (GE Healthcare) on laboratory prepared spin columns (BioRad) to remove unbound platinum. The eluent was dried to completion by SpeedVac and the remaining pellet was stored at –30 °C until use.

Platinum—DNA Single Strand Click reaction (Figure 3.2c): The platinum-bound DNA pellet was resuspended in a solution of Na_2PO_4 (pH 7.0) (88.5 μL, 100 mM), $CuSO_4$ (5 μL, 1 mM), dansyl alkyne (2.5 μL, 2 mM), and sodium ascorbate (4 μL, 5 mM). This solution was reacted at 50 °C for 1 h and subsequently purified with Sephadex G-25 Medium spin-columns. The samples were dried to completion by SpeedVac and the remaining pellet was stored at –30 °C until use.

MALDI Mass Spectrometry (Figure 3.2c): MALDI-MS samples were prepared according to the previously described protocol (Chapman, E. G.; DeRose, V. J. *J. Am Chem. Soc*. **2010**, *132*, 1946-1952). Briefly, dried DNA samples were re-suspended in deionized water and purified using C18 ZipTips. ZipTips were washed by aspiration three times with 1:1 MeCN/H_2O and equilibrated by washing three times with 0.1% trifluoroacetic acid (TFA). DNAs were bound to the tip by repeated aspiration of the analyte solution. Bound DNA was washed three times by aspiration with 0.1% TFA, three times with deionized water, and then eluted from the column using two washes of 1:1 MeCN/H_2O. The eluent was dried to completion by SpeedVac and re-suspended in a matrix consisting of 375 mM 2',4',6'-trihydroxyacetophenone (THAP, Sigma-Aldrich), 30 mM diammonium citrate in 3:1 EtOH/H_2O, with added NH_4^+ loaded Dowex cation exchange beads (Aldrich) and applied to the sample plate.

Platinum—DNA Hairpin Binding (Figure 3.3b): The DNA hairpin (400 μM of 5'-

TATGGTATTTTTATACCATA-3', typically 40 nmol) and added trace ^{32}P-labeled DNA hairpin was folded by rapid heating to 90 °C and slow cooling to 4 °C in 10 mM Na_2PO_4 (pH 7.0), 100 mM $NaNO_3$, and 1 mM $Mg(NO_3)_2$. An activated solution of *cis*-ammine(5-azidomethyl-2-methylpyridine)diiodoplatinum(II) was added in 2-fold excess and the solution was incubated at 37 °C for 18 h. Pt-bound DNA was purified with Sephadex G-25 Medium size exclusion resin (GE Healthcare) on laboratory prepared spin columns (BioRad) to remove unbound platinum. The eluent was dried to completion by SpeedVac and the remaining pellet was stored at –30 °C until use.

Platinum—DNA Hairpin Click reaction (Figure 3.3b): The platinum-bound DNA pellet was resuspended in one of two click-capable solutions: (A) Na_2PO_4 (pH 7.0) (88.5 μL, 100mM), $CuSO_4$ (5 μL, 1 mM), dansyl alkyne (2.5 μL, 2 mM), and sodium ascorbate (4 μL, 5 mM) or (B) Na_2PO_4 (pH 7.0) (88.5 μL, 100mM), CuI (5 μL, 1 mM), Et_3N (2 μL, 2 mM), dansyl alkyne (2.5 μL, 2 mM), and sodium ascorbate (4 μL, 5 mM). These solutions were prepared either in the presence or absence of 0.6% v/v CH_3CN.

Platinum—RNA Binding (Figure 3.4b): A solution of 100 μM SRL RNA (5'-UGA ACU UAG UAC GAG AGG AAC AGU UCA CCC CCC GCC GCG AAG CUA CCA UCC GCU-3', typically 10 nmol) was folded by rapid heating to 90 °C and slow cooling to 4 °C in 10 mM Na_2PO_4 (pH 7.0), 100 mM $NaNO_3$, and 1 mM $Mg(NO_3)_2$. Activated **1** was added in 4-fold excess and the mixture was incubated 37 °C for 18 h. Pt-bound RNA was purified with Sephadex G-25 Medium size exclusion resin (GE Healthcare) on laboratory prepared spin columns (BioRad) to remove unbound Pt. The eluent was dried to completion by SpeedVac and the remaining pellet was stored at –30 °C until use.

Platinum—RNA Click reaction (Figure 3.4b): The Pt-bound RNA pellet was resuspended in a buffered premixed solution containing 0.4 or 0.8 equivalents CuI (4 or 8 μL, 1 mM), Et_3N (2 μL, 2 mM), CH_3CN (6 μL , 10% v/v), excess dansyl alkyne (2.5 μL, 2 M), and pH 7.0-buffered sodium phosphate (85.5 μL or 81.5 μL, 100 mM, pH 7.0). This mixture was incubated at 50 °C for 1 h and purified by Sephadex G-25 Medium spin-columns. Samples were analyzed by dPAGE as described for DNA, on a 10 cm gel.

Cell Cultures and Treatments (Figure 3.5): *S. cerevisiae* strain BY4741 (MATa; his3Δ1; leu2Δ0; met15Δ0; ura3Δ0) was a gift from the Stevens laboratory at the University of Oregon. Plated cells were grown on YEPD agar plates (1% yeast extract, 2% peptone, 2% glucose, and 2% agar). Liquid cultures were grown on Synthetic Complete medium (SC) consisting of 0.67% yeast nitrogen base and 2% glucose supplemented with amino acids and nucleotide bases and maintained in the dark at 30°C with shaking at 200 rpm. Culture growth was measured by absorbance at 600 nm (1 $AU_{600} = 2.0 \times 10^7$ cells/mL). A 5 mM picazoplatin stock was used for all picazoplatin treatments. Yeast cultures were pregrown to an OD_{600} of 5 (10.0 x 10^7 cells/mL) and then diluted to an OD_{600} of 0.25 (5.0 x 10^6 cells/mL) in picazoplatin-containing media (final concentration of 0, 250, or 500 μM drug). 10 mL cultures were grown for 12 h at 30°C with shaking at 200 rpm. Total RNA was extracted from picazoplatin-treated yeast using the MasterPure Yeast RNA Purification Kit (Epicentre) according to a modified manufacturer's protocol. Total RNA concentration was calculated using absorbance at 260 nm (1AU = 40 μg/mL) and all samples were dried to completion by SpeedVac and resuspended in ddH_2O to a final normalized concentration of 1 ug/μL.

Total RNA Click Reaction: 1 μL of total RNA was added to a 10 μL aqueous solution containing 0.5 μL (20 U) RiboGuard RNAse Inhibitor (0.5 μL, 20 U, Epicentre) and excess Alexa Fluor 488 DIBO Alkyne (1 μL, 0.5 mM). The reaction proceeded overnight at 37°C. Unreacted fluorophore was removed using an RNeasy mini kit (Qiagen) according to a modified manufacturer's protocol. The 20 μL eluent from the spin column was diluted with 20 μL of formamide and the samples were analyzed on a 10% (29:1) mono/bis polyacrylamide gel (as described previously for *in vitro* click reactions).

Yeast 5.8S Ribosomal RNA Sequence: 5'-AAACUUUCAA CAACGGAUCU CUUGGUUCUC GCAUCGAUGA AGAACGCAGC GAAAUGCGAU ACGUAAUGUG AAΨUGCAGAA UUCCGUGAAU CAUCGAAUCU UUGAACGCAC AUUGCGCCCC UUGGUAUUCC AGGGGGCAUG CCUGUUUGAG CGUCAUUU-3'. Sequence from Rubin *et. al.*[1]

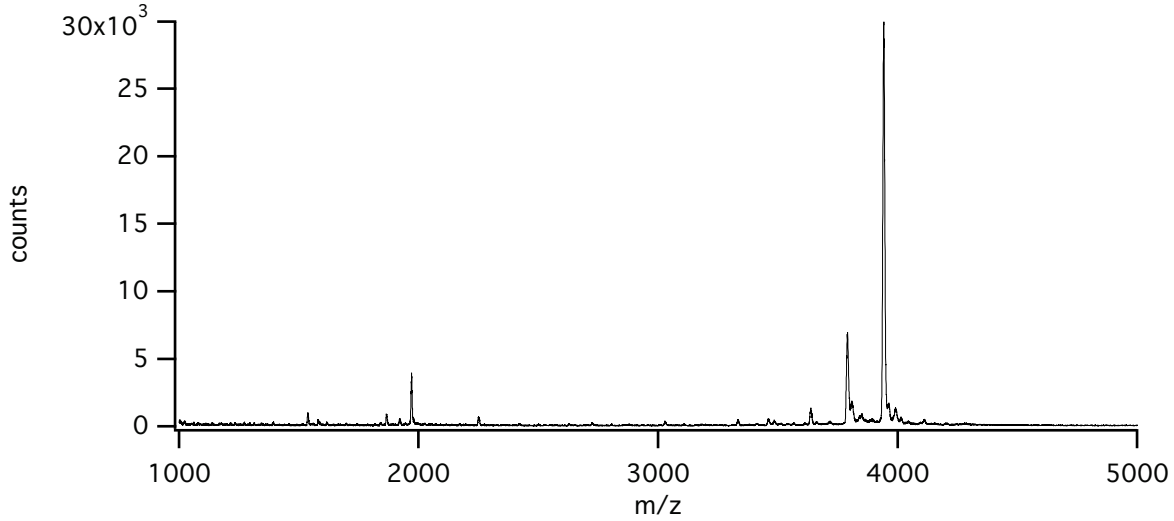

Figure B.1. Complete MALDI spectrum of T_6GGT_5 single-strand DNA oligomer.

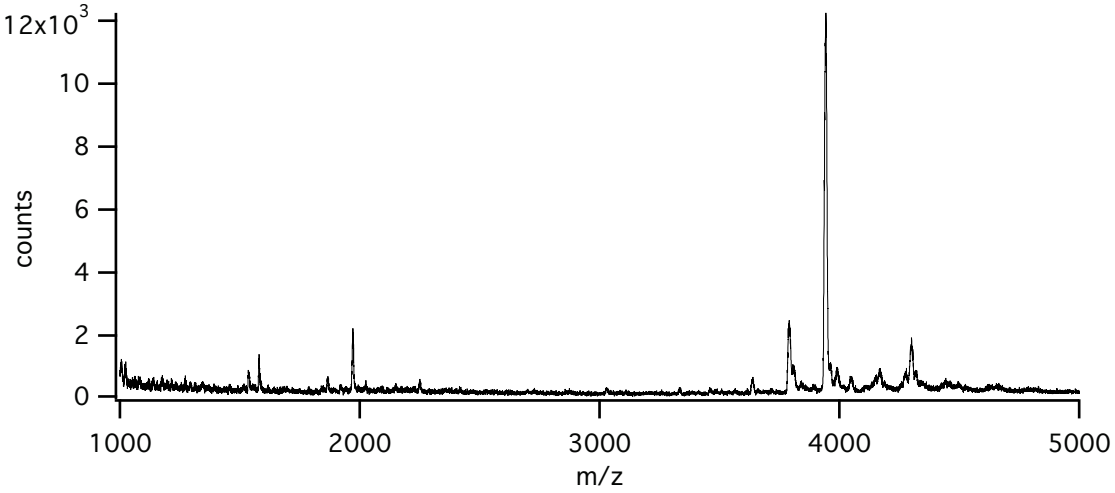

Figure B.2. Complete MALDI spectrum of T_6GGT_5 after binding with picazoplatin (**1**).

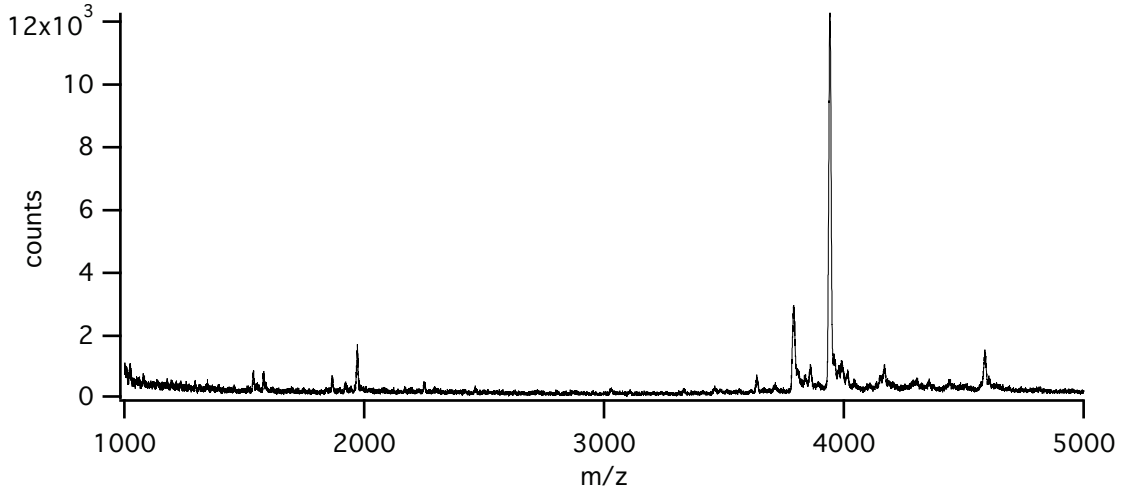

Figure B.3. Complete MALDI spectrum of platinated T_6GGT_5 after click to dansyl alkyne.

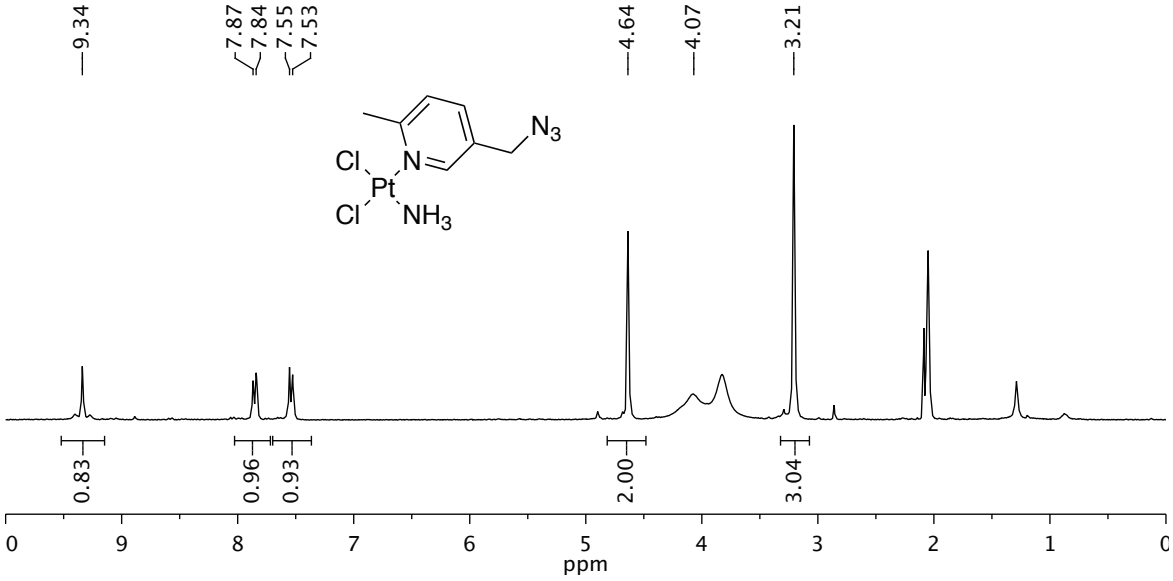

Figure B.4. ^{1}H NMR (300 MHz, d_6-acetone, 298 K) of picazoplatin, **1**.

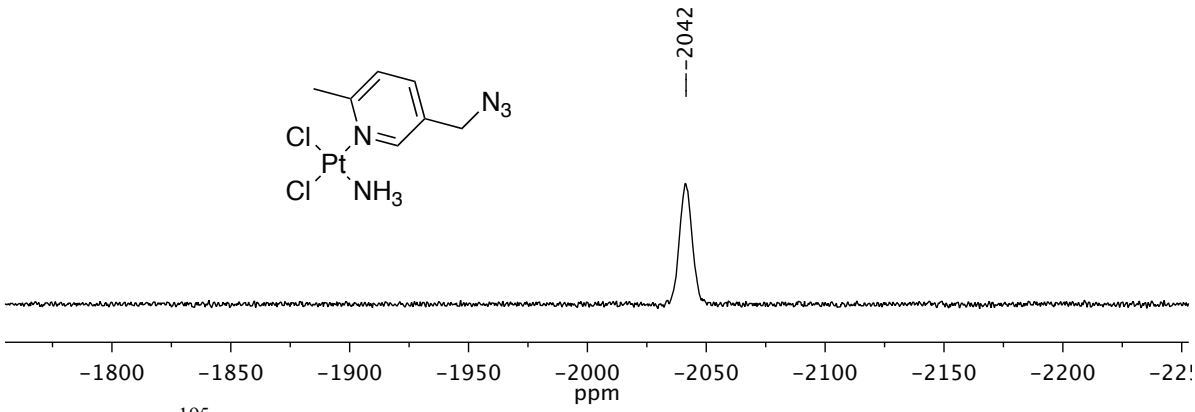

Figure B.5. ^{195}Pt NMR (129 MHz, d_6-acetone, 298 K) of picazoplatin, **1**, baseline corrected.

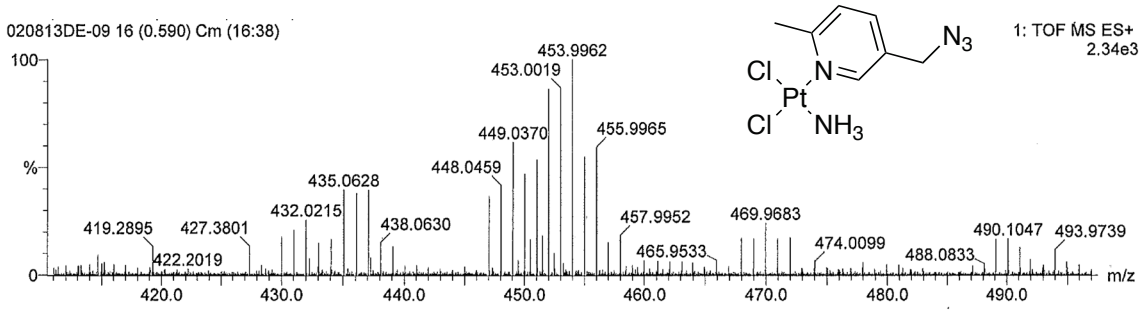

Figure B.6. High-resolution mass spec. of picazoplatin, **1**, with the molecular ion peak ($M+Na^+$) at 453.9962 m/z.

Figure B.7 (Materials and Methods):

Platinum—RNA Binding: A solution of 60 μM SRL RNA (5'-UGA ACU UAG UAC GAG AGG AAC AGU UCA CCC CCC GCC GCG AAG CUA CCA UCC GCU-3', typically 6 nmol) with added trace ^{32}P-labeled SRL RNA was folded by rapid heating to 90 °C and slow cooling to 4 °C in 10 mM phosphate buffer (pH 7.0), 100 mM $NaNO_3$, and 1 mM $Mg(NO_3)_2$. Activated **1** was added in 4-fold excess and the mixture was incubated 37 °C for 18 h. Pt-bound RNA was purified with Sephadex G-25 Medium size exclusion resin (GE Healthcare) on laboratory prepared spin columns (BioRad) to

remove unbound Pt. The eluent was dried to completion by SpeedVac and the remaining pellet was stored at –30 °C until use.

Platinum—RNA Click reaction: The Pt-bound RNA pellet was resuspended in one of two click-capable solutions: (A) Phosphate buffer (pH 7.0) (88.5 µL, 100 mM), $CuSO_4$ (5 µL, 1 mM), dansyl alkyne (2.5 µL, 2 mM), and sodium ascorbate (4 µL, 5 mM) or (B) Phosphate buffer (pH 7.0) (88.5 µL, 100mM), CuI (5 µL, 1 mM), Et_3N (2 µL, 2 mM), dansyl alkyne (2.5 µL, 2 mM), and sodium ascorbate (4 µL, 5 mM). Solutions were prepared in the presence or absence of 0.6% v/v CH_3CN. Reactions were incubated at 50 °C for 1 h ,purified by Sephadex G-25 Medium spin-columns, and analyzed as described for DNA, on an 8 cm PAGE gel.

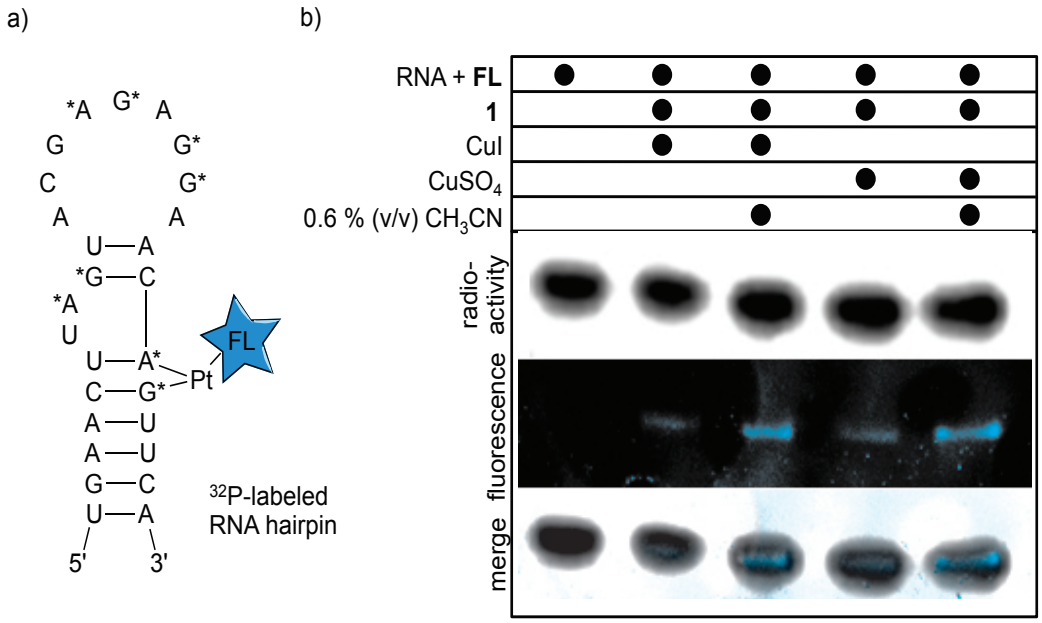

Figure B.7. (a) RNA SRL hairpin with **1** bound and tagged (clicked) with the alkyne fluorophore. Potential Pt binding sites are indicated by starred nucleotides. (b) Fluorescent labeling of RNA SRL mimic hairpin by click chemistry. Lane 1 contains nonplatinated RNA SRL and shows no nonspecific RNA-fluorophore interaction. Lanes 2-5 contain platinated RNA under varying click condition sets; lanes 3 and 5 show efficient RNA-fluorophore labeling in the presence of 0.6% acetonitrile.

APPENDIX C

SUPPORTING INFORMATION FOR CHAPTER IV: CLICK FLUORESCENT LABELING AND ENZYMATIC MAPPING OF PLATINUM (II) COVALENT DRUG MODIFICATIONS IN *SACCHAROMYCES CEREVISIAE* RIBOSOMAL RNA

Materials and Methods

Platinum Drug Treatment and RNA Extraction from *S. cerevisiae*: *S. cerevisiae* strain BY4741 (MATa; his3Δ1; leu2Δ0; met15Δ0; ura3Δ0) was a generous gift from the Stevens Laboratory at the University of Oregon. Cisplatin and oxaliplatin were purchased from Sigma Aldrich. Picazoplatin was synthesized as described previously (1). Plated cells were grown on YEPD agar plates (1% yeast extract, 2% peptone, 2% glucose, and 2% agar). Liquid cultures were grown on Synthetic Complete medium (SC) consisting of 0.67% yeast nitrogen base and 2% glucose supplemented with amino acids and nucleotide bases and maintained in the dark at 30°C with shaking at 200 rpm. Culture growth was measured by absorbance at 600 nm (1 AU600 = 2.0×10^7 cells/mL). A 5 mM cisplatin, oxaliplatin, or picazoplatin stock was used for all platinum treatments. Yeast cultures were pregrown to an OD600 of 5 (10.0×10^7 cells/mL) and then diluted to an OD600 of 0.25 (5.0×10^6 cells/mL) in platinum-containing media (final concentration varying between 0 and 500 μM drug). 10—50 mL cultures were grown for 12 h at 30°C with shaking at 200 rpm. Total RNA was extracted from cisplatin-, oxaliplatin-, or picazoplatin-treated yeast using the MasterPure Yeast RNA Purification Kit (Epicentre) according to a modified manufacturer's protocol. Total RNA concentration was calculated using absorbance at 260 nm (1AU = 40 μg/mL) and all samples were dried to completion by SpeedVac and resuspended in ddH_2O to a final normalized concentration of 10 ug/μL.

Fluorescent Post-Labeling of RNA from Picazoplatin-treated *S. cerevisiae*: 0.5 μL of total RNA was added to a 10 μL aqueous solution containing 0.5 μL (20 U) RiboGuard RNAse Inhibitor (0.5 μL, 20 U, Epicentre) and excess Alexa Fluor 488 DIBO Alkyne (1

μL, 0.5 mM). The reaction proceeded overnight at 37°C. Unreacted fluorophore was removed using an RNeasy mini kit (Qiagen) according to a modified manufacturer's protocol. The 20 μL eluent from the spin column was diluted with 20 μL of formamide and the samples were analyzed on a 10% (29:1) mono/bis polyacrylamide gel. RNA purity and content were assessed with a methylene blue stain. Fluorescence images were collected with an AlphaImager and processed (false colored) using Adobe Photoshop.

Platination of SRL RNA *in vitro*: Synthetic RNA was purchased from Dharmacon, consisting of the model SRL plus a short extended sequence designed for RT primer annealing (italicized). For all *in vitro* studies, cisplatin was aquated as described previously (1). A solution of 100 μM SRL RNA (5'-UGA ACU UAG UAC GAG AGG AAC AGU UCA *CCC CCC GCC GCG AAG CUA CCA UCC GCU*-3', typically 10 nmol) was folded by rapid heating to 90 °C and slow cooling to 4 °C in 10 mM Na_2PO_4 (pH 7.0), 100 mM $NaNO_3$, and 1 mM $Mg(NO_3)_2$. Activated cisplatin was added in 0—2 fold excess and the mixture was incubated 37 °C for 18 h. Non-activated oxaliplatin was added in 0—10 fold excess. Pt-bound RNA was purified with Sephadex G-25 Medium size exclusion resin (GE Healthcare) on laboratory prepared spin columns (BioRad) to remove unbound Pt. The eluent was dried to completion by SpeedVac and the remaining pellet was stored at –30 °C until use.

Primer Extension Analysis of Pt-bound RNA *in vitro*: DNA primers designed for reverse transcription of the model SRL and *S. cerevisiae* rRNA were purchased from Integrated DNA Technologies (5'-AGC GGA TGG TAG CTT CGC GGC-3' for the SRL region *in vitro* and *in vivo* and 5'-CTA TTG CGG TAA CAT TCA TC-3' for the PTC). γ-^{32}P 5′ end-labeling was performed as described previously (2). For primer extension of a synthetically platinated RNA, 100 pmol of the prepared RNA template was annealed to 10 pmol of the SRL DNA primer with trace γ-^{32}P primer and incubated with AMV Reverse Transcriptase (Fermentas) according to a modified manufacturer's protocol for 1.75 h at 42 °C. For the sequencing lanes, a synthetic template DNA (The resulting cDNA products were diluted in loading buffer containing 0.005% (w/v) xylene cyanol and bromophenol blue and analyzed by 12% dPAGE. Bands were visualized using a GE

phosphor screen in conjunction with a Storm phosphor screen imaging system and then quantified with ImageQuant 5.1 and normalized in Excel.

Sequencing reference lanes were generated with a Sequenase Version 2.0 DNA Sequencing kit (USB Corporation) following the manufacturer's protocol, using an appropriate DNA template (Integrated DNA Technologies) and the γ-^{32}P 5′ end-labeled primers used for the primer extension reactions.

Primer Extension Analysis of Pt-bound RNA *in vivo*: For primer extension, 1 μg of RNA template was annealed to 100 pmol of the specified 5′ end-labeled primer in the manufacturer's reaction buffer and incubated in the presence of AMV Reverse Transcriptase (Fermantas) for 1.75 h at 42 °C. The resulting cDNA products were diluted in loading buffer containing 0.005% (w/v) xylene cyanol and bromophenol blue and analyzed by 8% dPAGE. Bands were visualized using a GE phosphor screen in conjunction with a Storm phosphor screen imaging system and then quantified with ImageQuant 5.1 and normalized in Excel. Sequence reference lanes were generated as described above.

Figure Preparations: All figures containing crystal structure data were prepared in PyMOL (www.pymol.org) using PDB files obtained from the RCSB Protein Data Bank.

Table C.1. Estimation of Pt accumulation in different RNAs based on fluorescent labeling following treatment with 250 μM picazoplatin (5 ug reaction). The in-gel detection limit of clicked Alexa Fluor 488 alkyne (in 10% 29:1 mono/bis polyacrylamide) is approximately 1 pmol, and we estimate that we can visualize concentrations as low as 1 Pt per 10,000 nt in these RNA species (data not shown). Mol•nt RNA determined using an average nucleotide molecular weight of 340 g•nt.

RNA (ug)	mol•nt RNA	Total nt	mol RNAs	mol AF488*	Pt/RNA
rRNA 4.5 ug	1.4e-8	~6000/ribosome	2.2e-12	0.94e-12	~0.4
tRNA 0.5 ug	1.5e-9	~100/tRNA	1.5e-11	0.80e-12	~0.8

*Mol of Alexa Fluor 488 alkyne in each band, based on calibration gel. Each Alexa Fluor 488 alkyne corresponds to one Pt atom, assuming 100% click efficiency.

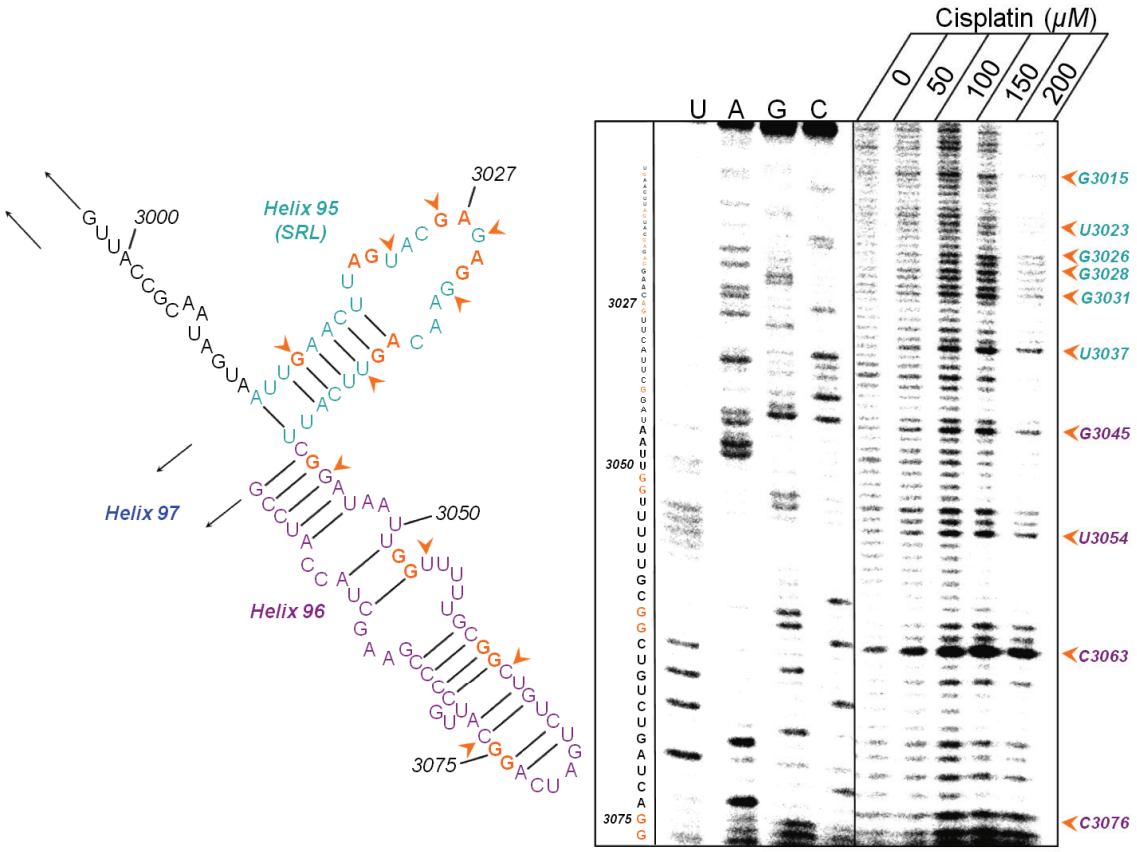

Figure C.1. Full sequence analyzed by primer extension analysis of the *S. cerevisiae* sarcin ricin loop and adjacent helices from ribosomal RNA treated with 0—200 μM cisplatin. Dideoxy sequencing ladder labeled by A, U, C, and G. Cisplatin-induced stop sites are denoted by arrowheads and summarized in the secondary structure with orange lettering. Nucleotides which were not analyzed in this particular experiment are in gray.

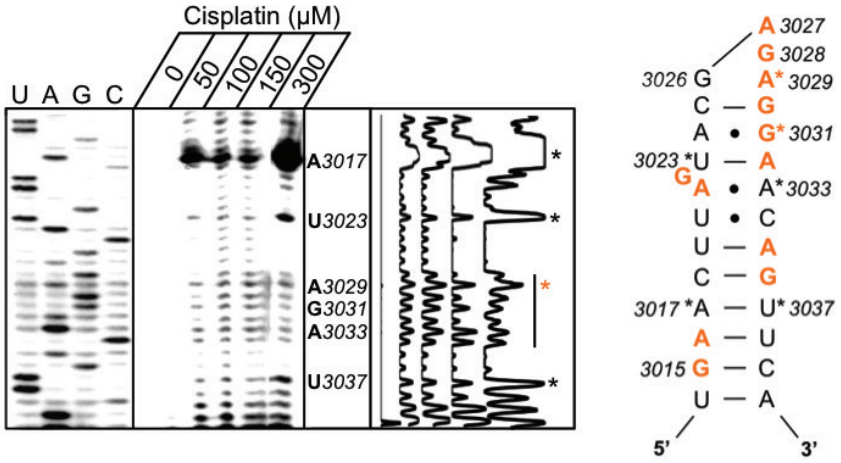

Figure C.2. Primer extension analysis of the sarcin-ricin loop (SRL) region in ribosomal RNA extracted from *S. cerevisiae* treated with 0—300 μM cisplatin. This experiment used a primer designed to probe further upstream than the one in Figure 3. Dideoxy sequencing ladder labeled by A, U, C, and G. Cisplatin-induced stop sites are denoted by asterisks (*) and represent nucleotides 3' to a stable platinum adduct. Colored asterisk denotes primary stop site in terminal SRL region according to line plot analysis. Predicted platinum crosslinks between adjacent purines based on experimental results are colored in bold on the *S. cerevisiae* secondary structure map.

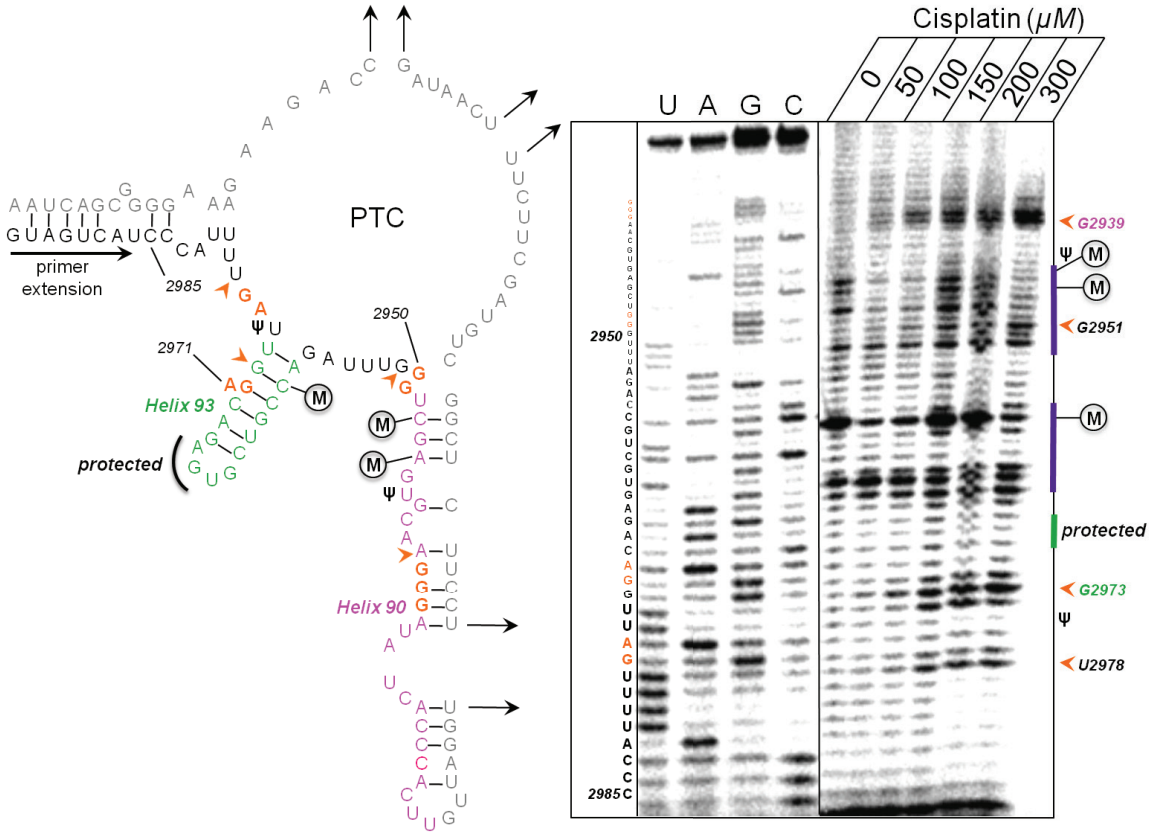

Figure C.3. Primer extension analysis of the *S. cerevisiae* peptidyl transferase center from ribosomal RNA treated with 0—300 μ M cisplatin. Cisplatin-induced stop sites are denoted by arrowheads and summarized in the secondary strucutre with orange lettering. Endogenous ribosomal RNA modifications (i.e. 2'-OCH_3) and regions of stable secondary structure which also inhibit primer extension in the absence of platinum are denoted by red lines. Nucleotides which were not analyzed in this particular experiment are in gray. Nucleotides protected from Pt indicated in green.

REFERENCES CITED

Chapter I:

(1) Chapman, E. G.; Hostetter, A. A.; Osborn, M. F.; Miller, A. L.; DeRose, V. J. *Met. Ions Life Sci.* **2011**, *9*, 347.

(2) Hostetter, A. A; Osborn, M. F.; DeRose, V. J. *ACS Chem. Biol.* **2012**, *7*, 218.

(3) White, J. D.; Osborn, M. F.; Moghaddam, A. D.; Guzman, L. E.; Haley, M. M.; DeRose, V. J. *J. Am. Chem. Soc.* **2013**, *135*, 11680.

(4) Rosenberg, B.; Van Camp, L.; Grimley, E. B.; Thomson, A. J. *J. Biol. Chem.* **1967**, *242*, 1347.

(5) Mjos, K. D.; Orvig, C. *Chem. Rev.* **2014**. [Epub ahead of print]

(6) Rosenberg, B. B. **1971**, *2*, 42.

(7) Deconti, R. C.; Toftness, B. R.; Lange, R. C.; Creasey, W. A. *Cancer Res.* **1973**, *33*, 1310.

(8) Wheate, N. J.; Walker, S.; Craig, G. E.; Oun, R. *Dalton Trans.* **2010**, *39*, 8113.

(9) Harder, H. C.; Rosenberg, B. *Int. J. Cancer* **1970**, *6*, 207.

(10) Jamieson, E. R.; Lippard, S. J. *Chem. Rev.* **1999**, *99*, 2467.

(11) Hambley, T. W. *Inorg. Chem.* **1991**, *30*, 937.

(12) Ciarimboli, G. *Anticancer Res.* **2014**, *1*, 547.

(13) Lippert, B. *Coord. Chem. Rev.* **1999**, *182*, 263.

(14) Fichtinger-Schepman, A. M.; Van der Veer, J. L.; den Hartog, J. H.; Lohman, P. H.; Reedijk, J. *Biochemistry* **1985**, *24*, 707.

(15) LeDoux, S. P.; Druzhyna, N. M.; Hollensworth, S. B.; Harrison, J. F.; Wilson, G. L. *Neuroscience* **2007**, *145*, 1249.

(16) Lindauer, E.; Holler, E. *Biochem. Pharmacol.* **1996**, *52*, 7.

(17) Akaboshi, M.; Kawai, K.; Tanaka, Y.; Takada, J.; Fujii, N. *Biol. Trace Elem. Res.* **1999**, *71-72*, 585.

(18) Gemba, M.; Nakatani, E.; Teramoto, M.; Nakano, S. *Toxicol. Lett.* **1987**, *38*, 291.

(19) Yang, Z.; Schumaker, L. M.; Egorin, M. J.; Zuhowski, E. G.; Guo, Z.; Cullen, K. J. *Clin. Cancer Res.* **2006**, *12*, 5817.

(20) Giurgiovich, A. J.; Diwan, B. A.; Olivero, O. A.; Anderson, L. M.; Rice, J. M.; Poirier, M. C. *Carcinogenesis* **1997**, *18*, 93.

(21) Olivero, O. A.; Semino, C.; Kassim, A.; Lopez-Larraza, D. M.; Poirier, M. C. *Mutat. Res.* **1995**, *346*, 221.

(22) Samimi, G.; Katano, K.; Holzer, A. K.; Safaei, R.; Howell, S. B. *Mol. Pharmacol.* **2004**, *66*, 25.

(23) Samimi, G.; Safaei, R.; Katano, K.; Holzer, A. K.; Rochdi, M.; Tomioka, M.; Goodman, M.; Howell, S. B. *Clin. Cancer Res.* **2004**, *10*, 4661.

(24) Klein, A. V.; Hambley, T. W. *Chem. Rev.* **2009**, *109*, 4911.

(25) Katano, K.; Safaei, R.; Samimi, G.; Holzer, A. K.; Tomioka, M.; Goodman, M.; Howell, S. B. *Clin. Cancer Res.* **2004**, *10*, 4578.

(26) Molenaar, C.; Teuben, J.-M.; Heetebrij, R. J.; Tanke, H. J.; Reedijk, J. *J. Biol. Inorg. Chem.* **2000**, *5*, 655.

(27) Kalayda, G. V.; Zhang, G.; Abraham, T.; Tanke, H. J.; Reedijk, J. *J. Med. Chem.* **2005**, *48*, 5191.

(28) Safaei, R.; Katano, K.; Larson, B. J.; Samimi, G.; Holzer, A. K.; Naerdemann, M.; Tomioka, M.; Goodman, M.; Howell, S. B. *Clin. Cancer Res.* **2005**, *756*, 756.

(29) Yu, F.; Megyesi, J.; Price, P. M. *J. Renal Physiol*. **2008**, *72205*, 44.

(30) Mandic, A.; Hansson, J.; Linder, S.; Shoshan, M. C. *J. Biol. Chem.* **2003**, *278*, 9100.

(31) Sharp, P. A. *Cell* **2009**, *136*, 577.

(32) Tay, Y.; Rinn, J.; Pandolfi, P. P. *Nature* **2014**, *505*, 344.

(33) Spacková, N.; Sponer, J. *Nucleic Acids Res.* **2006**, *34*, 697.

(34) Shi, X.; Khade, P. K.; Sanbonmatsu, K. Y.; Joseph, S. *J. Mol. Biol.* **2012**, *419*, 125.

(35) Guan, L.; Disney, M. D. *ACS Chem. Biol.* **2012**, *7*, 73.

(36) Auffinger, P.; Grover, N.; Westhof, E. *Met. Ions Life Sci.* **2011**, *9*, 1.

(37) Hermann, T.; Westhof, E. *Structure* **1998**, *6*, 1303.

(38) Freisinger, E.; Sigel, R. K. O. *Coord. Chem. Rev.* **2007**, *251*, 1834.

(39) Pyle, A. M. *J. Biol. Inorg. Chem.* **2002**, *7*, 679.

(40) Acharya, P.; Acharya, S.; Cheruku, P.; Amirkhanov, N. V.; Foldesi, A.; Chattopadhyaya, J. *J. Am. Chem. Soc.* **2003**, *125*, 9948.

(41) Legault, P.; Pardi, A. *J. Am. Chem. Soc.* **1997**, *119*, 6621.

(42) Chapman, E. G.; DeRose, V. J. *J. Am. Chem. Soc.* **2010**, *132*, 1946.

(43) Rijal, K.; Chow, C. S. *Chem. Commun. (Camb).* **2009**, *1*, 107.

(44) Papsai, P.; Snygg, A. S.; Aldag, J.; Elmroth, S. K. C. *Dalton Trans.* **2008**, *38*, 5225.

(45) Papsai, P.; Aldag, J.; Persson, T.; Elmroth, S. K. C. *Dalton Trans.* **2006**, *29*, 3515.

(46) Hedman, H. K.; Kirpekar, F.; Elmroth, S. K. C. *J. Am. Chem. Soc.* **2011**, *133*, 11977.

(47) Hägerlöf, M.; Hedman, H.; Elmroth, S. K. C. *Biochem. Biophys. Res. Commun.* **2007**, *361*, 14.

(48) Hostetter, A. A.; Chapman, E. G.; DeRose, V. J. *J. Am. Chem. Soc.* **2009**, *131*, 9250.

(49) Yu, Y. T.; Maroney, P. A.; Darzynkiewicz, E.; Nilsen, T. W. *RNA* **1995**, *1*, 46.

(50) Fabrizio, P.; Abelson, J. *Nucleic Acids Res.* **1992**, *20*, 3659.

(51) Woodson, S. A. *Curr. Opin. Chem. Biol.* **2005**, *9*, 104.

(52) Jung, Y.; Lippard, S. J. *J. Biol. Chem.* **2006**, *281*, 1361.

(53) Jordan, P.; Carmo-Fonseca, M. *Nucleic Acids Res.* **1998**, *26*, 2831.

(54) Tornaletti, S.; Patrick, S. M.; Turchi, J. J.; Hanawalt, P. C. *J. Biol. Chem.* **2003**, *287*, 35791.

(55) Ang, W. H.; Myint, M.; Lippard, S. J. *J. Am. Chem. Soc.* **2010**, *132*, 7429.

(56) Damsma, G. E.; Alt, A.; Brueckner, F.; Carrell, T.; Cramer, P. *Nat. Struct. Mol. Biol.* **2007**, *14*, 1127.

(57) Schmittgen, T. D.; Ju, J. F.; Danenberg, K. D.; Danenberg, P. V. *Int. J. Oncol.* **2003**, *23*, 785.

(58) Danenberg, P. V; Shea, L. C.; Danenberg, K. D.; Horikoshi, T. *Nucleic Acids Res.* **1991**, *19*, 3123.

(59) Rosenberg, J.; Sato, P. H. *Mol. Pharmacol.* **1987**, *33*, 611.

(60) Rosenberg, J.; Sato, P. H. *Mol. Pharmacol.* **1993**, *43*, 491.

(61) Heminger, K. A.; Hartson, S. D.; Rogers, J.; Matts, R. L. *Arch. Biochem. Biophys.* **1997**, *344*, 200.

(62) Parker, R. *Genetics* **2012**, *191*, 671.

(63) Isken, O.; Maquat, L. E. *Genes Dev.* **2007**, *21*, 1833.

(64) Hamill, S.; Wolin, S. L.; Reinisch, K. M. **2010**, *34*, 15045.

(65) Lafontaine, D. L. J. *Trends Biochem. Sci.* **2010**, *35*, 267.

(66) Alexandrov, A.; Chernyakov, I.; Gu, W.; Hiley, S. L.; Hughes, T. R.; Grayhack, E. J.; Phizicky, E. M. *Mol. Cell* **2006**, *21*, 87.

(67) Amitsur, M.; Levitz, R.; Kaufmann, G. *EMBO J.* **1987**, *6*, 2499.

(68) Schwer, B.; Sawaya, R.; Ho, C. K.; Shuman, S. *Proc. Natl. Acad. Sci. U. S. A.* **2004**, *101*, 2788.

(69) Nagy, P. D.; Carpenter, C. D.; Simon, A. E. *Proc. Natl. Acad. Sci. U. S. A.* **1997**, *94*, 1113.

(70) Ougland, R.; Zhang, C.-M.; Liiv, A.; Johansen, R. F.; Seeberg, E.; Hou, Y.-M.; Remme, J.; Falnes, P. Ø. *Mol. Cell* **2004**, *16*, 107.

(71) Vågbø, C. B.; Svaasand, E. K.; Aas, P. a; Krokan, H. E. *DNA Repair (Amst).* **2013**, *12*, 188.

(72) Mei, Y.; Stonestrom, A.; Hou, Y.-M.; Yang, X. *Protein Cell* **2010**, *1*, 795.

(73) Nawrot, B.; Sochacka, E.; Düchler, M. *Cell. Mol. Life Sci.* **2011**, *68*, 4023.

(74) Thompson, D. M.; Lu, C.; Green, P. J.; Parker, R. **2008**, *14*, 2095.

(75) Bellacosa, A.; Moss, E. G. *Curr. Biol.* **2003**, *13*, 482.

Chapter II:

1. Sharp, P. A. (2009) The centrality of RNA, *Cell 136*, 577–580.

2. Thomas, J. R., and Hergenrother, P. J. (2008) Targeting RNA with small molecules, *Chem. Rev. 108*, 1171–1224.

3. Chow, C. S., and Bogdan, F. M. (1997) A structural basis for RNA-ligand interactions, *Chem. Rev. 97,* 1489–1514.

4. Tor, Y. (2003) Targeting RNA with small molecules, *Chembiochem 4,* 998–1007.

5. Tibodeau, J. D., Fox, P. M., Ropp, P.A., R.; Theil, E. C., and Thorp, H. H. (2006) The up-regulation of ferritin expression using a small molecule ligand to the native mRNA. *Proc. Natl. Acad. Sci. U.S.A.*, *103*, 253–257.

6. Mattick, J. S. (2004) RNA regulation: a new genetics?, *Nat. Rev. Genet. 5*, 316–323.

7. Kong, Q. M., and Lin, C. L. G. (2010) Oxidative damage to RNA: mechanisms, consequences, and diseases, *Cell. Mol. Life Sci. 67*, 1817–1829.

8. Lee, J. T., and Raines, R. T. (2008) Ribonucleases as novel chemotherapeutics: the ranpirnase model, *BioDrugs 22*, 53–58.

9. Olmo, N., Turnay, J., González de Buitrago, G., López de Silanes, I., Gavilanes, J. G., and Lizarbe, M. A. (2001) Cytotoxic mechanism of the ribotoxin alpha-sarcin - Induction of cell death via apoptosis, *Eur. J. Biochem. 268*, 2113-23.

10. Jetzt, A. E., Cheng, J. S., Tumer, N. E., and Cohick, W. S. (2009) Ricin A-chain requires c-Jun N-terminal kinase to induce apoptosis in nontransformed epithelial cells, *Int. J. Biochem. Cell B. 41*, 2503–2510.

11. Dyson, P. J., and Sava, G. (2006) Metal-based antitumour drugs in the post genomic era, *Dalton Trans.* 1929–1933.

12. Akaboshi, M., Kawai, K., Maki, H., Akuta, K., Ujeno, Y., and Miyahara, T. (1992) The number of platinum atoms binding to DNA, RNA and protein molecules of HeLa-cells treated with cisplatin at its mean lethal concentration, *Jpn. J. Cancer Res. 83*, 522–526.

13. Boulikas, T., and Vougiouka, M. (2003) Cisplatin and platinum drugs at the molecular level, *Oncol. Rep. 10*, 1663–1682.

14. Jamieson, E. R., and Lippard, S. J. (1999) Structure, recognition, and processing of cisplatin-DNA adducts, *Chem. Rev. 99*, 2467–2498.

15. Schmittgen, T. D., Ju, J.-F., Danenberg, K. D., and Danenberg, P. V. (2003) Inhibition of pre-mRNA splicing by cisplatin and platinum analogs, *Int. J. Oncol. 23*, 785–789.

16. Rosenberg, J. M., and Sato, P. H. (1993) Cisplatin inhibits in vitro translation by preventing the formation of complete initiation complex, *Mol. Pharmacol. 43*, 491–497.

17. Heminger, K. A., Hartson, S. D., Rogers, J., and Matts, R. L. (1997) Cisplatin inhibits protein synthesis in rabbit reticulocyte lysate by causing an arrest in elongation, *Arch. Biochem. Biophys. 344*, 200–207.

18. Mazzoni, C. and Falcone, C. (2011) mRNA stability and control of cell proliferation., *Biochem. Soc. Trans., 39*, 1461-5.

19. Phizicky, E. M., and Hopper, A. K. (2010) tRNA biology charges to the front, *Genes Dev. 24*, 1832–1860.

20. Ishida, S., and Herskowitz, I. (2007) Genetic analysis of cisplatin resistance in yeast and mammals. In *Yeast as a Tool in Cancer Research* (Nitiss, J. L., and Heitman, J. Eds.), pp 393–408, Springer, The Netherlands.

21. Sinani, D., Adle, D. J., Kim, H., and Lee, J. (2007) Distinct mechanisms for Ctr1-mediated copper and cisplatin transport, *J. Biol. Chem. 282*, 26775–26785.

22. Liao, C., Hu, B., Arno, M., and Panaretou, B. (2007) Genomic screening in vivo reveals the role played by vacuolar H^+ ATPase and cytosolic acidification in sensitivity to DNA-damaging agents such as cisplatin, *Mol. Pharmacol. 71*, 416–425.

23. Fuertes, M. A., Castilla, J., Alonso, C., and Perez, J. M. (2003) Cisplatin biochemical mechanism of action: from cytotoxicity to induction of cell death through interconnections between apoptotic and necrotic pathways, *Curr. Med.Chem*. *10*, 257–266.

24. Carmona-Gutierrez, D., Eisenberg, T., Buttner, S., Meisinger, C., Kroemer, G., and Madeo, F. (2010) Apoptosis in yeast: triggers, pathways, subroutines, *Cell Death Differ. 17*, 763–773.

25. Almeida, B., Silva, A., Mesquita, A., Sarripalo-Marques, B., Rodrigues, F., and Ludovico, P. (2008) Drug-induced apoptosis in yeast, *Biochim. Biophys. Acta 1783*, 1436–1448.

26. Jung, Y., and Lippard S. J. (2007) Direct cellular responses to platinum-induced DNA damage, *Chem. Rev. 107*, 1387–1407.

27. Hoffmann, R. L. (1988) The effects of cisplatin and platinum (IV) on cell growth, RNA, protein, ribosome and DNA synthesis, *Toxicol. Environ. Chem. 17*, 139–151.

28. Beretta, G. L., Gatti, L., Tinelli, S., Corna, E., Colangelo, D., Zunino, F., and Perego P. (2004) Cellular pharmacology of cisplatin in relation to the expression of human copper transporter CTR1 in different pairs of cisplatin-sensitive and -resistant cells, *Biochem. Pharmacol. 68*, 283–291.

29. Song, I. S., Savaraj, N., Siddik, Z. H., Liu, P. M., Wei, Y. J., Wu, C. J., and Kuo, M. T. (2004) Role of human copper transporter Ctr1 in the transport of platinum-based antitumor agents in cisplatin-sensitive and cisplatin-resistant cells, *Mol. Cancer Ther. 3*, 1543–1549.

30. Zisowsky, J., Koegel, S., Leyers, S., Devarakonda, K., Kassack, M. U., Osmak, M., and Jaehde, U. (2007) Relevance of drug uptake and efflux for cisplatin sensitivity of tumor cells, *Biochem. Pharmacol*. *73*, 293–307.

31. Frohlich, K.-U., Fussi, H., and Ruckenstuhl, C. (2007) Yeast apoptosis—from genes to pathways, *Semin. Cancer Biol. 17*, 112–121.

32. Sorenson, C. M., and Eastman, A. (1988) Mechanism of cis-diamminedichloroplatinum(II)-induced cyto-toxicity - role of G2 arrest and DNA double-strand breaks, *Cancer Res. 48*, 4484–4488.

33. Grossmann, K. F., Brown, J. C., and Moses, R. E. (1999) Cisplatin DNA cross-links do not inhibit S-phase and cause only a G_2/M arrest in *Saccharomyces cerevisiae*, *Mutat. Res. 434*, 29–39.

34. Tyson, C. B., Lord, P. G., and Wheals, A. E. (1979) Dependency of size of *Saccharomyces cerevisiae* cells on growth rate, *J. Bacteriol. 138*, 92–98.

35. Eisenberg, T., Carmona-Gutierrez, D., Buttner, S., Tavernarakis, N., and Madeo, F. (2010) Necrosis in yeast, *Apoptosis 15*, 257–268.

36. Madeo, F., Frohlich, E., Ligr, M., Grey, M., Sigrist, S. J., Wolf, D. H., and Frohlich, K. U. (1999) Oxygen stress: A regulator of apoptosis in yeast, *J. Cell Biol. 145*, 757–767.

37. Li, X. P., Baricevic, M., Saidasan, H., and Tumer, N. E. (2007) Ribosome depurination is not sufficient for ricin-mediated cell death in Saccharomyces cerevisiae, *Infect. Immun. 75*, 417–428.

38. Liang, Q., and Zhou, B. (2007) Copper and manganese induce yeast apoptosis via different pathways, *Mol. Biol. Cell 18*, 4741–4749.

39. Lage, H., and Dietel, M. (1999) Involvement of the DNA mismatch repair system in antineoplastic drug resistance, *J. Cancer Res. Clin. Oncol. 125,* 156–65.

40. Zamble, D., Jacks, T., and Lippard, S.J. (1998) p53-dependent and –independent responses to cisplatin in mouse testicular terato carcinoma cells, *PNAS 95*, 6163-6168.

41. Dudgeon, D. D., Zhang, N., Ositelu, O. O., Kim, H., and Cunningham, K.W. (2008) Nonapoptotic Death of Saccharomyces cerevisiae Cells That Is Stimulated by Hsp90 and Inhibited by Calcineurin and Cmk2 in Response to Endoplasmic Reticulum Stresses, *Eukaryot. Cell. 12*, 2037–2051.

42. Burger, H., Capello, A., Schenk, P. W., Stoter, G., Brouwer, J., and Nooter, K. (2000) A genome-wide screening in Saccharomyces cerevisiae for genes that confer resistance to the anticancer agent cisplatin, *Biochem. Bioph. Res. Co. 269,* 767–774.

43. Schenk, P. W., Brok, M., Boersma, A. W. M. Brandsma, J. A., Den Dulk, H., Burger, H., Stoter, G., Brouwer, J., and Nooter, K. (2003) Anticancer drug resistance induced by disruption of the Saccharomyces cerevisiae NPR2 gene: a novel component involved in cisplatin- and doxorubicin-provoked cell kill, *Mol. Pharmacol. 64*, 259–268.

44. Moran, U., Phillips, R., and Milo, R. (2010) Snapshot: key numbers in biology, *Cell 141*, 1262–1262.

45. Tamaki, H., Yun, C.-W., Mizutani, T., Tsuzuki, T., Takagi, Y., Shinozaki, M., Kodama, Y., Shirahige, K., and Kumagai, H. (2005) Glucose-dependent cell size is regulated by a G protein-coupled receptor system in yeast Saccharomyces cerevisiae, *Genes Cells 10*, 193-206.

46. Bergamo, A., Messori, L., Piccoli, F., Cocchietto, M., and Sava, G. (2003) Biological role of adduct formation of the ruthenium(III) complex NAMI-A with serum albumin and serum transferrin, *Inv. New Drugs 21*, 401–411.

47. Eide, D. J., Clark, S., Nair, T. M., Gehl, M., Gribskov, M., Guerinot, M. L., and Harper, J. F. (2005) Characterization of the yeast ionome: a genome-wide analysis of nutrient mineral and trace element homeostasis in Saccharomyces cerevisiae, *Genome Biol. 6*, R77.

48. Bancroft, D. P., Lepre, C. A., and Lippard, S. J. (1990) Pt-195 NMR kinetic and mechanistic studies of cis-diamminedichloroplatinum and trans-diamminedichloroplatinum(II) binding to DNA, *J. Am. Chem. Soc. 112*, 6860–6871.

49. Cannone, J. J., Subramanian, S., Schnare, M. N., Collett, J. R., D'Souza, L. M., Du, Y., Feng, B., Lin, N., Madabusi, L.V., MÜller, K. M., Pande, N., Shang, Z., Yu, N., and Gutell, R. R. (2002). The Comparative RNA Web (CRW) Site: An Online Database of Comparative Sequence and Structure Information for Ribosomal, Intron, and Other RNAs, *BMC Bioinformatics 3*, 2.

50. Chapman, E. G., Hostetter, A. H., Osborn, M. F., Miller, A. L., and DeRose, V. J. (2011) Binding of kinetically inert metal ions to RNA: The case of Pt(II). In *Metal Ions in Life Sciences: Structural and Catalytic Roles of Metal Ions in RNA* (Sigel, A., Sigel, H., and Sigel, R. K. O., Eds.), pp 347–377, Royal Society of Chemistry, Cambridge.

51. Ju, Q., and Warner, J. R. (1994) Ribosome synthesis during the growth cycle of *Saccharomyces cerevisiae*, *Yeast 10*, 151–157.

52. Warner, J. R. (1999) The economics of ribosome biosynthesis in yeast, *Trends Biochem. Sci. 24*, 437–440.

53. Wilusz, C. J., Wormington, M., and Peltz, S. W. (2001) The cap-to-tail guide to mRNA turnover, *Nat. Rev. Mol. Cell Bio. 2*, 237–246.

54. Chapman, E. G., and DeRose, V. J. (2010) Enzymatic Processing of Platinated RNAs, *J. Am. Chem. Soc. 132*, 1946–1952.

55. Papsai, P., Snygg, A. S., Aldag, J., and Elmroth, S. K. (2008) Platination of full length tRNA(Ala) and truncated versions of the acceptor stem and anticodon loop, *Dalton Trans. 38,* 5225–5234.

56. Rijal, K., and Chow, C.S. (2009) A new role for cisplatin: probing ribosomal RNA structure, *Chem. Commun. 1,* 107–109.

57. Motorin, Y., Muller, S., Behm-Ansmant, I., and Brantant, C. (2007) Identification of modified residues in RNAs by reverse transcription-based methods, *Method. Enzymol. 425*, 21–53.

58. Rose, M. D., Winston, F., and Hieter, P. (1990) Yeast DNA miniprep. In *Methods in Yeast Genetics: a Laboratory Course Manual*. pp 140–142, Cold Spring Harbor Laboratory Press, NewYork.

59. Madeo, F., Frohlich, E., and Frohlich, K.-U. (1997) A yeast mutant showing diagnostic markers of early and late apoptosis, *J. Cell Biol. 139*, 729–734.

60. Sherman, F. (2002) Getting started with yeast, *Method. Enzymol. 350*, 3–41.

Chapter III:

(1) (a) Harper, B. W.; Krause-Heuer, A. M.; Grant, M. P.; Manohar, M.; Garbutcheon-Singh, K. B.; Aldrich-Wright, J. R. *Chem. Eur. J*. **2010**, *16*, 7064-7077. (b) Dyson, P. J.; Sava, G. *Dalton Trans*. **2006**, *16*, 1929-1933.

(2) (a) Sava, G.; Jaouen, G.; Hillard, E. A.; Bergamo, A. *Dalton Trans*. **2012**, *41*, 8226-8234. (b) Casini, A.; Reedijk, J. *Chem. Sci.* **2012**, *3*, 3135-3144. (c) Guggenheim, E.R.; Xu, D.; Zhang, C.X.; Chang, P.V.; Lippard, S.J. *Chem. Bio. Chem.* **2009**, *10*, 141-57. (d) Wexselblatt, E.; Yavin, E.; Gibson, D. *Inorg. Chim. Acta* **2012**, *393*, 75-83.

(3) (a) Wang, D.; Lippard, S. J. *Nat. Rev. Drug Discov*. **2005**, *4,* 307-320. (b) Boulikas, T.; Vougiouka, M. *Oncol. Rep*. **2003**, *10*, 1663-1682. (c) Jamieson, E. R.; Lippard, S. J. *Chem. Rev.* **1999**, *99*, 2467-2498.

(4) (a) Akaboshi, M.; Kawai, K.; Ujeno, Y.; Takada, S.; Miyahara, T. *Jpn. J. Can. Res*. **1994**, *85*, 106-111. (b) Akaboshi, M.; Kawai, K.; Maki, H.; Akuta, K.; Ujeno, Y.; Miyahara, T. *Jpn. J. Can. Res.* **1992**, *83*, 522-526. (c) DeConti, R. C.; Toftness, B. R.; Lange, R. C.; Creasy, W. A. *Cancer Res*. **1973**, *33*, 1310-1315.

(5) Kolb, H. C.; Finn, M. G.; Sharpless, K. B. *Angew. Chem. Int. Ed*. **2004**, *40*, 2004-2021.

(6) (a) Jewett, J. C.; Bertozzi, C. R. *Chem. Soc. Rev.* **2010**, *39*, 1272-1279. (b) Sletten, E. M.; Bertozzi, C. R. *Angew. Chem.* **2009**, *48*, 6974-6998.

(7) (a) El-Sagheer, A. H.; Brown, T. *Acc. Chem. Res.* **2012**, *45*, 1258-1267. (b) Jao, C. Y.; Salic, A. *PNAS* **2008**, *105*, 15779-15784.

(8) (a) Struthers, H.; Mindt, T. L.; Schibli, R. *Dalton Trans.* **2010**, *39*, 675-696. (b) Clough, M. C.; Zeits, P. D.; Bhuvanesh, N.; Gladysz, J. A. *Organometallics* **2012**, *31*, 5231-5234. (c) Stengel, I.; Strassert, C. A.; Plummer, E. A.; Chien, C.-H.; De Cola, L.; Bäuerle, P. *Eur. J. Inorg. Chem.* **2012**, 1795-1809. (d) Ding, S.; Qiao, X.; Kucera, G. L.; Bierbach, U. *J. Med. Chem*. **2012**, *55*, 10198-10203. (e) Urankar, D.; Košmrlj, J. *Inorg. Chim. Acta* **2010**, *363*, 3817-3822. (f) Struthers, H.; Mindt, T. L.; Schibli, R. *Dalton Trans*. **2010**, *39*, 675-696.

(9) Ding, S.; Qiao, X.; Suryadi, J.; Marrs, G. S.; Kucera, G. L.; Bierbach, U. *Angew. Chem. Int. Ed*. **2013**, *52,* 3350-3354.

(10) (a) Kelland, L. *Nat. Rev. Cancer* **2007**, *7*, 573-584. (b) Raynaud, F. I.; Boxall, F. E.; Goddard, P. M.; Valenti, M.; Jones, M.; Murrer, B. A.; Abrams, M.; Kelland, L. R. *Clin. Canc. Res.* **1997**, *3*, 2063-2074.

(11) Belluco, U.; Bertani, R.; Michelin, R. A.; Mozzon, M. *J. Organomet. Chem*. **2000**, *600*, 37-55.

(12) Kane, S. A.; Lippard, S. J. *Biochem*. **1996**, *35*, 2180-2188.

(13) Sletten, E. M.; Bertozzi, C. R. *Acc. Chem. Res*. **2011**, *44*, 666-676.

(14) (a) Chen, Y.; Guo, Z.; Parsons, S.; Sadler, P. J. *Chem. Eur. J*. **1998**, *4*, 672-676. (b) Chen, Y.; Guo, Z.; Parkinson, J. A.; Sadler, P. J. *Dalton Trans*. **1998**, 3577-3585. (c) Kelland, L. R.; Sharp, S. Y.; O'Neill, C. F.; Raynaud, F. I.; Beale, P. J.; Judson, I. R. *J. Inorg. Biochem*. **1999**, *77*, 111-115.

(15) Battle, A. R.; Choi, R.; Hibbs, D. E.; Hambley, T. W. *Inorg. Chem.* **2006**, *45*, 6317-6322.

(16) Chen, Y.; Parkinson, J. A.; Guo, Z.; Brown, T.; Sadler, P. J. *Angew. Chem. Int. Ed*. **1999**, *38*, 2060-2063.

(17) Bolletta, F.; Fabbri, D.; Lombardo, M.; Prodi, L.; Trombini, C.; Zaccheroni, N. *Organometallics*, **1996**, *15*, 2415-2417.

(18) (a) Chapman, E. G.; DeRose, V. J. *J. Am. Chem. Soc*. **2010**, *132*, 1946-1952. (b) Hostetter, A. A.; Chapman, E. G.; DeRose, V. J. *J. Am. Chem. Soc*. **2009**, *131*, 9250-9257.

(19) (a) Hostetter, A. A.; Osborn, M. F.; DeRose, V. J. *ACS Chem. Bio*. **2012**, *7*, 218-225. (b) Guan, L.; Disney, M. *ACS Chem. Bio*. **2012**, *7*, 73-86. (c) Hedman, H.K.; Kirpeker, F.; Elmroth, S. K. *J. Am. Chem. Soc.* **2011**, *133*, 11977-11984.

(20) Keshab, R.; Chow, C. S. *Chem. Commun*. **2009**, 107-109.

(21) (a) Shi, X.; Khade, P. K.; Sanbonmatsu, K. Y.; Joseph, S. *J. Mol. Biol.* **2012**, *419,* 125-138. (b) Moazed, D.; Robertson, J. M.; Moller, H. F. *Nature* **1988**, *334*, 362-364.

(22) (a) Paredes, E.; Das, S. R. *Bioorg. Med. Chem. Lett*. **2012**, *12*, 5313-5316. (b) Paredes, E.; Das, S. R. *Chem. Bio. Chem*. **2011**, *12*, 125-131.

(23) Dufour, E.; Reinbolt, J.; Castroviejo, M.; Ehresmann, B.; Litvak, S.; Tarrago-Litvak, L.; Andreola, M.-L. *J. Mol. Biol.* **1999**, *285*, 1339-1346.

Chapter IV:

1. Jamieson ER, Lippard SJ (1999) Structure, Recognition, and Processing of Cisplatin-DNA Adducts. *Chem Rev* 99:2467–98.

2. Wisnovsky SP, Wilson JJ, Radford RJ, Pereira MP, Chan MR, Laposa RR, Lippard SJ (2013) Targeting Mitochondrial DNA with a Platinum-Based Anticancer Agent. *Chem Biol* 20:1–6.

3. Hostetter AA, Osborn MF, DeRose VJ (2012) RNA-Pt adducts following cisplatin treatment of Saccharomyces cerevisiae. *ACS Chem Biol* 7:218–25.

4. Rijal K, Chow CS (2009) A new role for cisplatin: probing ribosomal RNA structure. *Chem Commun (Camb)* 1:107–9.

5. Papsai P, Aldag J, Persson T, Elmroth SKC (2006) Kinetic preference for interaction of cisplatin with the G-C-rich wobble basepair region in both tRNAAla and MhAla. *Dalton Trans* 29:3515–7.

6. Hägerlöf M, Papsai P, Hedman, HK, Jungwirth U, Jenei V, Elmroth, SKC (2008). Cisplatin and siRNA interference with structure and function of Wnt-5a mRNA. *J Biol Inorg Chem* 13:385–99.

7. Hägerlöf M, Hedman H, Elmroth SKC (2007) Platination of the siRNA sense-strand modulates both efficacy and selectivity in vitro. *Biochem Biophys Res Commun* 361:14–9.

8. Hedman HK, Kirpekar F, Elmroth SKC (2011) Platinum interference with siRNA non-seed regions fine-tunes silencing capacity. *J Am Chem Soc* 133:11977–84.

9. Polonyi C, Elmroth SKC (2013) Time dependence of cisplatin-induced duplex dissociation of 15-mer RNAs and mature miR-146a. *Dalton Trans* 42:14959–62.

10. Schmittgen TD, Ju JF, Danenberg KD, Danenberg PV (2003) Inhibition of pre-mRNA splicing by cisplatin and platinum analogs. *Int J Oncol* 23:785–789.

11. Danenberg PV, Shea LC, Danenberg KD, Horikoshi T (1991) Inactivation of Tetrahymena rRNA self-splicing by cis-platin proceeds through dissociable complexes. *Nucleic Acids Res* 19:3123–8.

12. Jordan P, Carmo-Fonseca M (1998) Cisplatin inhibits synthesis of ribosomal RNA in vivo. *Nucleic Acids Res* 26:2831–6.

13. Becker JP, Weiss J, Theile D (2013) Cisplatin, oxaliplatin, and carboplatin unequally inhibit in vitro mRNA translation. *Toxicol Lett*:1–5.

14. Bellacosa A, Moss EG (2003) RNA Repair: Damage Control. *Curr Biol* 13:R482–R484.

15. Mei Y, Stonestrom A, Hou Y-M, Yang X (2010) Apoptotic regulation and transfer RNA. *Protein Cell* 1:795–801.

16. White JD, Osborn MF, Moghaddam AD, Guzman LE, Haley MM, DeRose VJ (2013) Picazoplatin, an azide-containing platinum(II) derivative for target analysis by click chemistry. *J Am Chem Soc* 135:11680–3.

17. Ding S, Qiao X, Suryadi J, Marrs GS, Kucera GL, Bierbach U (2013) Using fluorescent post-labeling to probe the subcellular localization of DNA-targeted platinum anticancer agents. *Angew Chem Int Ed Engl* 52:3350–4.

18. Kelland L (2007) The resurgence of platinum-based cancer chemotherapy. *Nat Rev Cancer* 7:573–84.

19. Raynaud FI, Boxall FE, Goddard PM, Raynaud I, Goddard M (1997) cis-Amminedichloro(2-methylpyridine) platinum (II) (AMD473), a novel sterically hindered platinum complex : in vivo activity, toxicology, and pharmacokinetics in mice. *Clin Canc Res* 11:2063–2074.

20. Nawrot B, Sochacka E, Düchler M (2011) tRNA structural and functional changes induced by oxidative stress. *Cell Mol Life Sci* 68:4023–32.

21. Thompson DM, Lu C, Green PJ, Parker R (2008) tRNA cleavage is a conserved response to oxidative stress in eukaryotes. *RNA* 14:2095–2103.

22. Alexandrov A, Chernyakov I, Gu W, Hiley SL, Hughes TR, Grayhack EJ, Phizicky EM (2006) Rapid tRNA decay can result from lack of nonessential modifications. *Mol Cell* 21:87–96.

23. Motorin Y, Helm M (2010) tRNA stabilization by modified nucleotides. *Biochemistry* 49:4934–44.

24. Chapman EG, DeRose VJ (2010) Enzymatic processing of platinated RNAs. *J Am Chem Soc* 132:1946–52.

25. Shaheen HH, Hopper AK (2005) Retrograde movement of tRNAs from the cytoplasm to the nucleus in Saccharomyces cerevisiae. *Proc Natl Acad Sci U S A* 102:11290–5.

26. Pavon-Eternod M et al. (2009) tRNA over-expression in breast cancer and functional consequences. *Nucleic Acids Res* 37:7268–80.

27. Zhou Y, Goodenbour JM, Godley LA, Wickrema A, Pan T (2009) High levels of tRNA abundance and alteration of tRNA charging by bortezomib in multiple myeloma. *Biochem Biophys Res Commun* 385:160–4.

28. Dorner S, Polacek N, Schulmeister U, Panuschka C, Barta A (2002) Molecular aspects of the ribosomal peptidyl transferase. *Biochem Soc Trans* 30:1131–6.

29. Polacek N, Mankin AS (2005) The ribosomal peptidyl transferase center: structure, function, evolution, inhibition. *Crit Rev Biochem Mol Biol* 40:285–311.

30. Winter D, Polacek N, Halama I, Streicher B, Barta A (1997) Lead-catalysed specific cleavage of ribosomal RNAs. *Nucleic Acids Res* 25:1817–24.

31. Polacek N, Barta A (1998) Metal ion probing of rRNAs : evidence for evolutionarily conserved divalent cation binding pockets. *RNA* 4:1282–1294.

32. Iordanov MS, Pribnow D, Magun JL, Dinh T-H, Pearson JA, Magun BE (1998) Ultraviolet Radiation Triggers the Ribotoxic Stress Response in Mammalian Cells. *J Biol Chem* 273:15794–15803.

33. Magun BE, Iordanov MS, Pribnow D, Magun JL, Dinh T (1997) Ribotoxic stress response: activation of the stress-activated protein kinase JNK1 by inhibitors of the peptidyl transferase reaction and by sequence-specific RNA damage to the alpha-sarcin/ricin loop in the 28S rRNA . *Mol Cell Biol* 17:3373–3381.

34. Spacková N, Sponer J (2006) Molecular dynamics simulations of sarcin-ricin rRNA motif. *Nucleic Acids Res* 34:697–708.

35. Shi X, Khade PK, Sanbonmatsu KY, Joseph S (2012) Functional role of the sarcin-ricin loop of the 23S rRNA in the elongation cycle of protein synthesis. *J Mol Biol* 419:125–38.

36. Macbeth MR, Wool IG (1999) Characterization of in vitro and in vivo mutations in non-conserved nucleotides in the ribosomal RNA recognition domain for the ribotoxins ricin and sarcin and the translation elongation factors. *J Mol Biol* 285:567–80.

37. Hermann T, Westhof E (1998) Exploration of metal ion binding sites in RNA folds by Brownian-dynamics simulations. *Structure* 6:1303–14.

38. Mantri Y, Lippard SJ, Baik M-H (2007) Bifunctional binding of cisplatin to DNA: why does cisplatin form 1,2-intrastrand cross-links with ag but not with GA? *J Am Chem Soc* 129:5023–30.

39. Macbeth MR, Wool IG (1999) The phenotype of mutations of G2655 in the sarcin/ricin domain of 23 S ribosomal RNA. *J Mol Biol* 285:965–75.

40. Correll CC, Munishkin A, Chan Y-L, Ren Z, Wool IG, Steitz TA (1998) Crystal structure of the ribosomal RNA domain essential for binding elogation factors. *Proc Natl Acad Sci* 95:13436–13441.

41. Leshin JA, Heselpoth R, Belew AT, Dinman J (2011) High throughput structural analysis of yeast ribosomes using hSHAPE. *RNA Biol* 8:478–487.

42. Besseová I, Réblová K, Leontis NB, Sponer J (2010) Molecular dynamics simulations suggest that RNA three-way junctions can act as flexible RNA structural elements in the ribosome. *Nucleic Acids Res* 38:6247–64.

43. Rosenberg J, Sato PH (1992) Cisplatin Inhibits In Vitro Translation of Complete Initiation Complex by Preventing the Formation. *Mol Pharmacol* 43:491–497.

44. Havrila M, Réblová K, Zirbel CL, Leontis NB, Sponer J (2013) Isosteric and Nonisosteric Base Pairs in RNA Motifs: Molecular Dynamics and Bioinformatics Study of the Sarcin-Ricin Internal Loop. *J Phys Chem B*. 117:14302-14319.

45. Ahmad S, Isab AA, Ali S (2006) Structural and mechanistic aspects of platinum anticancer agents. *Transit Met Chem* 31:1003–1016.

46. Jerremalm E, Eksborg S, Ehrsson H (2003) Hydrolysis of oxaliplatin-evaluation of the acid dissociation constant for the oxalato monodentate complex. *J Pharm Sci* 92:436–8.

47. Cannone JJ, Subramanian S, Schnare MN, Collett JR, D'Souza LM, Du Y, Feng B, Lin N, Madabusi LV, Muller KM, Pande N, Shang Z, Gutell RR (2002) The comparative RNA web (CRW) site: an online database of comparative sequence and structure information for ribosomal, intron, and other RNAs. *BMC Bioinformatics* 3:2.

Chapter V:

(1) Chapman, E. G.; DeRose, V. J. *J. Am. Chem. Soc.* **2010**, *132*, 1946.

(2) Mjos, K. D.; Orvig, C. *Chem. Rev.* **2014**. [Epub ahead of print]

(3) Wheate, N. J.; Walker, S.; Craig, G. E.; Oun, R. *Dalton Trans.* **2010**, *39*, 8113.

(4) Ding, S.; Qiao, X.; Suryadi, J.; Marrs, G. S.; Kucera, G. L.; Bierbach, U. *Angew. Chem. Int. Ed. Engl.* **2013**, *52*, 3350.

(5) Bednarski, P. J.; Mackay, F. S.; Sadler, P. J. *Anticancer. Agents Med. Chem.* **2007**, *7*, 75.

(6) Xiao, H.; Noble, G. T.; Stefanick, J. F.; Qi, R.; Kiziltepe, T.; Jing, X.; Bilgicer, B. *J. Control. Release* **2013**, *173*, 11.

Appendix A:

1. Motorin, Y., Muller, S., Behm-Ansmant, I., and Brantant, C. (2007) Identification of modified residues in RNAs by reverse transcription-based methods, *Method. Enzymol. 425*, 21–53.

2. Rose, M. D., Winston, F., and Hieter, P. (1990) Yeast DNA miniprep. In *Methods in Yeast Genetics: a Laboratory Course Manual*. pp 140–142, Cold Spring Harbor Laboratory Press, NewYork.

3. Warner, J. R. (1999) The economics of ribosome biosynthesis in yeast, *Trends Biochem. Sci. 24*, 437–440.

4. Wilusz, C. J., Wormington, M., and Peltz, S. W. (2001) The cap-to-tail guide to mRNA turnover, *Nat. Rev. Mol. Cell Bio. 2*, 237–246.

5. Ben-Shem, A., Jenner, L., Yusupova, G., Yusupov, M. (2010) Crystal structure of the eukaryotic ribosome. *Science 330*, 1203-209.

6. Sherman, F. (2002) Getting started with yeast, *Method. Enzymol. 350*, 3–41.

Appendix B:

(1) Rubin, G. *J. Biol. Chem.* **1973**, *248*, 3860-3875.

(2) Chapman, E. G.; DeRose, V. J. *J. Am. Chem. Soc.* **2010**, *132*, 1946.

Appendix C:

(1) White JD, Osborn MF, Moghaddam AD, Guzman LE, Haley MM, DeRose VJ (2013) Picazoplatin, an azide-containing platinum(II) derivative for target analysis by click chemistry. *J Am Chem Soc* 135:11680–3.

(2) Chapman EG, DeRose VJ (2010) Enzymatic processing of platinated RNAs. *J Am Chem Soc* 132:194